Fundamental Equations of State for Parahydrogen, Normal Hydrogen, and Orthohydrogen

A Thesis
Presented in Partial Fulfillment of the Requirements for the
Degree of Master of Science
with a
Major in Mechanical Engineering
in the
College of Graduate Studies
University of Idaho

By
Jacob Leachman

May 2007

Major Professor: Richard T Jacobsen

Authorization to Submit Thesis

This thesis of Jacob Leachman, submitted for the degree of Master of Science with a major in Mechanical Engineering and titled "Fundamental Equations of State for Parahydrogen, Normal Hydrogen, and Orthohydrogen," has been reviewed in final form. Permission, as indicated by the signatures and dates given below, is now granted to submit final copies to the College of Graduate Studies for approval.

Major Professor _____Date_____

Richard T Jacobsen

Committee Members _____Date_____

Steven G. Penoncello

_____Date_____

Thomas E. Bitterwolf

Department Administrator _____Date_____

Donald Blackketter

Discipline's College Dean _____Date_____

Aicha Elshabini

Final Approval and Acceptance by the College of Graduate Studies

_____Date_____

Margrit von Braun

Abstract

The potential boom in the global hydrogen economy will increase the need for accurate hydrogen thermodynamic property standards. Based on these needs, new fundamental equations of state for parahydrogen and normal hydrogen were developed to replace the existing standards. To accurately predict thermophysical properties near the critical region and in liquid states, the Quantum Law of Corresponding States was applied to predict the vapor pressure curve for normal hydrogen and selected single phase data on the normal hydrogen surface. Once adequacy of the theory was established, pure orthohydrogen data were predicted and an orthohydrogen equation of state was developed.

All three equations of state have the same maximum pressure of 2000 MPa and temperature of 1000 K. The uncertainty in density is 0.04% in the region between 250 and 450 K and at pressures from 0.1-300 MPa. The uncertainties of vapor pressures and saturated liquid densities vary from 0.1-0.2%.

Acknowledgments

My sincere admiration goes to Professor Richard Jacobsen and Dr. Eric Lemmon. The system they have built for formulation of equations of state is truly world class, and this thesis would not be close to what it is without their assistance throughout or foresight to start the project. Professor Steven Penoncello should really be considered my major advisor and not just a committee member. I frequented his office doorway in search of advice countless times over the past year. I thank Professor Thomas Bitterwolf for helping me think about the quantum mechanics behind some of hydrogen's characteristics. It was no small task. I'd like to thank my fiancé Chelsea Sherman whose patience and understanding throughout this research has been unquestionably unmatched.

This work would not have been possible without the Center for Applied Thermodynamic Studies' Emeritus Director Richard B. Stewart. His early review of hydrogen properties placing a distinction between orthohydrogen and parahydrogen was very beneficial to the initial stages of this work. The Richard B. Stewart Thermodynamics Scholarship provided the funding for my summer research position at NIST and support for my graduate studies.

Table of Contents

Authorization to Submit Thesis ii
Abstract iii
Acknowledgments iv
Table of Contents v
List of Tables vii
List of Figures ix
List of Symbols xiv
1. Introduction 1
1.1 Hydrogen Generation 3
1.2 Hydrogen Storage 6
1.3 Hydrogen as a Commodity and the Standard Equation of State 8
2. The Hydrogen Molecule 11
2.1 Orthohydrogen and Parahydrogen 12
2.2 Self-Induced Conversion Between Orthohydrogen and Parahydrogen 17
2.3 Catalyzed Conversion Between Orthohydrogen and Parahydrogen 18
2.4 Determination of the Orthohydrogen and Parahydrogen Concentration 20
3. The Thermophysical Properties of Hydrogen 22
3.1 Ideal Thermodynamic Property Behavior of Hydrogen 22
3.2 Near Critical Region Property Behavior 23
3.3 Quantum Law of Corresponding States 25
4. Experimental Data for the Thermodynamic Properties of Hydrogen 31
4.1 Data Maps for Thermodynamic Properties of Parahydrogen. 35
4.2 Data Maps for Thermodynamic Properties of Normal Hydrogen 41
5. Current Thermodynamic Property Formulations for Hydrogen 45
5.1 Current Standard Thermodynamic Property Formulation for Parahydrogen. 45
5.2 Current Standard Thermodynamic Property Formulation for Normal Hydrogen 48
6. New Thermodynamic Property Formulations for Hydrogen 50
6.1 Theory and Design of Fundamental Equations of State 50

6.2 New Thermodynamic Property Formulation for Parahydrogen 55
6.3 New Thermodynamic Property Formulation for Normal Hydrogen..... 63
6.4 New Thermodynamic Property Formulation for Orthohydrogen..... 65
7. Comparison of Calculated Thermophysical Properties of Hydrogen to Data. 68
7.1 Comparison of Calculated Parahydrogen Properties to Data..... 68
7.2 Comparison of Calculated Normal Hydrogen Properties to Data 88
7.3 Comparison of Calculated Orthohydrogen Properties to Data 105
8. Current Status and Recommendations for Future Research 111
9. References 112
Appendix A. Tables of Hydrogen Thermodynamic Data 121

List of Tables

1.1 Selected Compilations of Thermophysical Properties of Hydrogen. 2
1.2 Estimated Experimental Measurement Accuracies 9
1.3 Estimated Uncertainty in the Normal Hydrogen and Methane EOS 9
3.1 Critical Point and Triple Point Properties for Normal Hydrogen and Parahydrogen. 24
3.2 Values of the Quantum Parameter for Several Fluids. 26
4.1 Summary of Thermodynamic Property Data for Parahydrogen. 32
4.2 Summary of Thermodynamic Property Data for Normal Hydrogen 33
5.1 Coefficients for the Parahydrogen Equation of State. 46
5.2 Fixed Point Properties and Correlation Limits for Parahydrogen. 46
5.3 Coefficients for the Ideal Gas Heat Capacity equation for Parahydrogen.... 47
5.4 Fixed Point Properties, Correlation Limits, and Fluid Constants for Normal Hydrogen. 48
5.5 Coefficients for the Ideal Gas Heat Capacity Equation for Normal Hydrogen. 49
6.1 Parameters and Coefficients of the New Parahydrogen Equation of State . 56
6.2 Parameters of the Gaussian Terms in the New Parahydrogen Equation of State. 56
6.3 Parameters and Coefficients of the Parahydrogen Ideal Gas Heat Capacity Equation. 57
6.4 Critical and Triple Point Properties used by the New Parahydrogen EOS.... 57
6.5 Parameters and Coefficients of the New Normal Hydrogen Equation of State. 63
6.6 Parameters of the Gaussian Terms in the New Normal Hydrogen Equation of State. 64
6.7 Parameters and Coefficients of the Normal Hydrogen Ideal Gas Heat Capacity Equation. 64
6.8 Critical and Triple Point Properties used by the New Normal Hydrogen EOS. 65
6.9 Data Sets Selected for Transformation to the Orthohydrogen Surface..... 66

6.10 Parameters and Coefficients of the Orthohydrogen Equation of State 66
6.11 Parameters of the Gaussian Terms in the Orthohydrogen Equation of State. 66
6.12 Parameters and Coefficients of the Orthohydrogen Ideal Gas Heat Capacity Equation. 67
6.13 Critical and Triple Point Properties used by the Orthohydrogen EOS. 67
A.1 Calculated Saturation Properties of the New Parahydrogen EOS..... 121
A.2 Calculated Saturation Properties of the New Normal Hydrogen EOS. 122
A.3 Calculated Saturation Properties of the New Orthohydrogen EOS. 123
A.4 Vapor Pressure Data Predicted Using the Quantum Law of Corresponding States. 124

List of Figures

1.1 Example Synthesis Gas Reactor for the Production of Hydrogen.. 4
1.2 Comparison of the Standard EOS Temperature Limit with Maximum Hydrogen Generation Process Temperatures. 6
2.1 Protium, Deuterium, and Tritium atoms. 11
2.2 The Differences in Molecular Architecture between Orthohydrogen and Parahydrogen. 14
2.3 The Equilibrium Concentration of Orthohydrogen and Parahydrogen. 16
2.4 Thermal Conductivity of Normal Hydrogen and Parahydrogen..... 21
3.1 Calculated Ideal Gas Heat Capacities of Parahydrogen, Normal Hydrogen, and Orthohydrogen. 23
3.2 Calculated Vapor Pressure Differences between Liquid Normal Hydrogen and Parahydrogen. 24
3.3 Reduced Temperatures plotted versus Quantum Parameter. 28
3.4 Reduced Pressures plotted versus Quantum Parameter. 28
3.5 Reduced Densities plotted versus Quantum Parameter. 29
4.1 P-ρ-T Data for Parahydrogen (P-T coordinates). 35
4.2 P-ρ-T Data for Parahydrogen (P- ρ coordinates). 37
4.3 Isochoric Heat Capacity Data for Parahydrogen..... 38
4.4 Isobaric Heat Capacity Data for Parahydrogen. 39
4.5 Speed of Sound Data for Parahydrogen. 40
4.6 P-ρ-T data for Normal Hydrogen (P-T coordinates). 41
4.7 P-ρ-T Data for Normal Hydrogen (P-rho coordinates). 43
4.8 Speed of Sound Data for Normal Hydrogen. 44
6.1 Rectilinear Diameter Plot of a Preliminary New Parahydrogen EOS Displaying an Incorrect Critical Density. 58
6.2 Calculated Isochoric Heat Capacity plotted versus Temperature for the Parahydrogen EOS of Younglove (top) and the New Parahydrogen EOS (bottom) (Isobars are shown between 0 and 10 MPa in 0.5 MPa increments)..... 59

6.3 Calculated Speed of Sound plotted versus Temperature for the Parahydrogen EOS of Younglove (top) and the new Parahydrogen EOS (bottom) (Isobars are shown between 0 and 10 MPa in 0.5 MPa increments)..... 60
6.4 Isothermal Behavior of the Parahydrogen EOS of Younglove (top) and the New Parahydrogen EOS (bottom) at Extreme Conditions of Density and Pressure. (Isotherms are spaced in 50 K increments starting with 50 K and ending at 1000 K)..... 62
7.1 Difference in Second Virial Coefficient plotted versus Temperature for the Parahydrogen EOS of Younglove (top) and the New Parahydrogen EOS (bottom) from experimental data. 72
7.2 Difference in Third Virial Coefficient plotted versus Temperature for the Parahydrogen EOS of Younglove (top) and the New Parahydrogen EOS (bottom) from experimental data. 73
7.3 Deviation of Saturation Heat Capacity for the Parahydrogen EOS of Younglove (top) and the new Parahydrogen EOS (bottom) from experimental data..... 74
7.4 Deviation of Isochoric Heat Capacity of the Parahydrogen EOS of Younglove (top) and the new Parahydrogen EOS (bottom) from experimental data..... 75
7.5 Deviation of Isobaric Heat Capacity of the Parahydrogen EOS of Younglove (top) and the new Parahydrogen EOS (bottom) from experimental data..... 76
7.6 Deviation of Sound Speed of the Parahydrogen EOS of Younglove (top) and the new Parahydrogen EOS (bottom) from experimental data..... 77
7.7 Deviation of Vapor Pressure of the Parahydrogen EOS of Younglove (top) and the new Parahydrogen EOS (bottom) from experimental data..... 78
7.8 Deviation of Density of the Parahydrogen EOS of Younglove (top) and the new Parahydrogen EOS (bottom) from experimental data (Data plotted against Pressure)..... 79

7.9 Deviation of Density of the Parahydrogen EOS of Younglove (right) and the new Parahydrogen EOS (left) from experimental data. (Data displayed in 10 K increments from 10-70 K) 80
7.10 Deviation of Density of the Parahydrogen EOS of Younglove (right) and the new Parahydrogen EOS (left) from experimental data. (Data displayed in 10 K increments from 30-40 K) 81
7.11 Deviation of Density of the Parahydrogen EOS of Younglove (right) and the new Parahydrogen EOS (left) from experimental data. (Data displayed in 10 K increments from 150-250 K) 82
7.12 Deviation of Density of the Parahydrogen EOS of Younglove (right) and the new Parahydrogen EOS (left) from experimental data. (Data displayed in 10 K increments from 270-360 K) 83
7.13 Deviation of Density of the Parahydrogen EOS of Younglove (right) and the new Parahydrogen EOS (left) from experimental data. (Data displayed in listed increments from 370-580 K) 84
7.14 Deviation of Density of the Parahydrogen EOS of Younglove (right) and the new Parahydrogen EOS (left) from experimental data. (Data displayed in 10 K increments from 670-880 K) 85
7.15 Deviation of Pressure of the Parahydrogen EOS of Younglove (top) and the new Parahydrogen EOS (bottom) from experimental data. (Data displayed in 10 K increment from 30-40 K) 86
7.16 Deviation of Density of the Parahydrogen EOS of Younglove (top) and the new Parahydrogen EOS (bottom) from experimental data. (Data plotted against temperature) 87
7.17 Difference in Second Virial Coefficient plotted versus Temperature for the Normal Hydrogen EOS of REFPROP (top) and the New Normal Hydrogen EOS (bottom) from experimental data. 90
7.18 Difference in Third Virial Coefficient plotted versus Temperature for the Normal Hydrogen EOS of REFPROP (top) and the New Normal Hydrogen EOS (bottom) from experimental data. 91

7.19 Deviation of Sound Speed plotted versus Pressure for the Normal Hydrogen EOS of REFPROP (top) and the New Normal Hydrogen EOS (bottom) from experimental data. 92
7.20 Deviation of Sound Speed plotted versus Pressure for the Normal Hydrogen EOS of REFPROP (top) and the New Normal Hydrogen EOS (bottom) from high pressure experimental data. 93
7.21 Deviation of Vapor Pressure plotted versus Temperature for the Normal Hydrogen EOS of REFPROP (top) and the New Normal Hydrogen EOS (bottom) from experimental data. 94
7.22 Deviation of Vapor Pressure plotted versus Temperature for the New Normal Hydrogen EOS with Transformed Parahydrogen data. 95
7.23 Deviation of Density plotted versus Pressure for the New Normal Hydrogen EOS. 96
7.24 Deviation of Density plotted versus Pressure for the Normal Hydrogen EOS of REFPROP (right) and the New Normal Hydrogen EOS (left) from experimental data (Data plotted in 10 K increments from 10-80 K). 97
7.25 Deviation of Density plotted versus Pressure for the Normal Hydrogen EOS of REFPROP (right) and the New Normal Hydrogen EOS (left) from experimental data (Data plotted in 10 K increments from 70-140 K). 98
7.26 Deviation of Density plotted versus Pressure for the Normal Hydrogen EOS of REFPROP (right) and the New Normal Hydrogen EOS (left) from experimental data (Data plotted in 10 K increments from 150-250 K). 99
7.27 Deviation of Density plotted versus Pressure for the Normal Hydrogen EOS of REFPROP (right) and the New Normal Hydrogen EOS (left) from experimental data (Data plotted in 10 K increments from 270-360 K). 100
7.28 Deviation of Density plotted versus Pressure for the Normal Hydrogen EOS of REFPROP (right) and the New Normal Hydrogen EOS (left) from experimental data (Data plotted in listed increments from 370-580 K). 101
7.29 Deviation of Density plotted versus Pressure for the Normal Hydrogen EOS of REFPROP (right) and the New Normal Hydrogen EOS (left) from experimental data (Data plotted in listed increments from 670-880 K). 102

7.30 Deviation of Density plotted versus Temperature for the Normal Hydrogen EOS of REFPROP (top) and the New Normal Hydrogen EOS (bottom) from experimental data. 103
7.31 Deviation of Pressure plotted versus Density for the Normal Hydrogen EOS of REFPROP (top) and the New Normal Hydrogen EOS (bottom) from experimental data (Data displayed in one 10 K increment from 30-40 K). 104
7.32 Deviation of Vapor Pressure plotted versus Temperature for the New Orthohydrogen EOS from experimental and Predicted data. 106
7.33 Deviation of Sound Speed plotted versus Pressure for the New Orthohydrogen EOS from Predicted data. 107
7.34 Deviation of Density plotted versus Pressure for the New Orthohydrogen EOS from Experimental and Predicted data. (Data shown in increments from 10-150 K) 108
7.35 Deviation of Density plotted versus Pressure for the New Orthohydrogen EOS from Experimental and Predicted data. (Data shown in increments from 150-350 K) 109
7.36 Deviation of Density plotted versus Pressure for the New Orthohydrogen EOS from Experimental and Predicted data. (Data shown in increments from 350-880 K) 110

List of Symbols

Symbol	Physical Quantity	Unit
a	Helmholtz free energy	J
B	Second virial coefficient	L/mol
C	Third virial coefficient	L^2/mol^2
C_p	Isobaric heat capacity	J/(mol·K)
C_v	Isochoric heat capacity	J/(mol·K)
ħ	Planck's constant	J·s
h	Enthalpy	J/mol
M	Molar mass	g/mol
N	Avogadro's number	/mol
P	Pressure	MPa
R	Molar gas constant	J/(mol·K)
r	Radius of interaction	Å
s	Entropy	J/(mol·K)
T	Temperature	K
U	Intermolecular Potential	/m
w	Speed of sound	m/s
Z	Compressibility Factor	
α	Reduced Helmholtz energy	
ε	Characteristic temperature	/K
δ	Reduced density	
Λ	Quantum parameter	
ρ	Molar density	mol/L
φ	Fugacity coefficient	
τ	Reduced temperature	
ψ	Wave function	
	Subscripts	
c	Critical point property	
r	Reduced property	
o	Orthohydrogen property	
p	Parahydrogen property	
N	Normal hydrogen property	
t	Triple point property	
o	Dilute gas property	
	Superscripts	
*	Quantum reduced property	
r	Real fluid property	
o	Ideal gas property	

1. Introduction

Hydrogen's role as a fuel and energy carrier (energy transfer medium) came into perspective in the 1960s with the success of NASA's liquid hydrogen fueled space program. Hydrogen is an excellent rocket propellant due to its wide range of flammability, high flame speed, efficient combustion, and because it has the highest energy content per unit weight of any known fuel. Recently hydrogen has been recommended as an energy carrier or fuel for environmentally-friendly domestic vehicles. A hydrogen highway infrastructure is being constructed in Canada from Vancouver to Whistler for transportation during the 2010 Winter Olympics [1]. The state of California is also building a network of hydrogen fueling stations for both urban and rural highways that currently has 16 stations in operation [2].

Although relatively new as an energy carrier for transportation, hydrogen has long been utilized in the production of chemicals, particularly fertilizers, in petroleum refining, in metals treatment, and it is a component in every living organism. Hydrogen offers several advantages as an energy carrier or fuel for transportation in addition to its advantages as a rocket fuel:

- When ideally combusted or reacted with oxygen it produces water vapor as the only byproduct.
- It can be produced from many sources within the United States (US).
- It is safer in some aspects than many other fuels [3].

The commercial sale of hydrogen as a commodity demands accurate and precise metering standards. For the design and calibration of systems, engineers must use accurate values for the properties of the working fluids. These values are usually obtained from an Equation of State (EOS). For large scale production, these calculated properties must be very accurate to prevent large uncertainties in the quantity of product produced. The currently accepted standard EOS for thermophysical properties of hydrogen is based on work

conducted from the 1970s through mid 1980s at the National Institute of Standards and Technology (NIST), then the National Bureau of Standards (NBS). The EOS is accurate to the upper limits in pressure and temperature of 121 megapascals (MPa) and 400 kelvins (K), respectively [4]. These limits may not allow for accurate property calculations in the operating temperature range of many of the proposed commercial hydrogen generation processes.

For the sustainable production and distribution of hydrogen, a revision of the thermophysical property models of hydrogen and the data used to develop those models are provided. Because the available literature for hydrogen is so extensive, the bibliography of this report is limited to those papers and other references containing formulations and data used in this presentation. A summary of prior compilations is presented in Table 1.1. This thesis builds upon previous research in the Center for Applied Thermodynamic Studies (CATS) at the University of Idaho. One report and two papers document previous work [5,6,7]. Some material has been taken from that work and included here for completeness without specific reference.

Table 1.1 Selected Compilations of Thermophysical Properties of Hydrogen.

Author(s) [Ref.#]	Date
Woolley *et al.* [8]	1948
Hust & Stewart [9]	1965
McCarty & Weber [10]	1972
McCarty [11]	1975
Vargaftik [12]	1975
McCarty *et al.* [13]	1981
Younglove [14]	1985
Souers [15]	1986
Verkin *et al.* [16]	1991
NIST Web Site for H_2 Data [17]	2006
Jacobsen *et al.* [6]	2006
Leachman *et al.* [7]	2006

1.1 Hydrogen Generation

Although hydrogen is the most abundant element in the universe, pure hydrogen is extremely limited on earth. To obtain pure hydrogen, the hydrogen is usually extracted from complex compounds. This extraction of hydrogen requires energy from another source. Hydrogen atoms are found in water (H_2O), hydrocarbons (C_xH_y), fertilizers, and many other common chemical compounds. The long term source of hydrogen fuel that can be used to support the hydrogen economy must be naturally occurring and abundant. In addition, the processes used to liberate hydrogen from the source compounds must not create greenhouse gases like carbon dioxide (CO_2) or carbon monoxide (CO). The short term requirements to establish a stable hydrogen economy may require hydrogen production from fossil fuels while the technology for production from renewable energy sources gains a foothold. Regardless of the source, the extraction of hydrogen from compounds requires energy from one of three categories: fossil fuels, nuclear power, or renewable energy resources.

Commercial production of hydrogen from fossil fuels and renewable biomass involves expansion of existing technology. Biomass production of hydrogen requires the heating of biomass slurry. When driven to pressures and temperatures of 24 MPa and 950-1100 K, respectively, the biomass produces a mixture of CO_2, H_2O, molecular hydrogen (H_2), methane (CH_4) and CO [18]. This gas mixture is in many ways similar to natural gas that occurs within the earth's crust. The partial oxidation of coal produces a similar gas mixture. When the fuel is refined to primarily CO and H_2 it is called synthesis gas or syngas [19]. Syngas can be used to create synthetic liquid hydrocarbons or it can be used to create hydrogen gas. Synthetic liquid hydrocarbons are produced using syngas in the Fischer-Tropsch process. Fischer-Tropsch technology was pioneered in petroleum-poor, but coal-rich, Germany in the 1920s and was used by Germany to produce as many as 124,000 barrels of synthetic fuel per day in 1944 [20]. An example of a syngas commercial reactor system is shown in Figure 1.1.

Although there are several different reactor types and feed fuels, most steam methane reforming reactors operate at temperatures in the range of 1000-1400 K [18]. The water gas shift reaction converts the CO present with steam to CO_2 at temperatures from 550-700 K [19]. In 2004, 50 million metric tons of hydrogen were produced globally, of which 48 % was by steam reforming of natural gas [21].

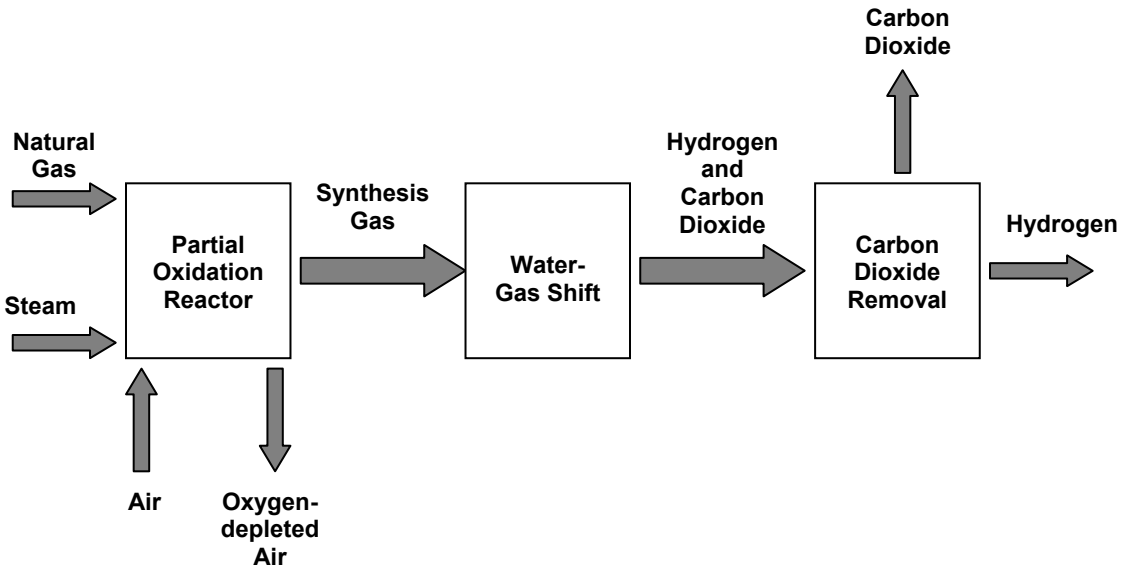

Figure 1.1 Example Synthesis Gas Reactor for the Production of Hydrogen.

Nuclear production of hydrogen is accomplished using a high temperature nuclear reaction to boost the operating temperature of either high-temperature electrolysis processes or thermochemical water-splitting processes. High-temperature electrolysis of water produces hydrogen gas through the separation of water's hydrogen-oxygen bond. Conventional electrolysis separates water into its constituent elements by charging water with an electrical current. Ideally, water can be dissociated directly without electricity if the temperature is high enough (thermolysis); however this process requires temperatures in excess of 2800 K [22]. Combining conventional electrolysis and thermolysis by capturing heat from a nuclear reaction, the amount of electrical energy required can be reduced.

Thermochemical water-splitting cycles use a series of chemical reactions at high temperatures. The cycles are designed so that water is fed into the process, hydrogen and oxygen gases are collected, and all of the reactants are regenerated and recycled. Although more than 100 thermochemical water-splitting cycles have been identified, only a few have been selected for further research. Important characteristics of candidate cycles are the simplicity of the cycle, the efficiencies of the processes, and the ability to separate pure hydrogen from the products [23]. The sulfur family of cycles is of particular commercial interest and typically sees a high reaction temperature of 1150 K.

Hydrogen can also be generated from renewable energy resources through either biological production with algae, photovoltaic cells, or electrolytic production from wind turbines. Photolytic cells and electrolytic production of hydrogen from windmills both use water at ambient conditions and apply the necessary voltage difference to cause electrolysis of the water. The minimum voltage required for these processes is 1.23 electron volts at 298 K. Biological production of hydrogen with algae occurs at normal ambient pressure and temperature ranges because the algae require a controlled life-promoting environment.

The only cycles being investigated for the production of hydrogen that lie within the temperature limits of the accepted standard hydrogen EOS are cycles using photolytic cells, electrolytic production from wind turbines, and biological production with algae [Figure 1.2]. The EOS will be discussed further in Section 1.3. The maximum pressure of the generation cycles is well within the range of the current standard EOS maximum pressure limit. To be able to make correct and rapid calculations in the design of these systems, accurate thermodynamic and transport property values are required. The limits on the current standard EOS do not always allow for this.

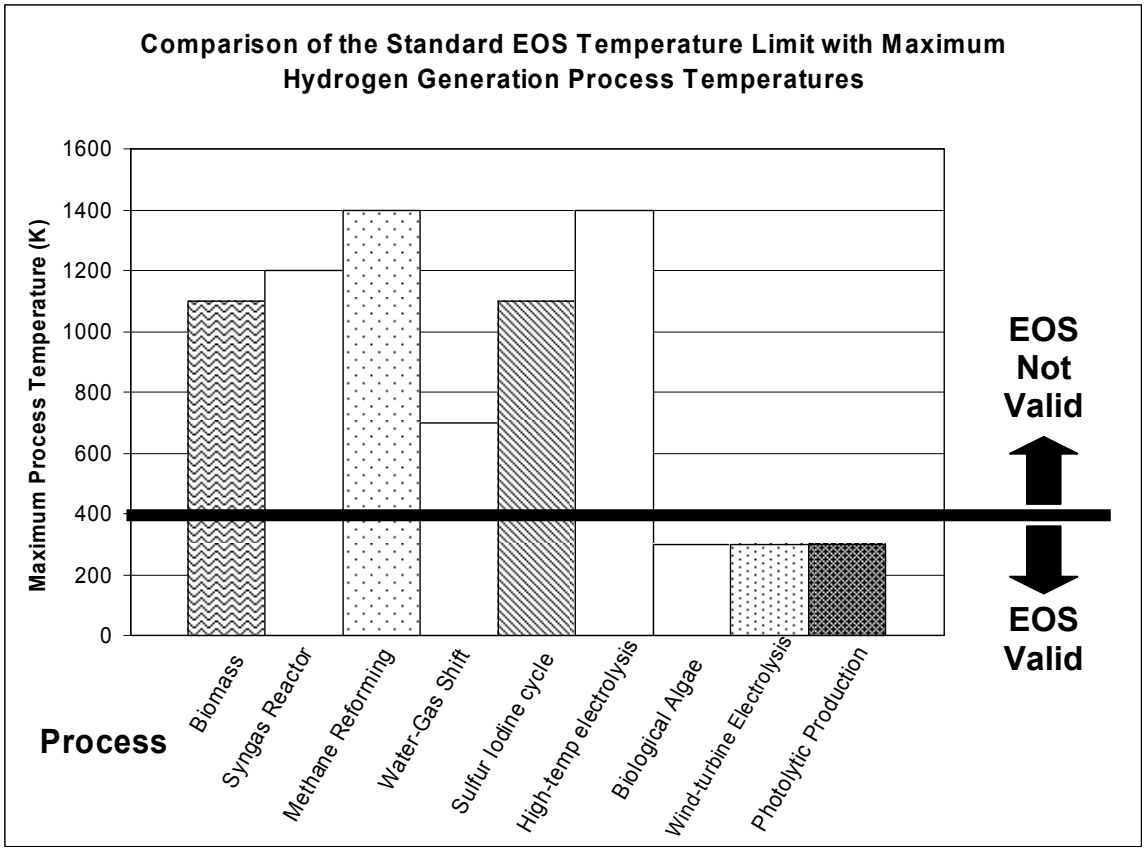

Figure 1.2 Comparison of the Standard EOS Temperature Limit with Maximum Hydrogen Generation Process Temperatures.

1.2 Hydrogen Storage

Focusing on transportation applications, once the hydrogen has been generated, the hydrogen may be stored for distribution to another location, or used immediately. The goal of any energy storage system is to safely provide the greatest energy with the least mass, in the smallest possible volume. The Department of Energy (DOE) mandates a storage capacity of 5-10 kg of usable hydrogen to power a vehicle for 300 miles [24]. There are primarily three methods for hydrogen storage:

- compressed gas
- cryogenic liquid
- adsorbed in a chemical or physical structure.

Compression of hydrogen gas is currently the simplest method for hydrogen storage and loses the smallest amount of the available energy. 7.5 kg of hydrogen at 298 K and 0.1 MPa pressure occupy just over 90 cubic meters in volume. To reduce the volume occupied by a storage tank, composite tanks have been constructed for hydrogen that contain gas at pressures up to 70 MPa [25]. At these pressures, a tank containing 7.5 kg of hydrogen at 298 K is 0.1864 cubic meters [4].

Storage of liquid hydrogen offers several advantages over storage of gaseous hydrogen. Liquid hydrogen storage has a higher energy density, and can operate at atmospheric pressures, allowing lightweight tanks to be used. However, the process to liquefy hydrogen is complex. Liquefying a gas normally involves throttling the gas through an expansion valve. Gases usually cool upon expansion; however hydrogen will not drop in temperature during expansion until it is cooled below its abnormally low Joule-Thompson inversion temperature of 200 K at 0.1 MPa [13]. Phenomena unique to gases like hydrogen can be responsible for the boil-off of significant amounts of the liquid. This is discussed in Section 2.

Adsorbing hydrogen in a chemical or physical structure has the potential to offer higher energy densities than liquid hydrogen. Once the hydrogen is chemically adsorbed on a structure, a chemical reaction is required to release the hydrogen to be used. Significant breakthroughs will be required to make this technology affordable and reusable. However, due to the potential for high gravimetric densities, hydrogen storage by adsorption is being researched extensively. The gravimetric density of hydrogen is defined as the hydrogen mass divided by the total mass of a storage system expressed as a percentage. Ideally, a large mass of hydrogen could be contained in a light-weight storage system. The preferred storage systems are those with a high percentage of hydrogen by mass and a high mass of hydrogen to volume ratio.

1.3 Hydrogen as a Commodity and the Standard Equation of State

Once hydrogen has been generated, the hydrogen must be metered for distribution and sale. Measurement of the quantity of hydrogen as a commodity can be more challenging than for a quantity of gasoline. Hydrogen can be distributed as a gas, cryogenic liquid or a mixture of both and can be compressed to achieve a higher energy density. Unlike gasoline, a fixed volume of gas can possess varying numbers of molecules depending on compressibility. To determine the amount of commodity sold, the number of molecules (mass) of hydrogen is usually determined by calculating density based upon the measurable thermodynamic properties, pressure and temperature, using a standard equation of state (EOS).

The EOS is a semi-empirical equation that takes the ideal gas law and corrects it to model real behavior of particular fluids. Using compiled experimental data, accurate data points are selected and fitted using linear and nonlinear methods to create coefficients of terms in a functional representation. Generally a minimum number of terms in the equation is desired to reduce computation time. The EOS is checked for accuracy, and error estimates are made based on deviations from experimental measurements. The range and quantity of experimental measurements is the limiting factor in the range of an EOS although some judicious extrapolation is possible. The EOS created is generally programmed into a computer software package like REFPROP© from NIST [4]. This software can then be used to determine densities or other property values used in the calibration of flow meters or in engineering calculations.

The estimated accuracies of the state-of-the-art experimental measurements in the vapor and liquid phases are shown in Table 1.2. The estimated accuracies of the hydrogen EOS and current standard methane EOS are shown in Table 1.3. The hydrogen supercritical region is the vapor region above 35 K.

Table 1.2 Estimated Experimental Measurement Accuracies

Estimated Experimental Measurement Accuracies		
Property	State of the Art Accuracy	
	Vapor Phase	Liquid Phase
Density	±0.05 %	±0.02 %
Pressure	±0.02 %	±0.02 %
Temperature	± 0.001 K	± 0.001 K
Isochoric Heat Capacity	±0.5 %	±1 %
Isobaric Heat Capacity	±0.5 %	±1 %
Speed of Sound	±0.01 %	±0.03 %

Table 1.3 Estimated Uncertainty in the Normal Hydrogen and Methane EOS [4].

Property	Estimated Uncertainty in the Normal Hydrogen and Methane EOS			
	Liquid H_2	Vapor H_2	Supercritical H_2	Methane
Density	0.1 %	0.25 %	0.2 %	0.03-0.07 %
Heat Capacity	3 %	3 %	3 %	<1 %
Speed of Sound	2 %	1 %	1 %	0.03-0.3 %

In 2003, the annual worldwide hydrogen production was estimated to be 500 billion normal cubic meters [21]. This is approximately 41.9 billion kilograms of hydrogen per year. A deviation of 0.2 percent in mass calculated using properties from the standard EOS becomes an 83.8 million kilogram uncertainty each year.

Hydrogen is considered by many to be the fuel of the future for the transportation industry. To make a comparison the scenario of hydrogen replacing finished motor gasoline in the United States is applied. In 2005, the US annual finished motor gasoline usage per was 103.6 billion gallons [21]. 1 kg of hydrogen has the equivalent energy of 2.8 kg of gasoline, and with 1 gallon of gasoline having a mass of approximately 3 kg, 1 gallon of gasoline is roughly equivalent, from an energy standpoint, to 1 kg of hydrogen. For hydrogen to completely replace gasoline consumption in the US, 103.6 billion kg of hydrogen will be used every day. A 0.2 percent deviation in mass calculated using properties from the standard EOS becomes a 207 million kilogram uncertainty each year in the US

alone. The current average price for a kilogram of hydrogen in the US varies from $2.10 to $9.10 depending on location [26]. The average price of gasoline will be used for this comparison. At the 2006 average sale price of $2.62 per gallon of gasoline [27], if 1 gallon of gasoline is replaced by 1 kg of hydrogen at the same price, a $543 million dollar annual uncertainty in gross product sale occurs. This figure becomes approximately $1.5 million dollars per day. Due to the volatility of gasoline prices, this number will fluctuate considerably.

Accurate and precise custody transfer of hydrogen depends on the standard EOS used to calibrate the devices and processes involved in the custody exchange. In addition, the safety, efficiency, and longevity of engineered hydrogen storage vessels and generation processes require accurate thermodynamic and transport property values. To create a new hydrogen standard, the physical characteristics of hydrogen must be considered and will be discussed in Section 2.

2. The Hydrogen Molecule

The hydrogen atom is arguably one of the most studied structures in chemistry, with almost every textbook on fundamental chemistry including a chapter or section on the subject. While the simplicity of the atomic and molecular structure is appealing, the behavior of the allotropic modifications must be taken into account.

Two stable isotopes and one unstable isotope of atomic hydrogen exist: Protium (H), Deuterium (D), and Tritium (T) [Figure 2.1]. Protium is by far the most abundant isotope, outnumbering Deuterium almost 6400 to 1 [28]. Tritium is radioactive and has a half-life of 12.26 years and is created only in nuclear reactions or through exposure to cosmic rays.

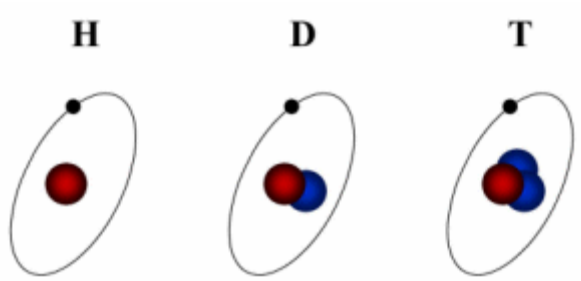

Figure 2.1 Protium, Deuterium, and Tritium atoms.

As a result Tritium makes up only 10^{-18} % of all hydrogen isotopes [28]. When shielded from ultraviolet radiation and subjected to the pressures in an environment like earth, two hydrogen atoms combine into one stable diatomic molecule. For this thesis, only the combination of two protium atoms will be considered in this thesis. Reference 15 contains a comprehensive review of hydrogen properties including deuterium, tritium, and their combinations.

2.1 Orthohydrogen and Parahydrogen

In 1929 Bonhoeffer and Harteck [29], about the same time as Eucken and Hiller [30], were able to observe changes in property values of samples of hydrogen held at low temperatures for quite some time. Since the samples were nearly isolated, the only possible cause for the change was a conversion of the molecules from one energy state to another energy state possessing different property values. This observation came as no surprise, as Heisenberg and Hund [31,32] had explained with quantum theory the existence of two different energy states for helium, orthohelium and parahelium, two years earlier and postulated a similar occurrence for hydrogen. Bonhoeffer and Harteck [29] chose the names orthohydrogen and parahydrogen for the different forms similar to the nomenclature chosen by Heisenberg [31] for the helium molecule [32]. Heisenberg chose 'ortho', meaning straight, right, and proper, from the Greek prefix (orthos) to represent the dominant concentration at room temperature and chose the prefix 'para', meaning abnormal, incorrect, to describe the form prevalent at low temperatures.

Today it is widely accepted that diatomic hydrogen has two modifications called orthohydrogen and parahydrogen, the differentiating feature of the two being the relative orientation of the nuclear spin of the individual atoms. The cause of the difference in spins is due to the parity in structure of the hydrogen molecule.

It is well established from particle physics that electrons and protons have a magnetic quantum number or spin of ½ and an anti-symmetric Schrödinger wave function. Fundamental particles having a spin of ½ are also said to be indistinguishable from another and are classified as Fermions. Fermions combine with other Fermions to yield molecules with *total* antisymmetric wave functions. To elucidate the indistinguishable nature of the particles, consider the two electrons on a hydrogen molecule. When the two electrons interact to form a new combination state, the two spins of ½ combine by quantum addition to yield 0 and 1. To calculate the binding energy of the molecule created by this

interaction, it is necessary to exchange the positions of the electrons. This does not mean that the actual electrons switch nuclei, but that both electrons can be near both nuclei at once through the probability of their wave functions. This quantum mechanical degree of freedom contributes approximately 60% of the binding energy of the molecule. If one of these electrons is excited to a higher orbital, the particles become distinguishable, the probability of their wave functions do not overlap, the binding energy from the electrons is lost and the particle may dissociate [15].

Extending the treatment to the protons provides further insight into the hydrogen molecule. Unlike the electron wave functions, the nuclei are positioned so far apart that their wave functions do not overlap. One proton is the only particle present in each of the two nuclei in a hydrogen molecule. Like electrons, protons are fermions and have a magnetic quantum number (nuclear spin) of ½. Applying quantum mechanical addition, when the spins are anti-symmetric they cancel each other and sum to 0, when they are summed symmetric they equal 1. When the sum of the overall nuclear spin wave function is 0 the nuclear state is antisymmetric. When the sum is 1, the overall nuclear spin is symmetric. The significance of this becomes apparent when the vibrational, rotational, and nuclear spin wave functions are combined into the total nuclear wave function for the molecule:

$$\psi_{tot} = \psi_{vib}\psi_{rot}\psi_{spin} \tag{2.1}$$

The vibrational contribution is always symmetric due to the linear-diatomic nature of the molecule and the lack of particle exchange between nuclei [15]. Combining the two possible states of the nuclear spin, the one possible state of the vibration contribution, and the requirement that the total nuclear wave function be antisymmetric, two possible cases arise:

$$(antisym) = (sym)(sym)(antisym), \tag{2.2}$$

$$(antisym) = (sym)(antisym)(sym) \tag{2.3}$$

An easy way to think about the total wave function of these being antisymmetric is in Equations 2.2, -1=(1)(1)(-1), and Equation 2.3, -1=(1)(-1)(1). But the question remains whether the symmetric rotational contribution or the antisymmetric rotational contribution has even rotational (ψ_{rot} =0,2,4,…) and the other odd (ψ_{rot} =1,3,5,…). Dennison [32] proved that only the symmetric rotational contribution can occupy the even levels as this was the only combination that could explain the experimental behavior observed in the heat capacities. The differences in heat capacity will be discussed further in Section 3.1. Thus, Equation 2.2 represents the even (ψ_{rot} =0,2,4,…) rotational energy levels associated with parahydrogen due to the antisymmetric (antisymmetric) nuclear spin, and Equation 2.3 represents the odd (ψ_{rot} =1,3,5,…) rotational energy levels associated with orthohydrogen due to the symmetric (symmetric) nuclear spin [Figure 2.2].

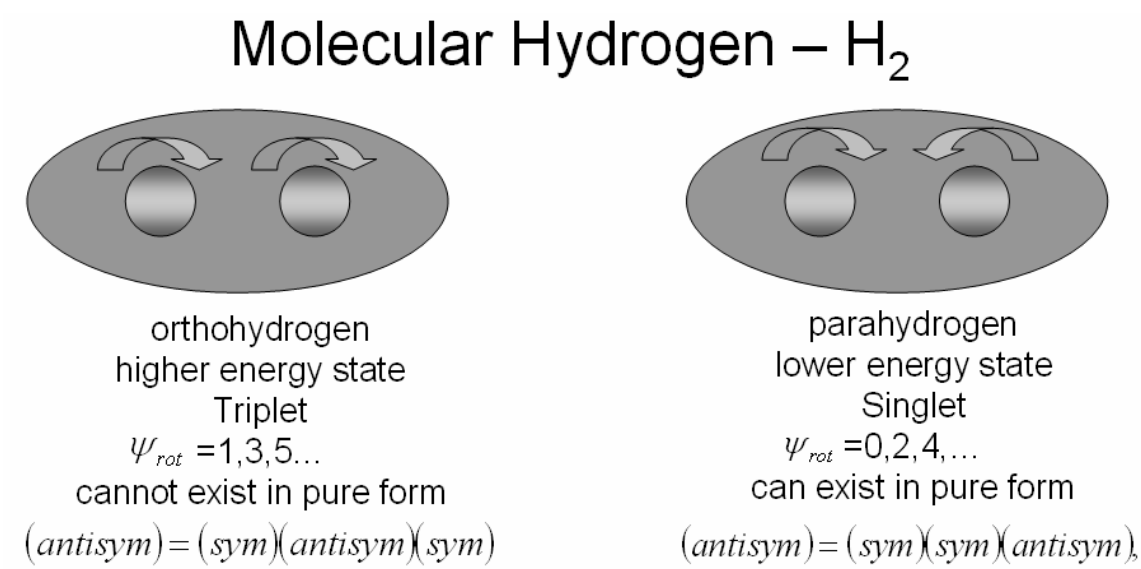

Figure 2.2 The Differences in Molecular Architecture between Orthohydrogen and Parahydrogen.

The three to one ratio in Figure 2.2 corresponds to the ratio of orthohydrogen to parahydrogen molecules. This ratio is due to the difference in nuclear spin. The antisymmetric nuclear spin wave function of parahydrogen has only one possible

sub state and is called a singlet. The symmetric nuclear spin wave function has a degeneracy of three and is called a triplet. Therefore, when the temperature is high enough to excite all of the sub-states, a 3:1 ratio of orthohydrogen to parahydrogen will exist. Before this temperature is attained, an equilibrium ratio of less than 3:1 will exist; this ratio of orthohydrogen to parahydrogen molecules at a given temperature is defined as equilibrium hydrogen. The ideal gas equilibrium ratio of orthohydrogen to parahydrogen at a given temperature is shown in Figure 2.3. Since parahydrogen has the lower energy level of the two, an equilibrium sample of hydrogen at 19 K is 99.75 % parahydrogen. At a temperature of 80 K the equilibrium concentration is approximately 50 % orthohydrogen and 50 % parahydrogen, while at room temperature the equilibrium mixture is 75 % orthohydrogen and 25 % parahydrogen which is defined as normal hydrogen [Figure 2.3]. Above room temperature, each of the four possible energy states will remain equally populated, maintaining the 3:1 distribution ratio, which is why orthohydrogen cannot naturally exist in a pure form.

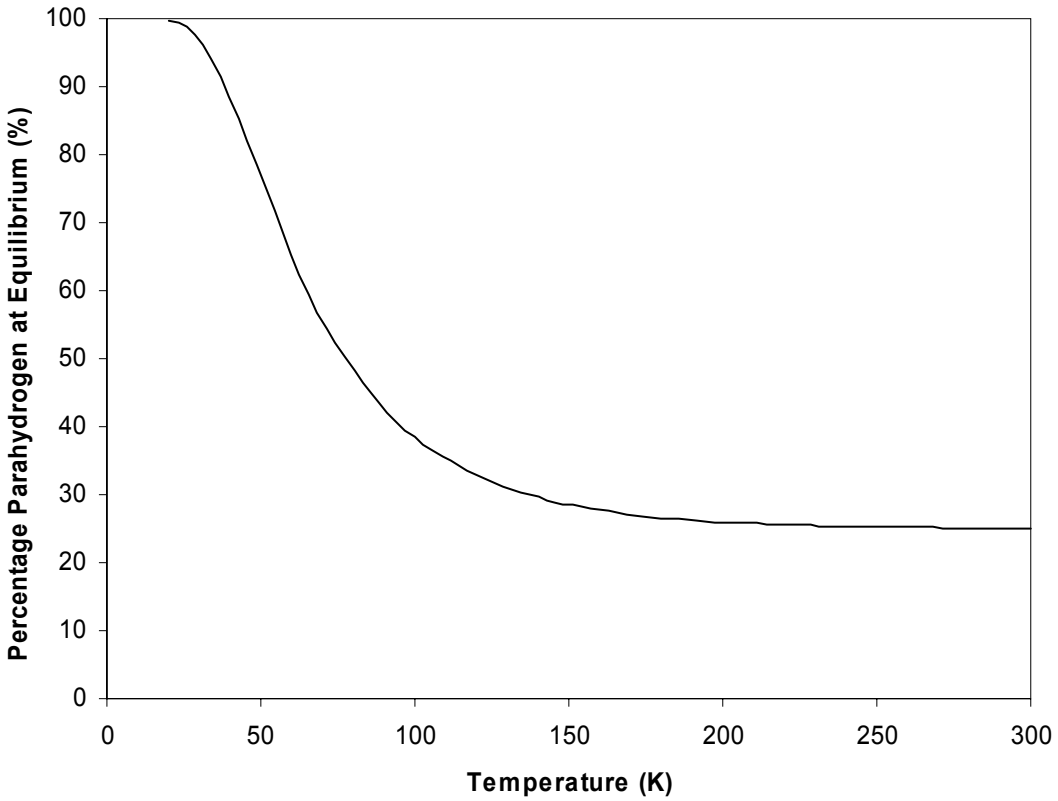

Figure 2.3 The Equilibrium Concentration of Parahydrogen.

Although orthohydrogen cannot exist naturally in a pure form, Sandler discovered that orthohydrogen is more strongly adsorbed on a solid than parahydrogen [33]. This preferential adsorption is due to the splitting of the rotational levels under the influence of the surface electric potential [33]. As a result, arbitrary concentrations of orthohydrogen and parahydrogen from nearly 0 to almost 100% orthohydrogen can be prepared. In addition to this artificial altering of the sample concentration, the concentration of an isolated sample at a fixed temperature can change over time.

2.2 Self-Induced Conversion Between Orthohydrogen and Parahydrogen

Since the equilibrium concentration of a sample is defined at an equilibrium temperature, one would expect that determining the concentration of a sample is as simple as taking the sample temperature. This is not the case, however. If the temperature of a sample is changed over time, the hydrogen molecules do not instantaneously change to the equilibrium sample concentration. The hydrogen molecules must interact with a magnetic field in a way to cause the spin reversal of one of the nuclei. They do not spontaneously change spin direction.

Due to the non-overlap of the nuclear spin wave functions, the overlap of the electron wave function is not enough to keep the nuclear spin vectors oriented in a fixed direction under all of the magnetic field gradients a molecule may encounter. As a result, if a magnetic field gradient is high across a hydrogen molecule, the gradient can create a torque on one of the nuclei and reverse one of the nuclear spin vectors.

Natural conversion of hydrogen in the gaseous form is a slow process [32]. Coincidently, the higher energy form of hydrogen, orthohydrogen, has a magnetic dipole and a non-spherical charge distribution due to the symmetric alignment of the nuclear spin of the nuclei. Parahydrogen does not have a magnetic dipole, however, owing to its spherical charge distribution and anti-symmetric nuclei spin alignment. The main mechanism of natural orthohydrogen/parahydrogen transformation is the magnetic dipole interaction of the nuclear moments of orthohydrogen molecules [34]. This method of conversion between the hydrogen molecules themselves is called self-induced conversion. The number of interactions between hydrogen molecules increases with density so the orthohydrogen-parahydrogen conversion occurs slowly in the gaseous state, becoming more rapid as density increases [34].

Whether the reaction goes from orthohydrogen to parahydrogen or vice versa depends on the direction the sample temperature is changing. If the sample is rising in temperature, the equilibrium concentration will become higher in orthohydrogen, and the molecules will convert from parahydrogen to orthohydrogen. If the sample is reducing in temperature, the equilibrium concentration will become higher in parahydrogen and the conversion will go from orthohydrogen to parahydrogen.

Due to the relative rarity in collisions between molecules that can cause a conversion, the self-induced conversion rate is slow allowing time for non-equilibrium sample concentrations to be measured over a wide range of temperatures. The rate of self-induced conversion has been measured by several authors [34] and varies between liquid and vapor phases.

When hydrogen is converted to a liquid, the significance of the orthohydrogen-parahydrogen concentration comes into play. If liquid normal hydrogen is stored in a vessel, the heat of conversion from one form to another (555 kJ/kg at the normal boiling point, 20.39 K [13]) is greater than the latent heat of vaporization (444.93 kJ/kg [4]). This energy will be released in the storage vessel, and the boil-off will be greater than that associated with the heat leak into the vessel. The conversion energy is enough to boil away over 60 % of the stored liquid over 1000 hours [13].

2.3 Catalyzed Conversion Between Orthohydrogen and Parahydrogen

The catalytic conversion of orthohydrogen to parahydrogen is typically used in engineering applications involving liquefaction [35]. Since the pioneering work of Wigner [36], a vast array of experimental and theoretical treatments has appeared in the literature. The most recent all-encompassing report appeared in 1992 by Ishii [33]. The highlights pertinent to this thesis are discussed. Further details are given by Ishii [33]. Three methods for increasing the rate of conversion catalytically exist: 1) Conversion through dissociation; 2) Magnetically

induced conversion; 3) Non-dissociative, non-magnetic conversion on noble metals at low temperatures.

The first method involves dissociating the molecules with a catalyst and then inducing them to recombine. Upon dissociation, the nuclei of the respective hydrogen atoms lose their relative nuclear spin orientation. Since the equilibrium concentration is temperature dependent, the hydrogen atoms will recombine at the equilibrium ratio for the given temperature [37]. This chemical process occurs in proton exchange membrane fuel cells. The second method involves using the inhomogeneous magnetic surface of a catalyst material to influence one of the nuclei of the molecule, causing a decoupling and spin reversal of the nuclei affected, similar to self-induced conversion [33]. The third and most recently discovered method occurs when hydrogen is brought in contact with noble metal catalysts at low temperatures [33].

2.4 Determination of the Orthohydrogen and Parahydrogen Concentration

Four names for fluid hydrogen have been discussed: equilibrium hydrogen, normal hydrogen, orthohydrogen and parahydrogen. Equilibrium hydrogen and normal hydrogen both are used to describe mixtures of orthohydrogen and parahydrogen.

The equilibrium orthohydrogen-parahydrogen concentration changes with temperature and subsequently the macroscopic properties of the sample change as well. The ratio of orthohydrogen to parahydrogen molecules must be known before properties of the mixture can be calculated. Several methods for determining the ratio exist:

1) Metering transmission of slow neutrons,
2) Nuclear resonance methods,
3) Velocity of sound measurements,
4) Heat capacity measurements,
5) Vapor pressure measurements,
6) Thermal conductivity measurements.

Metering of slow neutrons is used primarily in solid states. The nuclear resonance methods measure the perturbation of the nuclei and are employed over the entire working range of the fluid. Methods 3-6 are based solely on macroscopic thermophysical properties. Of these options, the latter is preferred due to size of sample required, simplicity of equipment, and speed with which the measurements can be taken [38,39,40].

The thermal conductivities of normal hydrogen and parahydrogen are shown in Figure 2.4 with the maximum difference between the forms existing around 145K. The transient hot wire approach to measuring thermal conductivity can be accomplished through holding the current of a wire immersed in a sample and the pressure of the sample constant. The equilibrium temperature of the wire, found by measuring its resistance, depends on the thermal conductivity of the

gas. To determine the orthohydrogen/parahydrogen ratio of the sample, the thermal conductivity does not need to be explicitly calculated. The measured wire resistance is compared to those of wires in known mixtures of orthohydrogen and parahydrogen as a calibration [32,39].

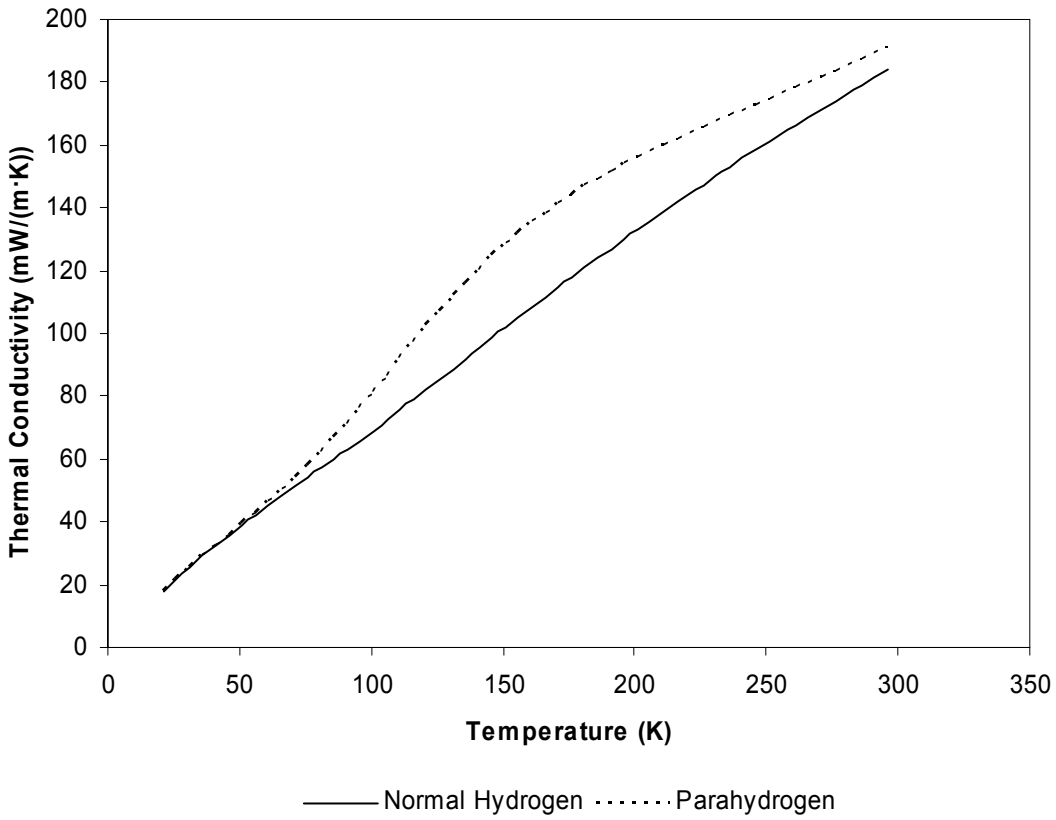

Figure 2.4 Thermal Conductivity of Normal Hydrogen and Parahydrogen.

The differences in these and other thermophysical properties between orthohydrogen and parahydrogen are discussed further in Section 3.

3. The Thermophysical Properties of Hydrogen

Since it is possible to create and verify the concentration of samples of nearly pure parahydrogen, normal hydrogen and equilibrium hydrogen, experimental measurements have been conducted to determine properties such as pressure, compressibility, temperature, speed of sound, specific heat, viscosity, and thermal conductivity of the mixtures. In addition, some of the properties of the critical point and triple point of the fluid surface have been measured. For nearly all of the properties, differences have been detected between the orthohydrogen and parahydrogen forms.

NBS Report 8812 [9] summarizes the property differences of orthohydrogen and parahydrogen. As will be pointed out in later sections, two primary areas see significant differences in orthohydrogen and parahydrogen property values: 1) ideal gas values associated with caloric properties, 2) values near and including the critical region.

3.1 Ideal Thermodynamic Property Behavior of Hydrogen

For the ideal gas properties of the forms of hydrogen, larger differences occur in caloric properties. The specific heats of the orthohydrogen and parahydrogen forms can be theoretically calculated through consideration of the vibrational, translational, rotational, electronic, and nuclear contributions of the molecules. At temperatures below 300 K the vibrational and electronic contributions are small and the rotational term becomes dominant. A statistical treatment for the rotational heat capacities below 300 K exists in the literature and can be found in the work of Farkas [32].

Orthohydrogen and parahydrogen have considerably different rotational energies at these temperatures with a maximum difference occurring at around 145 K. These differences become evident in the values of ideal gas specific heats as shown in Figure 3.1. Properties like constant volume specific heat, constant pressure specific heat, thermal conductivity and properties derived from specific

heats like enthalpy and entropy show significant differences between the different forms.

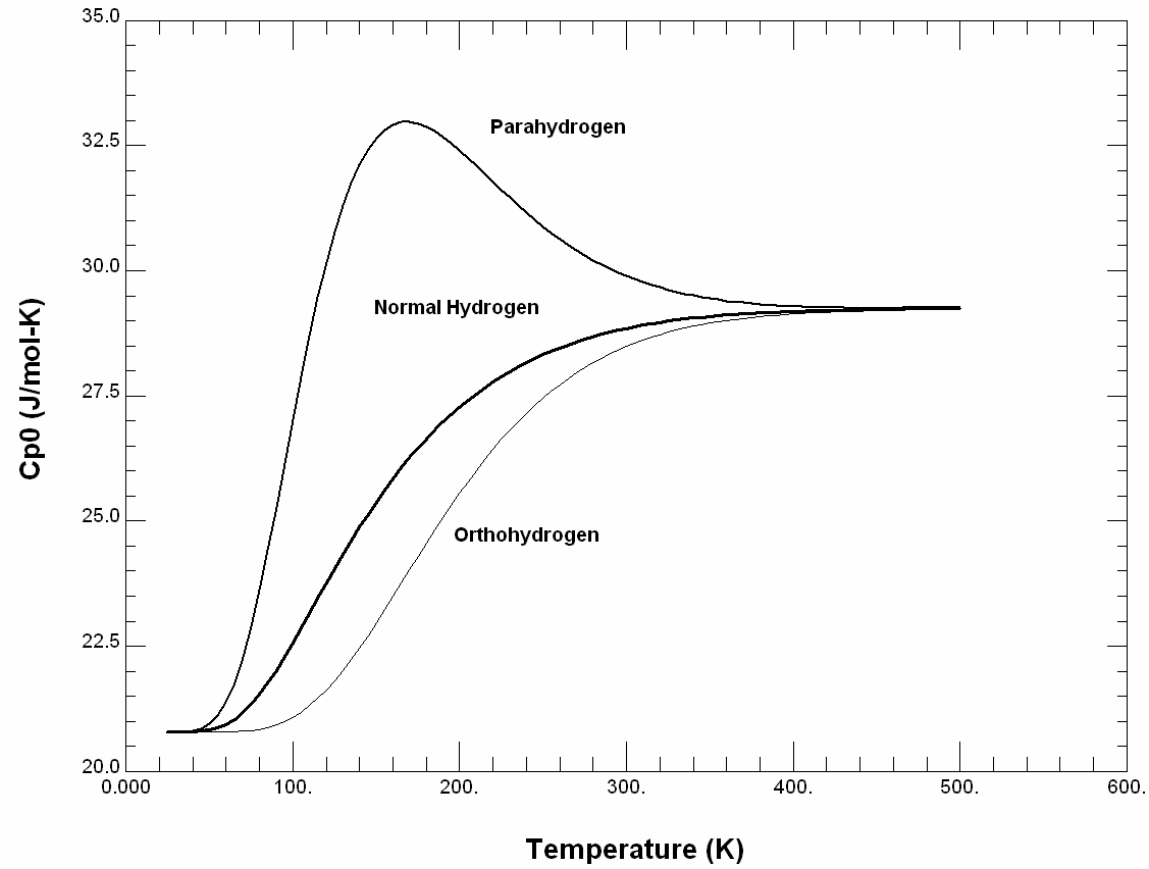

Figure 3.1 Calculated Ideal Gas Heat Capacities of Parahydrogen, Normal Hydrogen, Orthohydrogen.

3.2 Near Critical Region Property Behavior

In addition to differences in ideal properties related to specific heat, differences in the near critical region properties have been observed between orthohydrogen and parahydrogen. Since the critical region properties of pure orthohydrogen have never been measured, the difference is based on a sample of normal hydrogen compared to a sample of parahydrogen. The critical point and triple point properties used in the current standard equations of state for normal hydrogen and parahydrogen are given in Table 3.1.

Table 3.1 Critical Point and Triple Point Properties for Normal Hydrogen and Parahydrogen [4].

	T (K)	P (MPa)	ρ (mol·L^{-1})
Parahydrogen Critical Point	32.938	1.28377	15.556
Parahydrogen Triple Point	13.8033	0.007042	38.215
Normal Hydrogen Critical Point	33.19	1.315	14.94
Normal Hydrogen Triple Point	13.952	0.0077	38.3

The vapor pressure curve experiences differences between normal hydrogen and parahydrogen similar to the differences in Table 3.1. The differences between the vapor pressure of normal hydrogen and parahydrogen are shown in Figure 3.2.

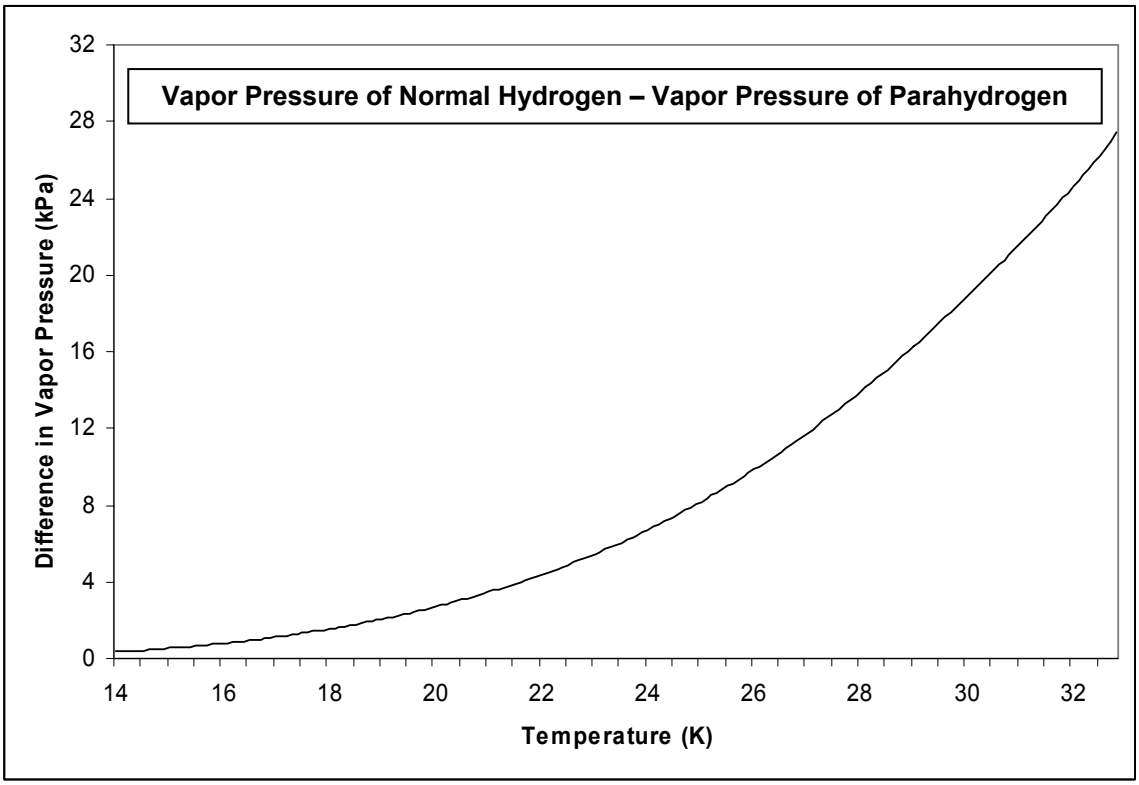

Figure 3.2 Calculated Vapor Pressure Differences between Liquid Normal Hydrogen and Parahydrogen.

The differences in vapor pressure cannot be explained based on molecular weight, because orthohydrogen and parahydrogen have identical molecular

weights. However, the differences can be explained through differences in intermolecular potential.

3.3 Quantum Law of Corresponding States

This section is the subject of a separate publication [41], and the details are given here for completeness. Due to the small differences in the parahydrogen and normal hydrogen real fluid surfaces, one would expect the traditional molecular theory of corresponding states to yield fairly accurate transformations between the hydrogen forms. This is not the case, however, because of the quantum characteristics of hydrogen. As early as 1937, Pitzer recognized that the primary contributor to deviations from the classical theory of corresponding states was quantum mechanical characteristics of the molecules being studied [42].

As the molecular weight is reduced, the deviation from classical molecular interactions increases owing to the increased effect quantum mechanics plays on intermolecular interactions. The classical theoretical approach to treating molecular interactions is the Lennard-Jones 6-12 potential:

$$U = 4\varepsilon\left[\left(\frac{\sigma}{r}\right)^{12} - \left(\frac{\sigma}{r}\right)^{6}\right], \tag{3.1}$$

where r is the intermolecular distance and epsilon (ε) and sigma (σ) are constants [15]. The constant epsilon is the maximum well depth in J/mol. The first term represents the hard-core repulsive force and the second term is the attractive force between molecules. In 1944 de Boer was the first to use the interaction parameters of the Lennard-Jones potential to create a useful quantum parameter for comparison with traditional molecules [43].

$$\Lambda^{*} = \frac{N\hbar}{\sigma(M\varepsilon)^{1/2}} \tag{3.2}$$

In this equation, N is Avogadro's number, h is Plank's constant, and M the molecular weight. The quantum parameter gives an indication of the effect of

quantum behavior on a molecular interaction. Table 3.2 lists the quantum parameters for several quantum fluids.

Table 3.2 Values of the Quantum Parameter for Several Fluids [44].

Fluid	Quantum Parameter
Xenon	0.064
Krypton	0.10
Argon	0.19
Neon	0.58
Tritium	1.0-1.1
Deuterium	1.22
Hydrogen	1.73
Helium-3	3.08

In Table 3.2 there is a row labeled “Hydrogen” that is not specified as orthohydrogen or parahydrogen. Since the quantum parameter is based on the intermolecular potential, a difference in quantum parameters for orthohydrogen and parahydrogen cannot exist unless a difference in intermolecular potentials exists. Most modern statistical thermodynamics texts do not specify the difference in statistical parameters between orthohydrogen and parahydrogen because the differences are small.

The differences in vapor pressure discussed in Section 3.2 cannot be reproduced without making a distinction between the statistical parameters for orthohydrogen and parahydrogen. Knaap and Beenakker [45] used the differences in polarizability of orthohydrogen and parahydrogen to deduce different intermolecular parameters. The difference in polarizability was based on differences in the internuclear separation distance between orthohydrogen nuclei in the ψ_{rot} =1 rotational state and parahydrogen nuclei in the ψ_{rot} =0 rotational state. From this they found that:

$$\frac{\varepsilon_o}{\varepsilon_p} = 1.006\,, \tag{3.3}$$

$$\frac{\sigma_o}{\sigma_p} = 1.0003\,, \tag{3.4}$$

where the subscript o and p denote orthohydrogen and parahydrogen respectively. The values for normal hydrogen can be determined by interpolation:

$$\frac{\varepsilon_n}{\varepsilon_p} = 1.0045 \,, \tag{3.5}$$

$$\frac{\sigma_n}{\sigma_p} = 1.00023 \,. \tag{3.6}$$

The parameters for the Lennard-Jones potential for normal hydrogen were determined from Hirschfelder *et al.* [44] to be 36.7 per kelvin (ε) and 2.959 angstroms (σ). With these new parameters for the intermolecular potential, it was then possible to differentiate between properties of orthohydrogen and parahydrogen with respect to the quantum parameter. By rewriting P, ρ, and T in terms of these new constants we obtain the dimensionless quantities [15]:

$$P^* = \frac{N\sigma^3 P}{\varepsilon} \,, \tag{3.7}$$

$$\rho^* = N\sigma^3 \rho \,, \tag{3.8}$$

$$T^* = \frac{RT}{\varepsilon} \,. \tag{3.9}$$

Plotting reduced thermodynamic properties versus the quantum parameter, a functional relationship between the quantum parameter and temperature, pressure, or density for light fluids can be determined. Figure 3.3 shows the reduced critical temperature, triple point temperature, temperature half way between the critical and triple point, and temperature at a pressure half way between the critical and triple point for fluids Neon, Deuterium, Normal Hydrogen, Parahydrogen, and Helium-4. Figures 3.4 and 3.5 display reduced pressures and densities plotted against the quantum parameter respectively.

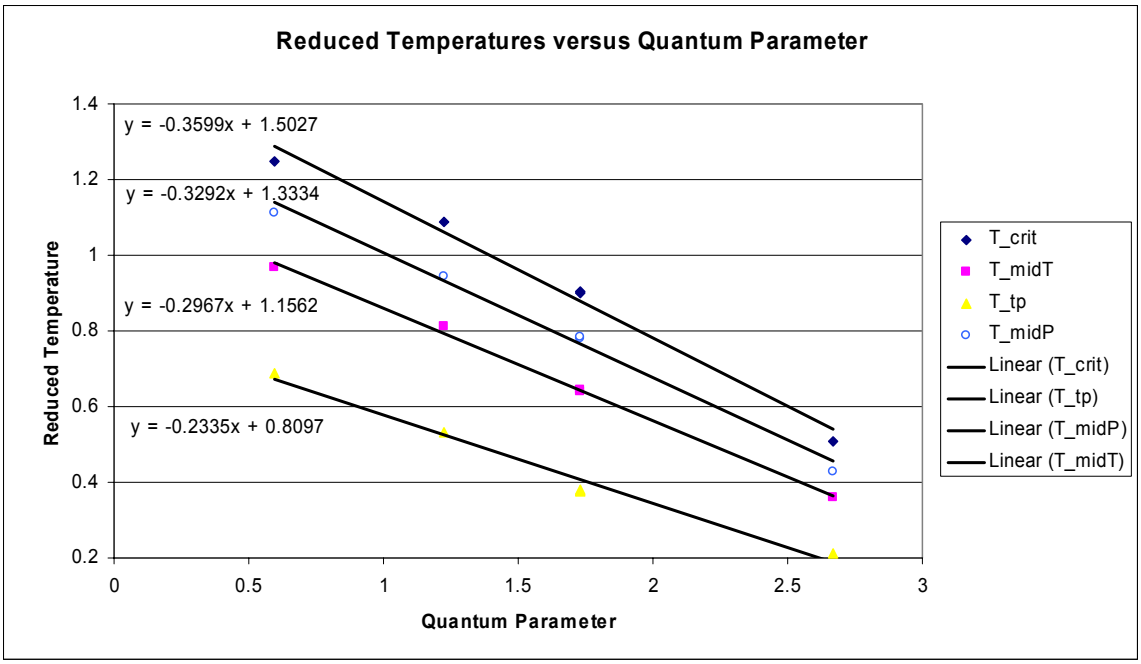

Figure 3.3 Reduced Temperatures plotted versus Quantum Parameter.

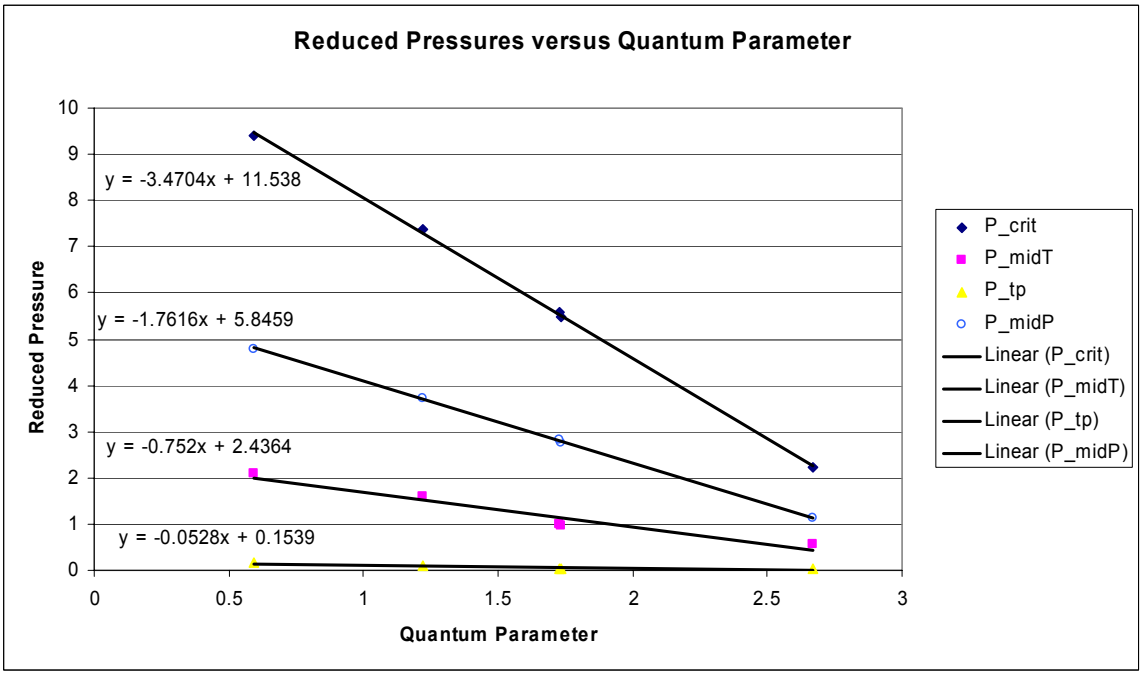

Figure 3.4 Reduced Pressures plotted versus Quantum Parameter

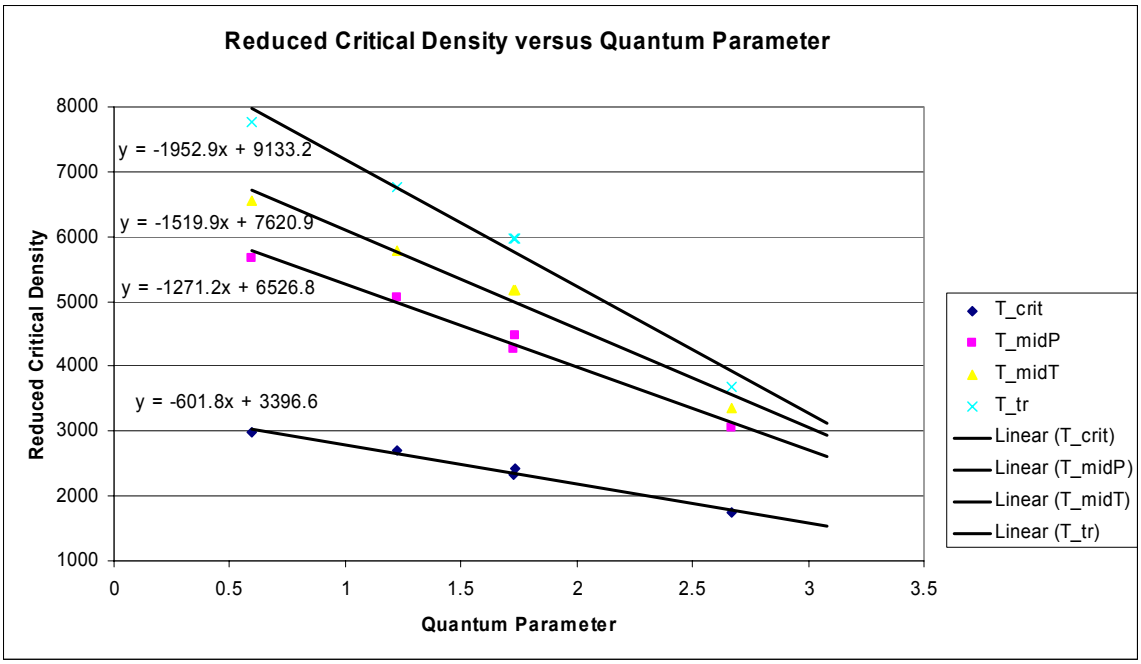

Figure 3.5 Reduced Densities plotted versus Quantum Parameter.

Van Dael *et al.* [46] used a corresponding states approach assuming a constant slope of the critical temperature versus change in quantum parameter to explain the change in critical temperatures between normal hydrogen and parahydrogen. Their equation for the reduced critical temperature of parahydrogen was:

$$T^*_{c,p} = T^*_{c,n} + \left(\Lambda^*_p - \Lambda^*_n\right)\frac{\Delta T^*_c}{\Delta\Lambda^*}\,. \tag{3.10}$$

A similar equation using pressures or densities could also be employed. It can also be noticed from Figures 3.3 and 3.4 that the slope of a line passing through constant ratio values in between the critical and triple points can be adjusted simply by taking:

$$\frac{\Delta T^*}{\Delta\Lambda^*} = \left(\frac{T - T_t}{T_c - T_t}\right)\left(\frac{\Delta T^*_c}{\Delta\Lambda^*} - \frac{\Delta T^*_t}{\Delta\Lambda^*}\right) + \frac{\Delta T^*_t}{\Delta\Lambda^*}\,, \tag{3.11}$$

$$\frac{\Delta P^*}{\Delta\Lambda^*} = \left(\frac{P - P_t}{P_c - P_t}\right)\left(\frac{\Delta P^*_c}{\Delta\Lambda^*} - \frac{\Delta P^*_t}{\Delta\Lambda^*}\right) + \frac{\Delta P^*_t}{\Delta\Lambda^*}\,, \tag{3.12}$$

thus enabling property calculation away from the critical point.

Additional properties can be found using combinations of reduced T, P, and ρ using dimensional analysis. For example, the reduced speed of sound can be described as [46]:

$$w^* = \frac{w}{\left(\frac{N\varepsilon}{M}\right)^{1/2}}. \tag{3.13}$$

However, if the data point includes a measured pressure and temperature, the pressure and temperature can be transformed while holding the third experimental value (e.g. density or speed of sound) constant. The theory was tested and shown to transform data from parahydrogen to normal hydrogen within the accuracy of the existing normal hydrogen experimental data. Comparisons of the transformed data to experimental data are shown in Section 7.2.

4. Experimental Data for the Thermodynamic Properties of Hydrogen

This section includes information on all published experimental data for the thermodynamic properties of parahydrogen and normal hydrogen. As mentioned in Section 1, some of the material in this Section has been updated from preliminary publications [5,6,7]. Portions of these previous works are repeated here for clarity. For reasons explained earlier, there are no direct experimental measurements of properties of orthohydrogen. The data are presented in a summary form in Tables 4.1, and 4.2, and are illustrated graphically in Figures 4.1 through 4.8. The Absolute Average Deviation (AAD) for each data set is calculated through comparison with the current standard formulations and are determined by:

$$AAD = \frac{1}{n}\sum_{i=1}^{n}\left|\%\Delta X_i\right|, \tag{4.1}$$

$$\%\Delta X = 100\left(\frac{X_{data} - X_{calc}}{X_{data}}\right). \tag{4.2}$$

For the formulation of an EOS, precise and accurate data over a wide range of values are needed. The experimental method and apparatus must also be taken into account in the selection of accurate data points to be used in developing a model. The current standard formulations for the thermodynamic properties of normal hydrogen and parahydrogen are listed with bibliographic information in Section 5.

Table 4.1 Summary of Thermodynamic Property Data for Parahydrogen.

Author	Year	Number of Points	Temperature Range (K)	Pressure Range (MPa)	Absolute Average Deviation
P- ρ -T					
Goodwin *et al.* [47]	1963	1234	15-100	1.5-35.5	0.87
Goodwin *et al.* [48]	1961	17	17.0-33.0	sat	0.02
Hoge and Lassiter [49]	1951	46	32.9-33.3	1.3-1.4	4.41
Roder *et al.* [50]	1963	46	33.0-40.0	1.3-2.8	2.33
Isochoric Heat Capacity					
Younglove and Diller [51]	1962	162	19.9-90.4	1.1-63.26	1.24
Isobaric Heat Capacity					
Medvedev [52]	1971	319	20.9-50.3	0.2-3.04	4.56
Speed of Sound					
Younglove [53]	1965	251	14.5-100.0	sat-32.0	1.58
van Dael *et al.* [46]	1965	23	20.3-32.0	sat	4.25
van Itterbeek *et al.* [54]	1961	48	14.1-20.4	sat	2.88
van Itterbeek *et al.* [55]	1963	116	15.1-20.5	sat-23.5	1.52
Vapor Pressure					
Barber and Horsford [56]	1963	10	13.8-20.3	sat	0.20
Hoge and Arnold [57]	1951	45	15.8-32.9	sat	0.16
Keesom *et al.* [58]	1931	31	17.2-20.5	sat	1.12
Kemp and Kemp [59]	1978	3	13.8-20.3	sat	0.34
van Itterbeek *et al.* [60]	1964	42	20.6-32.3	sat	0.86
Weber *et al.* [61]	1962	32	20.3-32.7	sat	0.32
Saturation Heat Capacity					
Brouwer *et al.* [62]	1970	12	24.5-30.0	sat	0.73
Smith *et al.* [63]	1954	8	18.3-31.5	sat	1.04
Johnston *et al.* [64]	1950	16	12.7-19.0	sat	2.45
Younglove and Diller [65]	1962	32	14.8-31.5	sat	2.73
Second Virial Coefficient					
Goodwin *et al.* [66]	1964	58	15.0-423.2	--	0.78
Third Virial Coefficient					
Goodwin *et al.* [66]	1964	52	20.0-423.2	--	0.29

Table 4.2 Summary of Thermodynamic Property Data for Normal Hydrogen.[1]

Author	Year	Number of Points	Temperature Range (K)	Pressure Range (MPa)	Absolute Average Deviation
		P-ρ-T			
Amagat [67]	1893	73	273.2-320.4	0.1-304.0	0.44
Bartlett [68]	1927	8	273.2	5.1-101.3	0.37
Bartlett *et al.* [69]	1928	43	273.2-673.0	5.1-101.3	0.29
Bartlett *et al.* [70]	1930	54	203-293	2.6-102.7	0.38
David and Hamann [71]	1953	12	65-79	30.4-126.7	0.53
Holborn and Otto [72]	1925	30	65.25-223.1	2.0-10.0	0.17
Jaeschke and Humphreys [73]					
Gasunie	1990	68	273.2-353	0.2-26.3	0.04
Ruhrgas	1990	221	273.2-353	0.5-28.1	0.04
Johnston *et al.* [74]	1953	227	33-300	0.5-20.6	0.69
Liebenberg *et al.* [75][2]	1978	19	75.0-163.9	473.3-1871	--
Liebenberg *et al.* [76]	1977	1953	75-307	200-2000	4.78
Machado *et al.* [77]	1988	60	130-159	1.2-105.5	5.16
Michels and Goudeket [78]	1941	283	273-423	0.9-300.9	0.13
Michels *et al.* [79]	1959	482	98.2-423.2	0.7-299.2	0.11
Presnall [80]	1969	108	473.1-873.0	10.1-182.4	1.34
Scott [81]	1929	18	298	0.1-17.2	0.14
Townend and Bhatt [82]	1931	40	273-298	0.1-60.8	0.11
van Itterbeek *et al.* [83]	1966	161	21.2-40.7	0.3-16.1	1.25
Verschoyle [84]	1926	25	273-293	5.0-21.0	0.15
Wiebe and Gaddy [85]	1938	47	273-573	2.5-101.3	0.08
		Speed of Sound			
Gusewell *et al.* [86]	1970	7	25-31	0.1	6.37
Liebenberg *et al.* [75][2]	1978	19	75.0-163.9	473.3-1871	--
Liebenberg *et al*. [76]	1977	1953	75-307	200-2000	12.33
Matsuishi *et al.* [87][2]	2003	42	293-526	1190-10840	--
van Dael *et al.* [46]	1965	175	22.2-33	0.2-24.8	1.82
van Itterbeek *et al.* [88]	1961	42	14.1-20.4	0.009-0.1	1.69
van Itterbeek *et al.* [89]	1963	110	15.1-20.5	0.02-23.5	6.37
		Vapor Pressure			
Aston *et al.* [90]	1935	4	18.0-20.7	sat	4.65
Barber [91]	1964	1	13.816	sat	3.02
Grilly [92]	1951	8	19.3-24.5	sat	3.53
Henning [93]	1926	25	14.0-20.5	sat	6.78
Henning and Otto [94]	1936	19	13.93-20.38	sat	13.11
Hiza [95]	1981	12	20.0-30.0	sat	2.40
Keesom *et al.* [96]	1931	31	17.2-20.5	sat	4.25
Scott [97]	1934	10	15.2-20.3	sat	2.86
Traver *et al.* [98]	1902	9	14.9-20.4	sat	3.53
van Itterbeek *et al.* [99]	1964	42	20.6-32.3	sat	3.54
White [100]	1950	17	20.9-33.1	sat	3.79
White [101]	1950	6	33.08-33.25	sat	3.33

Table 4.2 (cont). Summary of Thermodynamic Property Data for Normal Hydrogen.[1]

Author	Year	Number of Points	Temperature Range (K)	Pressure Range (MPa)	Absolute Average Deviation
Second Virial Coefficient					
Bartlett *et al.* [69]	1928	5	273.2-572.3		0.52
Beenakker *et al.* [102]	1959	1	20.4		10.02
Cottrell *et al.* [103]	1956	1	303.2		1.04
Dehaas [104]	1912	3	289.1-293.7		15.99
El Hadi *et al.* [105]	1969	7	19.3-26.3		1.48
Gibby *et al.* [106]	1929	7	298.2-448.2		0.48
Holborn and Otto [72]	1925	8	90.2-473.2		3.05
Holborn and Otto [107]	1926	9	65.3-473.2		11.12
Johnston *et al.* [74]	1953	18	35.1-300		0.20
Kerl [108]	1982	1	293.1		--
Knaap *et al.* [109]	1962	23	20.5-65.0		5.69
Long and Brown [110]	1937	7	20.9-46.5		1.83
Lopatinskii *et al.* [111]	1991	2	293.2		0.43
Michels and Goudeket [78]	1941	20	273.2-423.2		1.14
Michels *et al.* [79]	1959	17	98.2-423.2		0.77
Mihara *et al.* [112]	1977	3	298.2-348.2		0.57
Mueller *et al.* [113]	1961	6	73.2-323.2		8.85
Nijhoff and Keesom [114]	1927	8	24.84-373.15		1.54
Perez *et al.* [115]	1980	5	300-500		0.75
Schramm *et al.* [116]	1991	1	296.2		0.92
Scott [81]	1929	1	298.2		0.45
Townend and Bhatt [82]	1931	2	273.2-298.2		0.59
van Agt and Onnes [117]	1925	9	14.6-90.3		3.90
Varekamp and Beenakker [118]	1959	8	14.0-21.0		8.87
Verschoyle [84]	1926	2	273.2-293.2		0.44
Wiebe and Gaddy [85]	1938	6	273.2-573.2		0.39
Third Virial Coefficient					
Holborn and Otto [72]	1925	5	90.2-273.2		0.99
Johnston *et al.* [74]	1953	18	35.1-300.0		0.11
Michels and Goudeket [78]	1941	20	273.2-423.2		0.53
Michels *et al.* [79]	1959	17	98.2-423.2		0.14
Mihara *et al.* [112]	1977	3	298.2-348.2		0.12
Scott [81]	1929	1	298.2		0.20
Townend and Bhatt [82]	1931	2	273.2-298.2		0.12
Verschoyle [84]	1926	2	273.2-293.2		0.03

[1] Data reported prior to 1933 are assumed to be normal hydrogen; the orthohydrogen-parahydrogen ratio is uncertain.

[2] Some of the data in these data sets crossed the current phase boundary and have been omitted from comparisons.

4.1 Data Maps for Thermodynamic Properties of Parahydrogen.

Data maps give a graphical representation to the available experimental data over differing regions of the fluid surface.

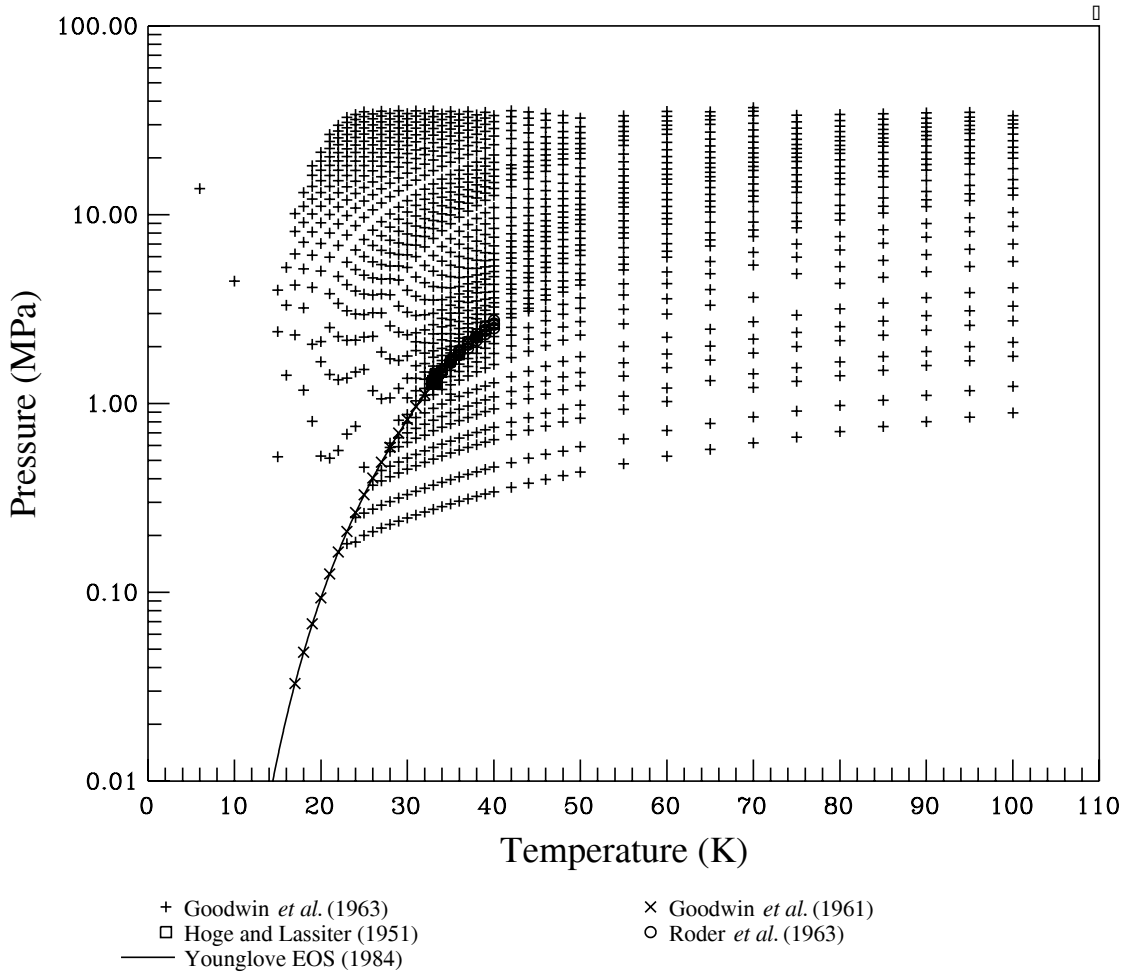

Figure 4.1 P-ρ-T Data for Parahydrogen (P-T coordinates).*

Figure 4.1 displays the available density data for parahydrogen. The Goodwin *et al.* [47] data from 1963 is the most wide ranging accurate density data available near the critical region of parahydrogen or normal hydrogen. Hoge and Lassiter [49] measured the critical density in 1951 and Roder *et al.* [50] superseded these measurements in 1963 on the same apparatus as the Goodwin data set [47]. All

* Consistent with internal CATS bibliographic format, references in graphs show years in parentheses. Numbers are given in Tables 4.1 and 4.2.

of the parahydrogen density measurements were taken at the National Bureau of Standards (now NIST).

Figure 4.2 displays the same data as Figure 4.1 but in P- ρ coordinates. The Goodwin *et al.* [48] data of 1961 are along the saturated liquid line and are the lowest temperature parahydrogen density data available. The saturation curve in this and other figures was calculated using the current standard EOS in REFPROP [4].

Figure 4.3 displays the only set of isochoric heat capacity data available for parahydrogen. Luckily the data set is wide ranging and extends to over 90 K. The data were taken at NBS [51].

Figure 4.4 displays the available isobaric heat capacity data. The only available isobaric heat capacity data available for parahydrogen are those from Medvedev *et al.* [52]. Although the data set is wide ranging, the large absolute average deviation of the data set displayed in Table 4.1 is due to a large amount of scatter in the data that will make an empirical fit difficult.

Four different data sets for parahydrogen sound speed are displayed in Figure 4.5. The Younglove [53] set was taken on the same apparatus as the isochoric heat capacity data and is the most wide ranging set. The speed of sound over the entire saturation curve was determined by the groups of van Itterbeek *et al.* [54,55] and van Dael *et al.* [46].

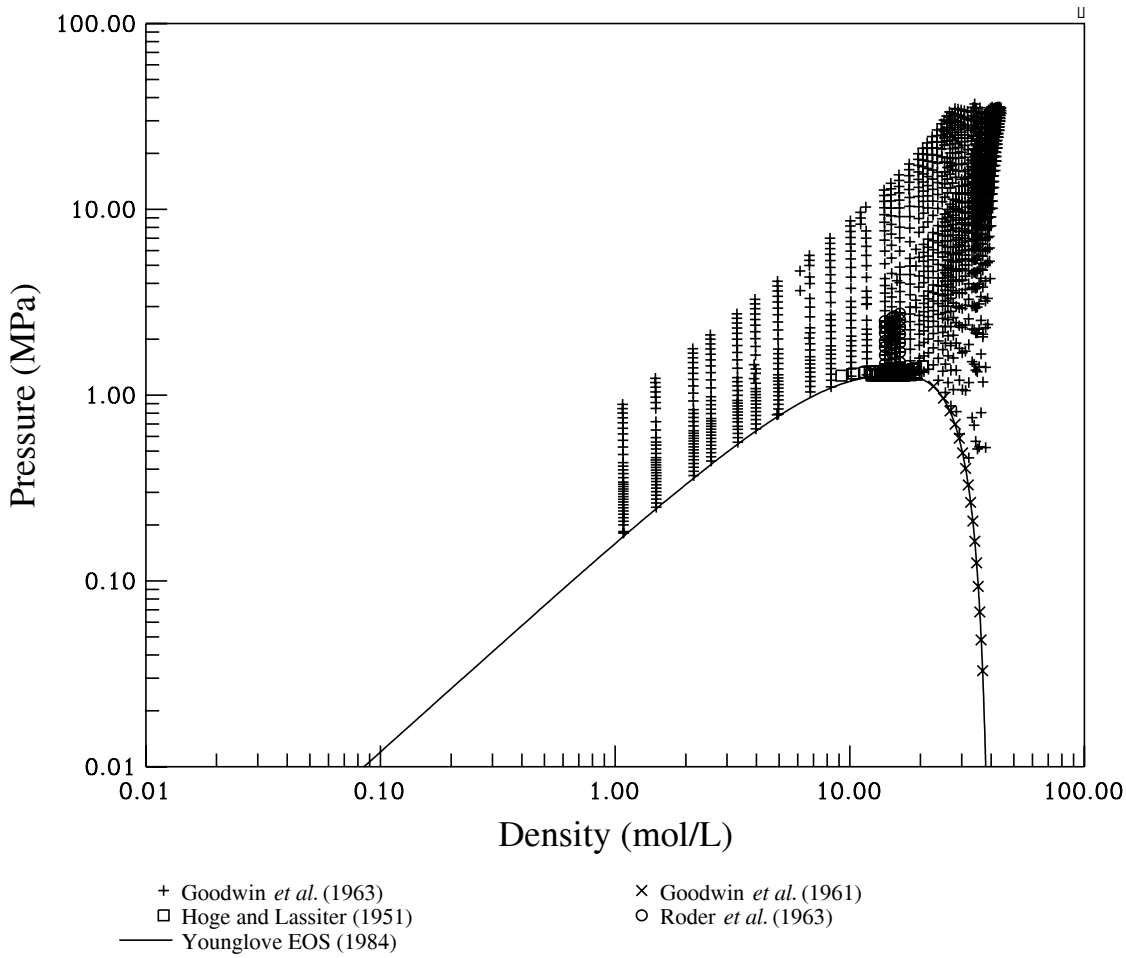

Figure 4.2 P-ρ-T Data for Parahydrogen (P- ρ coordinates).

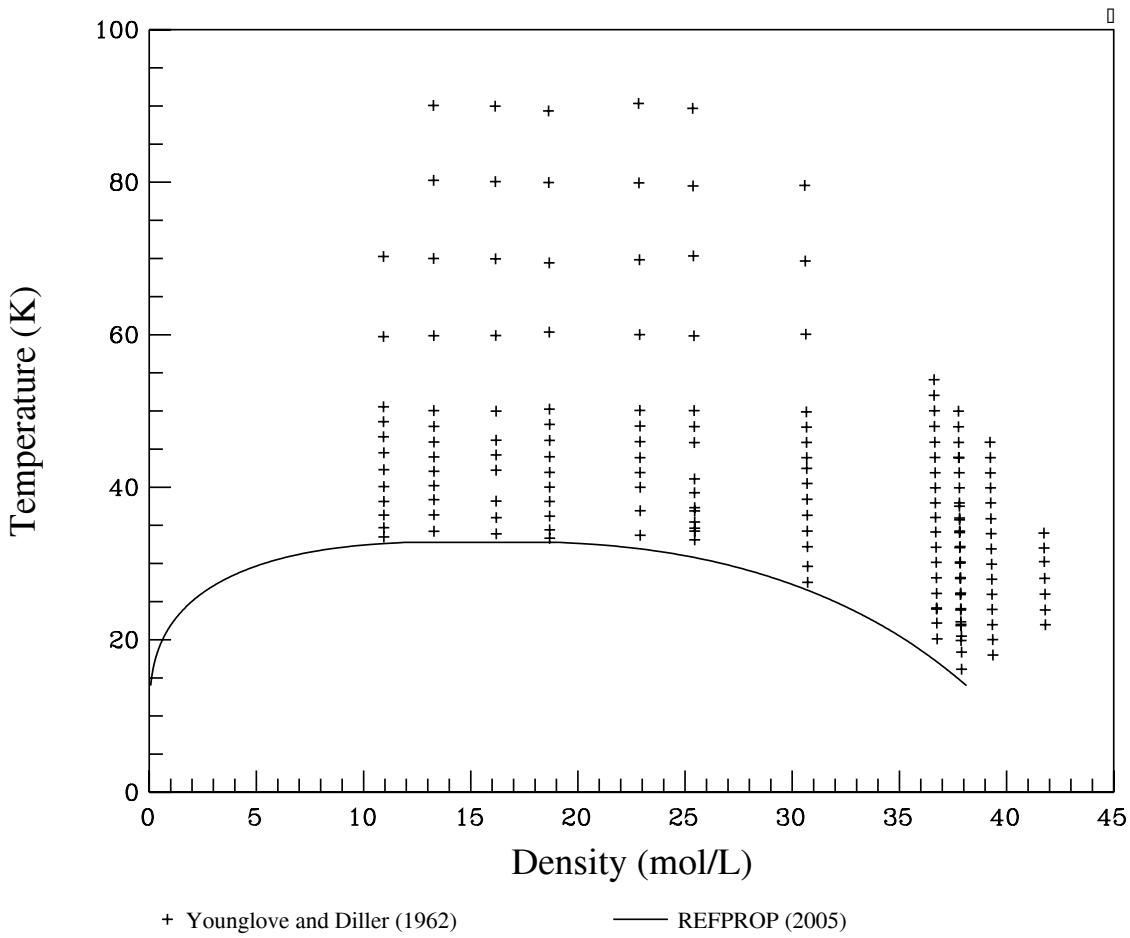

Figure 4.3 Isochoric Heat Capacity Data for Parahydrogen.

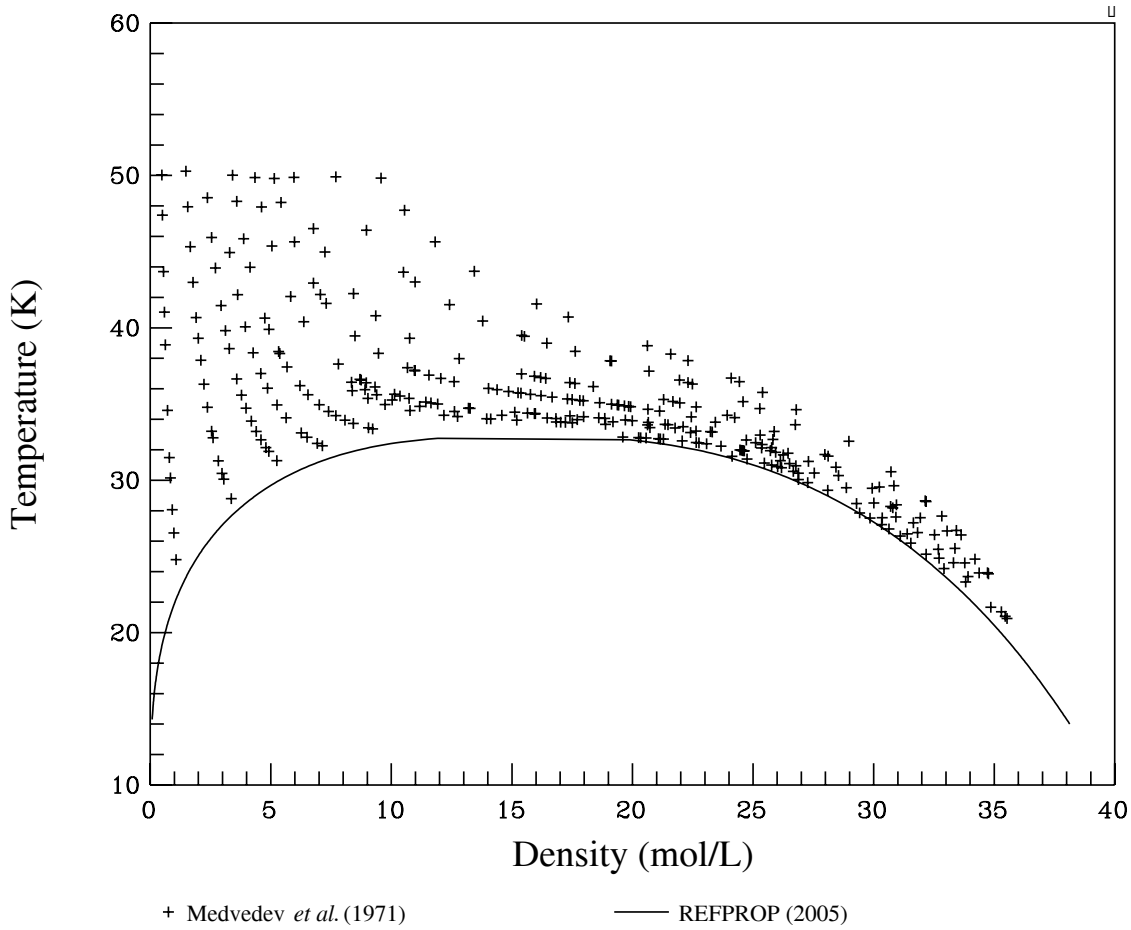

Figure 4.4 Isobaric Heat Capacity Data for Parahydrogen.

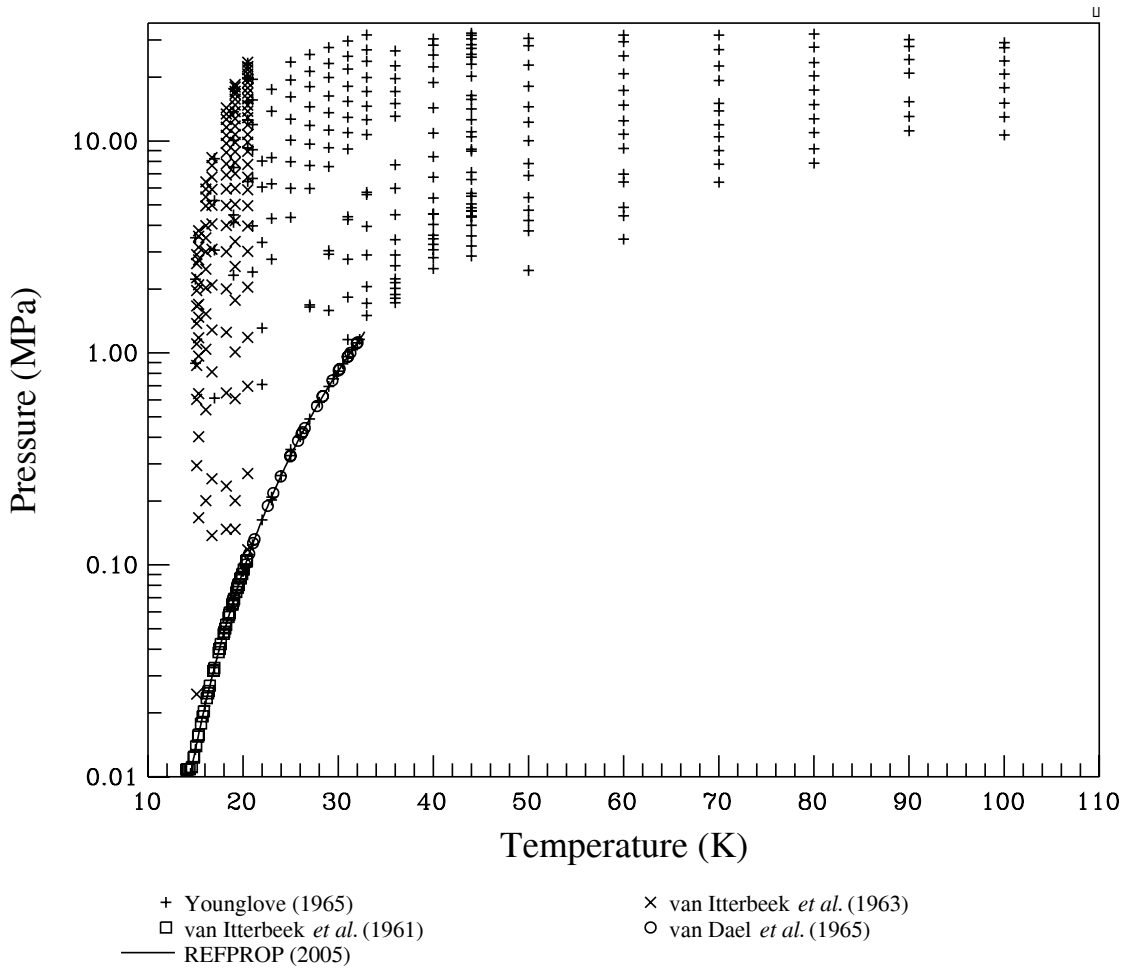

Figure 4.5 Speed of Sound Data for Parahydrogen.

4.2 Data Maps for Thermodynamic Properties of Normal Hydrogen.

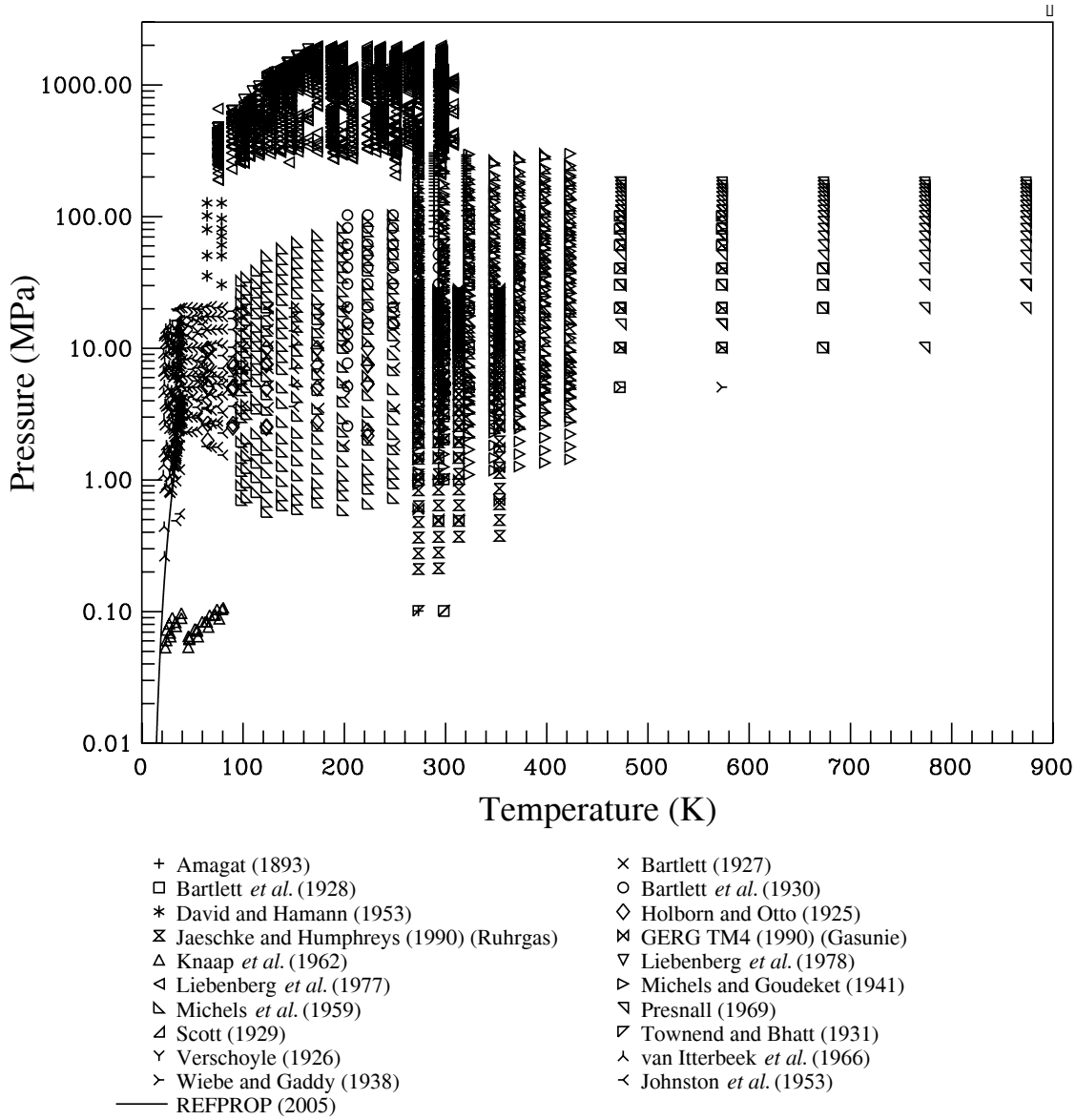

Figure 4.6 P-ρ-T data for Normal Hydrogen (P-T coordinates).

A large number of data sets exist for normal hydrogen in the vapor phase. The primary data set is that of Michels *et al.* [79]. Two sets of liquid phase and near critical region data exist for normal hydrogen and were taken by van Itterbeek *et al.* [83] and Johnston *et al.* [74].

The normal hydrogen speed of sound surface was measured extensively by the van Itterbeek group [46,88,89]. Gusewell *et al.* [86] also measured points along the saturated liquid line. The high pressure high temperature speed of sound data of Liebenberg *et al.* and Matsuishi *et al.* [75,76,87] are not displayed here. Although extensive data sets in the liquid phase exist, no speed of sound data exist in the vapor phase excluding these.

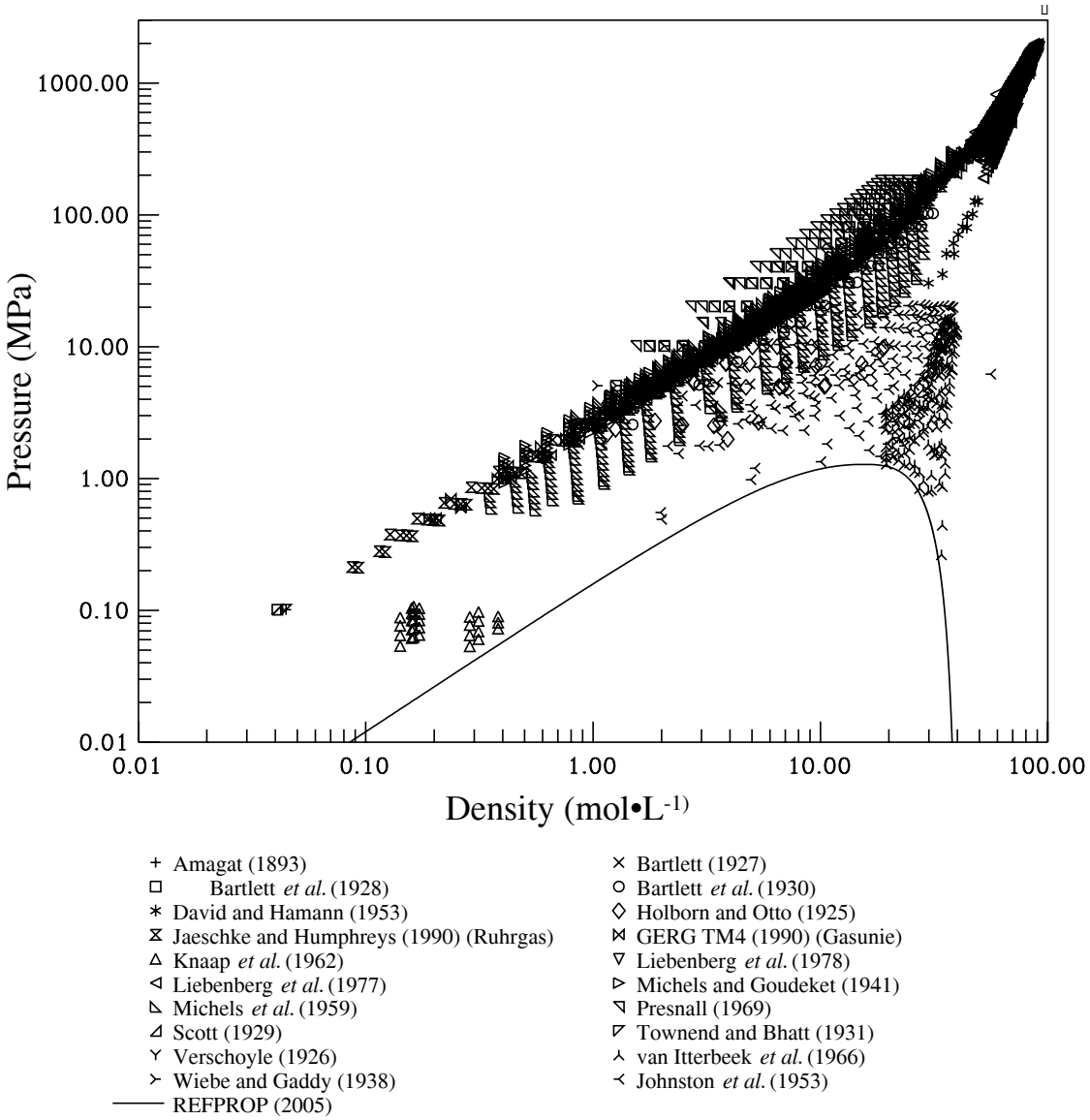

Figure 4.7 P-ρ-T Data for Normal Hydrogen (P-ρ coordinates).

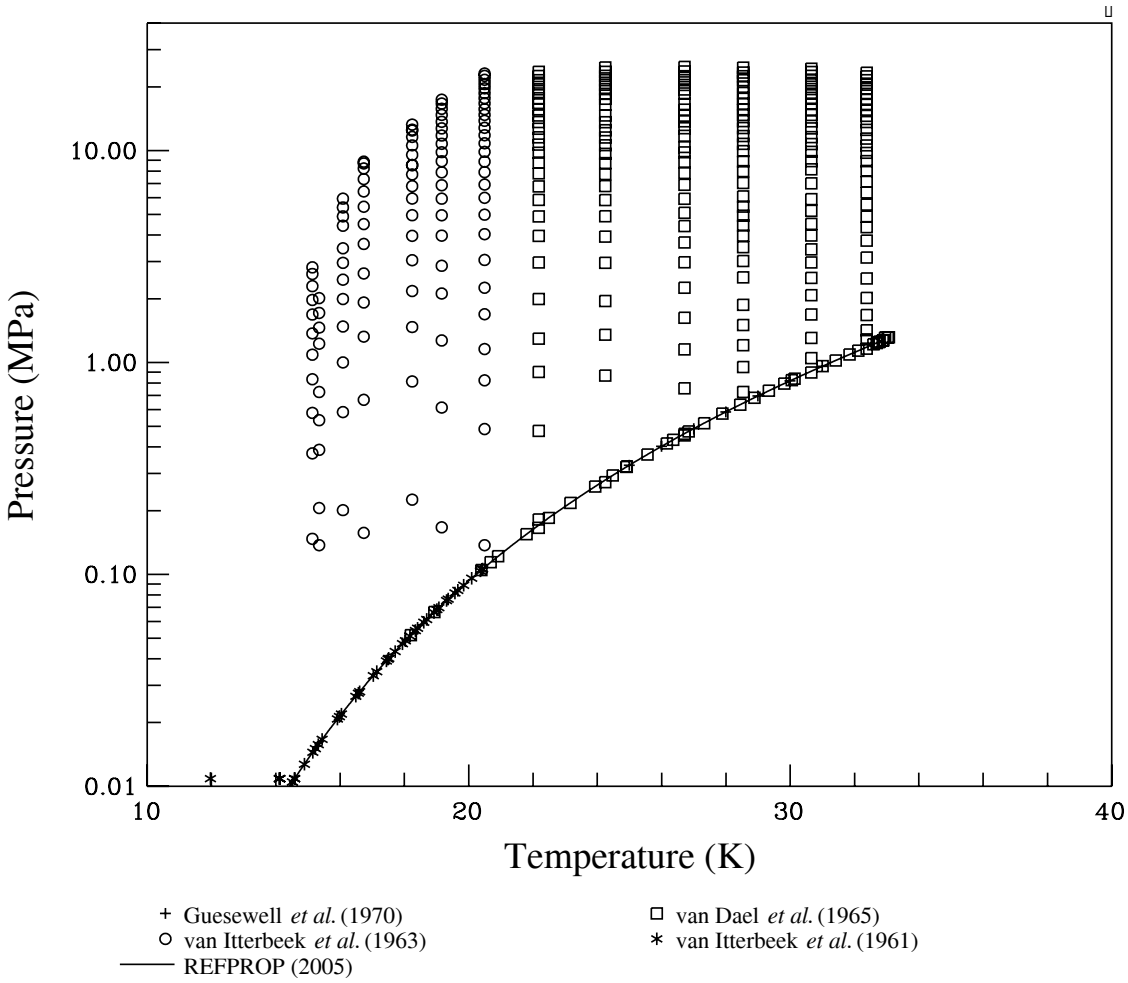

Figure 4.8 Speed of Sound Data for Normal Hydrogen.

5. Current Thermodynamic Property Formulations for Hydrogen

This section contains information about the currently accepted formulations for thermodynamic properties of parahydrogen and normal hydrogen. These formulations are those that are used in the current version of REFPROP [4]. Details of the data analysis and correlation methods used for these published formulations are not repeated here.

5.1 Current Standard Thermodynamic Property Formulation for Parahydrogen.

The standard equation of state for parahydrogen originally published in [14] is a 32 term modified Benedict-Webb-Rubin (MBWR) of the form

$$
\begin{aligned}
P = {} & \rho RT + \rho^2\left(G(1)T + G(2)T^{1/2} + G(3) + \frac{G(4)}{T} + \frac{G(5)}{T^2} \right) + \\
& \rho^3\left(G(6)T + G(7) + \frac{G(8)}{T} + \frac{G(9)}{T^2} \right) + \rho^4\left(G(10)T + G(11) + \frac{G(12)}{T} \right) + \\
& \rho^5\left(G(13)\right) + \rho^6\left(\frac{G(14)}{T} + \frac{G(15)}{T^2} \right) + \rho^7\left(\frac{G(16)}{T} \right) + \rho^8\left(\frac{G(17)}{T} + \frac{G(18)}{T^2} \right) + \\
& \rho^9\left(\frac{G(19)}{T^2} \right) + \rho^3\left(\frac{G(20)}{T^2} + \frac{G(21)}{T^3} \right)\exp\left(\gamma\rho^2\right) + \\
& \rho^5\left(\frac{G(22)}{T^2} + \frac{G(23)}{T^4} \right)\exp\left(\gamma\rho^2\right) + \rho^7\left(\frac{G(24)}{T^2} + \frac{G(25)}{T^3} \right)\exp\left(\gamma\rho^2\right) + \\
& \rho^9\left(\frac{G(26)}{T^2} + \frac{G(27)}{T^4} \right)\exp\left(\gamma\rho^2\right) + \rho^{11}\left(\frac{G(28)}{T^2} + \frac{G(29)}{T^3} \right)\exp\left(\gamma\rho^2\right) + \\
& \rho^{13}\left(\frac{G(30)}{T^2} + \frac{G(31)}{T^3} + \frac{G(32)}{T^4} \right)\exp\left(\gamma\rho^2\right)
\end{aligned}
\qquad . \qquad (5.1)
$$

In this equation, $G(x)$ is the coefficient corresponding to the term number in Table 5.1. The fixed point properties, and correlation limits are listed in Table 5.2.

Table 5.1 Coefficients for the Parahydrogen Equation of State.

Term Number	Nterm
1	0.00046755283934160
2	0.042892742514540
3	-0.51640855965040
4	2.9617902798010
5	-30.271949684120
6	0.000019081003203790
7	-0.0013397768592880
8	0.30564731154210
9	51.611971595320
10	0.00000019999815502240
11	0.00028963670593560
12	-0.022578039390410
13	-0.0000022873927618260
14	0.000024462614786450
15	-0.0017181816011190
16	-0.00000054651426034590
17	0.0000000040519414013150
18	0.0000011575951239610
19	-0.000000012691627283890
20	-49.830236055190
21	-160.66760920980
22	-0.1926799185310
23	9.3198946389280
24	-0.00032225965544340
25	0.0012068393076690
26	-0.0000003841588197470
27	-0.000040361574536080
28	-0.000000000125086812351 30
29	0.000000001976107321888 0
30	-0.000000000000241188347401 10
31	-0.000000000000412755149825 10
32	0.000000000008917972883610

Table 5.2 Fixed Point Properties and Correlation Limits for Parahydrogen.

Fixed Point Properties and Correlation Limits for Parahydrogen			
	Pressure (MPa)	Temperature (K)	Density (mol·L^{-1})
Critical point	1.28377	32.938	15.556
Triple point	0.007042	13.8	38.21
Upper limit	121	400	44
Lower limit	--	13.8	--

The ideal heat capacity equation used by the standard formulation was taken from [4] and is of the form

$$\frac{c_p^0}{R} = \sum_i n_i T^{t_i} + \sum_i v_i \left(\frac{u_i}{T}\right)^2 \frac{\exp(u_i/T)}{[\exp(u_i/T)-1]^2}. \tag{5.2}$$

The coefficients for the equation for parahydrogen are listed below in Table 5.3 [4].

Table 5.3 Coefficients for the Ideal Gas Heat Capacity equation for Parahydrogen.

n_i	t_i
2.49951690	0.0
-0.00111251850	1.0
0.000274914610	1.50
-0.0000100052690	2.0
0.00000000226954040	3.0
-0.000000000000210310290	4.0
v_i	u_i
12.3533880	598.0
-17.7776760	778.0
6.43091740	1101.0
7.33475210	6207.0

The vapor pressure ancillary equation used in REFPROP [4] for parahydrogen is of the form

$$\ln(p/p_c) = \frac{A(1-T_r) + B(1-T_r)^{1.5} + C(1-T_r)^{2.1} + D(1-T_r)^{2.8}}{T_r}, \tag{5.3}$$

where $T_r = T/T_c$, A=-4.9718, B=1.3191, C=-0.15747, and D=0.79468. In contradiction with the findings of Section 3, REFPROP does not have a separate ancillary vapor pressure equation for normal hydrogen.

The sublimation line given in REFPROP for parahydrogen is:

$$\ln(p/p_t) = A + B/T + C\ln(T), \tag{5.5}$$

where for parahydrogen: p_t=0.13332237 kPa, A=4.009857354, B=–90.77568949, and C=2.489830940.

5.2 Current Standard Thermodynamic Property Formulation for Normal Hydrogen.

It has been established that the normal hydrogen surface is very similar to the parahydrogen surface with the differences primarily in the ideal gas heat capacities and the near critical region and fluid properties. Due to the preliminary real fluid part of the equation of state for normal hydrogen being piecewise, the real fluid portion of the formulation was replaced in REFPROP [4] by the non-piecewise real fluid equation for parahydrogen. By changing the critical and triple point values with those for normal hydrogen and substituting in a new normal hydrogen ideal gas heat capacity equation, an approximate normal hydrogen surface was created. The only differences between the parahydrogen and the normal hydrogen formulations in REFPROP [4], are the critical and triple point values, the sublimation line, and the ideal gas heat capacity equation.

The fixed point properties, and correlation limits for the normal hydrogen formulation are listed in Table 5.4.

Table 5.4 Fixed Point Properties, Correlation Limits, and Fluid Constants for Normal Hydrogen.

Fixed Point Properties and Correlation Limits for Normal Hydrogen			
	Pressure (MPa)	Temperature (K)	Density ($mol \cdot L^{-1}$)
Critical point	1.315	33.19	14.94
Triple point	0.0077	13.957	38.3
Upper limit	121	400	38.148
Lower limit	--	13.957	--

Although the same functional form for the ideal gas heat capacity equation is used for normal hydrogen and parahydrogen (Eq. 5.2), for normal hydrogen the second term (the Einstein function) in the equation is zero. The coefficients for the ideal gas heat capacity equation for normal hydrogen are listed in Table 5.5.

Table 5.5 Coefficients for the Ideal Gas Heat Capacity Equation for Normal Hydrogen.

n_i	t_i
12155215000.0	-7.00
-3639676300.0	-6.00
433752650.0	-5.00
-23085817.0	-4.00
-3868.09270	-3.00
88240.1360	-2.00
-7858.70850	-1.00
724.802090	0.00
-184.268060	0.50
21.801550	1.00
-1.3051820	1.50
0.0210031750	2.00
0.00239116040	2.50
-0.000182405470	3.00
0.00000561495610	3.50
-0.000000073803310	4.00
0.00000000000663577550	5.00

The normal hydrogen sublimation line equation is of the form

$$\ln(p/p_t) = \frac{-8.065\left(1-T_r\right)^{0.93}}{T_r}, \tag{5.6}$$

where for normal hydrogen: T_r=T/13.957 K and p_t=7.7 kPa [4].

6. New Thermodynamic Property Formulations for Hydrogen

To meet the demands for accurate thermophysical property predictions over a wide range of temperatures and pressures for the present and future hydrogen economy, new equations of state for hydrogen are required. The formulations must correctly model differing property behavior between the hydrogen surfaces of state for the various forms of hydrogen, and must correctly model derivative properties such as speed of sound and heat capacity to ensure the best extrapolation behavior possible.

6.1 Theory and Design of Fundamental Equations of State

Modern thermodynamic property formulations allow for calculation of all thermodynamic properties using mathematical differentiation. Classical equations of state based on the virial equation of state are typically pressure explicit, like the current standard formulations for parahydrogen. This means that two properties, typically temperature and density, are the input independent variables for the equation which is used to calculate a dependent variable, pressure. The difficulty associated with this classical approach is that once the pressure value is calculated, complex integration may be required to determine the derivative property desired. For example, to calculate the enthalpy and entropy from a pressure explicit equation of state the relations below must be evaluated:

$$h(T,\rho) = h_{T_0}^0 + T\int_0^{\rho}\left[\left(\frac{P}{T\rho^2}\right) - \left(\frac{1}{\rho^2}\right)\left(\frac{\partial\rho}{\partial T}\right)_{\rho}\right]_T d\rho + \left(\frac{P-\rho RT}{\rho}\right) + \int_{T_0}^{T} c_p^0 dT\,, \qquad (6.1)$$

$$s(T,\rho) = s_{T_0}^0 + \int_{T_0}^{T}\left(\frac{c_p^0}{T}\right)dT - R\ln(RT\rho) + \int_0^{\rho}\left[\frac{R}{\rho} - \left(\frac{1}{\rho^2}\right)\left(\frac{\partial\rho}{\partial T}\right)_{\rho}\right]_T d\rho\,. \qquad (6.2)$$

To overcome this difficulty, modern thermodynamic formulations are explicit in a fundamental property like Helmholtz free energy. The fundamental properties,

internal energy, enthalpy, Gibbs free energy, and Helmholtz free energy, are integrals of other properties from a calculus point of view. In other words, with a fundamental property output from the formulation, any other thermodynamic property can be obtained through much simpler derivative calculations.

The Helmholtz free energy is obtained by:

$$\frac{a(T,\rho)}{RT} = \alpha(\tau,\delta). \tag{6.3}$$

Where τ and δ are the reciprocal reduced temperature and reduced density, respectively.

$$\tau = \frac{T_c}{T} \tag{6.4}$$

$$\delta = \frac{\rho}{\rho_c} \tag{6.5}$$

The subscript c denotes a critical point property. The actual Helmholtz free energy is composed of two parts, the ideal gas contribution and the residual contribution:

$$\alpha(\tau,\delta) = \alpha^0(\tau,\rho) + \alpha^r(\tau,\rho) \ . \tag{6.6}$$

The ideal gas contribution to the Helmholtz free energy is based on the ideal gas heat capacity given by Equation 5.2.

$$\alpha^0(\tau,\delta) = \ln\delta - \ln\tau + \sum a_k \tau^{i_k} + \sum a_k \ln[1-\exp(-b_k\tau)] \tag{6.7}$$

The subscript k in this case is the index of each term of the ideal gas heat capacity equation. The residual contribution to the Helmholtz free energy is from the actual equation of state.

$$\begin{aligned}\alpha^r(\tau,\delta) = &\sum_{i=1}^{l} N_i \delta^{d_i} \tau^{t_i} + \sum_{i=l+1}^{m} N_i \delta^{d_i} \tau^{t_i} \exp\left(-\delta^{p_i}\right) + \\ &\sum_{i=m+1}^{n} N_i \delta^{d_i} \tau^{t_i} \exp\left[+\varphi_i(\delta - D_i)^2 + \beta_i(\tau - \gamma_i)^2\right]\end{aligned}\ ^{*}, \tag{6.8}$$

where each summation typically contains 4-20 terms and the index i points to each individual term. The first summation of terms is a simple polynomial, with

* The sign on the coefficients φ_i, β_i, was changed to '+' to account for '-' values in Tables 6.2, 6.6, and 6.11 in copies of this manuscript after 2-14-08.

exponents d_i and t_i on the reduced density and temperature respectively. The second summation contains an exponential density term to aid in liquid phase property calculation. The third summation contains modified Gaussian terms that were originally introduced by Setzmann and Wagner [120]. The purpose of the Gaussian terms is to improve modeling of the critical region. The critical region has the most extreme changes and curvature of the entire surface, is the most difficult to measure experimentally, and is the most difficult to model. Although the values of N_i, d_i, t_i, p_i, φ_i, β_i, γ_i, and D_i are somewhat arbitrary, bounds on some of their values must be set to obtain correct equation behavior. The values of d_i, p_i, t_i, γ_i, and D_i are typically positive with those of d_i, and p_i being integer values. The values of φ_i, and β_i are typically negative.

The advantages of an equation explicit in Helmholtz free energy become apparent in the calculation of various properties. For example Equations 6.1 and 6.2 when using a "Helmholtz explicit" equation become:

$$h(T,\rho) = RT\tau\left[\left(\frac{\partial\alpha^0}{\partial\tau}\right)_\delta + \left(\frac{\partial\alpha^r}{\partial\tau}\right)_\delta\right] + \delta\left(\frac{\partial\alpha^r}{\partial\delta}\right)_\tau + 1, \tag{6.9}$$

$$s(T,\rho) = R\tau\left[\left(\frac{\partial\alpha^0}{\partial\tau}\right)_\delta + \left(\frac{\partial\alpha^r}{\partial\tau}\right)_\delta\right] - \alpha^0 - \alpha^r. \tag{6.10}$$

Helmholtz free energy is the fundamental property of choice due to the ability to map out the critical region. Other properties can be obtained using Equations 6.11-6.20 [119].

$$P(T,\rho) = \rho RT\left[1 + \left(\frac{\partial\alpha^r}{\partial\delta}\right)_\tau\right] \tag{6.11}$$

$$Z(T,\rho) = \frac{P}{\rho RT} = 1 + \left(\frac{\partial\alpha^r}{\partial\delta}\right)_\tau \tag{6.12}$$

$$u(T,\rho) = RT\tau\left[\left(\frac{\partial\alpha^0}{\partial\tau}\right)_\delta + \left(\frac{\partial\alpha^r}{\partial\tau}\right)_\delta\right] \tag{6.13}$$

$$g(T,\rho) = RT\left[1 + \alpha^0 + \alpha^r + \delta\left(\frac{\partial \alpha^r}{\partial \delta}\right)_\tau\right] \tag{6.14}$$

$$c_v(T,\rho) = -R\tau^2\left[\left(\frac{\partial^2 \alpha^0}{\partial \tau^2}\right)_\delta + \left(\frac{\partial^2 \alpha^r}{\partial \tau^2}\right)_\delta\right] \tag{6.15}$$

$$c_p(T,\rho) = c_v + R\frac{\left[1 + \delta\left(\frac{\partial \alpha^r}{\partial \delta}\right)_\tau - \delta\tau\left(\frac{\partial^2 \alpha^r}{\partial \delta \partial \tau}\right)\right]^2}{\left[1 + 2\delta\left(\frac{\partial \alpha^r}{\partial \delta}\right)_\tau + \delta^2\left(\frac{\partial^2 \alpha^r}{\partial \delta^2}\right)_\tau\right]} \tag{6.16}$$

$$w(T,\rho) = \sqrt{\frac{RT}{M}\left[\frac{1 + 2\delta\left(\frac{\partial \alpha^r}{\partial \delta}\right)_\tau + \delta^2\left(\frac{\partial^2 \alpha^r}{\partial \delta^2}\right)_\tau - \frac{\left[1 + \delta\left(\frac{\partial \alpha^r}{\partial \delta}\right)_\tau - \delta\tau\left(\frac{\partial^2 \alpha^r}{\partial \delta \partial \tau}\right)\right]^2}{\tau^2\left[\left(\frac{\partial^2 \alpha^0}{\partial \tau^2}\right)_\delta + \left(\frac{\partial^2 \alpha^r}{\partial \tau^2}\right)_\delta\right]}\right]} \tag{6.17}$$

$$\phi(T,\rho) = \exp\left[Z - 1 - \ln(Z) + \alpha^r\right] \tag{6.18}$$

$$B(T) = \lim_{\delta \to 0}\left[\frac{1}{\rho_c}\left(\frac{\partial \alpha^r}{\partial \delta}\right)\right] \tag{6.19}$$

$$C(T) = \lim_{\delta \to 0}\left[\frac{1}{\rho_c^2}\left(\frac{\partial^2 \alpha^r}{\partial \delta^2}\right)\right] \tag{6.20}$$

Although there are many different types of equations of state applicable to many different fluids, the primary goals of the formulations are the same:

1) Represent available experimental data to within the accuracy of the data;
2) Include a minimum number of terms to decrease computation time;
3) Represent the ranges of experimental data available from the triple point up to significant dissociation or the melting line;
4) Have fundamentally correct extrapolation behavior.

To achieve these goals, there are many different approaches. The methods employed for this thesis are discussed here.

After a survey of existing literature was completed and the available data had been compared to the existing formulations, primary data sets were selected for use in a regression based on a set of characteristics:

1) The date and laboratory of the experiment;
2) The reputation of the experimentalist taking the data;
3) The type of apparatus used to take the data;
4) The precision of the data set;
5) Comparison of the data set with data from other experimentalists in the same location on the surface of state.

The order of importance in this list is somewhat arbitrary and sometimes becomes a matter of instinct on the part of the person correlating the data based on iterative analysis of deviation plots. The number of individual data points from each data set selected to be used in the fit is kept to a minimum to increase the speed of convergence. The minimum number of points required depends on the number of points needed to obtain the correct behavior in a location of the surface. For example, the complex curvature of the surface near the critical region requires more data points to obtain correct behavior than nearly linear data like the speed of sound in the vapor or liquid phase.

Each of the terms is modified using a fitting algorithm that adjusts values based on sum of the squares of deviations between a set of experimental data for the fluid and values calculated from the model. In this work, a non-linear fitting algorithm based on the Levenberg-Marquardt method was used to optimize the terms. The algorithm minimizes the function:

$$S = \sum W_\rho F_\rho^2 + \sum W_P F_P^2 + \sum W_{c_v} F_{c_v}^2 + \ldots, \tag{6.21}$$

where W specifies the weight of a particular type of property and F specifies the deviation of the property. These deviation calculations are shown in Equations 6.22-6.24 and similar equations exist for other properties.

$$F_P = \frac{\left(P_{data} - P_{calc}\right)}{P_{data}} \tag{6.22}$$

$$F_{c_v} = \frac{\left(c_{v\,data} - c_{v\,calc}\right)}{c_{v\,data}} \tag{6.23}$$

$$F_\rho = \frac{\left(P_{data} - P_{calc}\right)}{\rho_{data}} \left(\frac{\partial \rho}{\partial P}\right)_T \tag{6.24}$$

The non-linear regression technique allows for the critical point properties to be determined as part of the optimization process and for limits in numerical values of the terms to improve the empirical behavior of the functional form via the selected data. As a result, the calculated critical point for the equation of state may not exactly match the experimental critical point of the actual fluid. There are some instances where the predicted critical state may be more accurate than the measured values, but no generalization of this behavior can be made.

6.2 New Thermodynamic Property Formulation for Parahydrogen

The parahydrogen equation was created first because parahydrogen had the most comprehensive data set with the most caloric properties near the critical region. From observations of deviations of calculated properties of the current standards it was determined that deviations in experimental density measurements between normal hydrogen and parahydrogen were smaller than the experimental uncertainty away from the critical region. These differences will be discussed in Section 7. To expand the range of the parahydrogen equation, the Michels *et al.* [79], Liebenberg *et al.* [76], and Presnal [80] normal hydrogen isothermal density data were used at temperatures over 90 K. Further selection of data for use in the regression will be discussed in Section 7.

The final equation of state has 9 polynomial terms and 5 Gaussian critical region terms as described by Equation 6.8. The polynomial parameters and coefficients are shown in Table 6.1, and the parameters of the Gaussian terms are shown in Table 6.2.

Table 6.1 Parameters and Coefficients of the New Parahydrogen Equation of State.

i	N_i	t_i	d_i	p_i
1	-7.33375	0.6855	1	0
2	0.01	1	4	0
3	2.60375	1	1	0
4	4.66279	0.489	1	0
5	0.682390	0.774	2	0
6	-1.47078	1.133	2	0
7	0.135801	1.386	3	0
8	-1.05327	1.619	1	1
9	0.328239	1.162	3	1
10	-0.0577833	3.96	2	--
11	0.0449743	5.276	1	--
12	0.0703464	0.99	3	--
13	-0.0401766	6.791	1	--
14	0.119510	3.19	1	--

Table 6.2 Parameters of the Gaussian Terms in the New Parahydrogen Equation of State.

i	φ_i	β_i	γ_i	D_i
10	-1.7437	-0.194	0.8048	1.5487
11	-0.5516	-0.2019	1.5248	0.1785
12	-0.0634	-0.0301	0.6648	1.28
13	-2.1341	-0.2383	0.6832	0.6319
14	-1.777	-0.3253	1.493	1.7104

The parahydrogen ideal gas heat capacity equation is of the same form as Equation 5.2 but was fitted to match the existing ideal heat capacity data. The parameters and coefficients are shown in Table 6.3.

Table 6.3 Parameters and Coefficients of the Parahydrogen Ideal Gas Heat Capacity Equation.

n_i	t_i
2.5	0.0
v_i	u_i
4.30256	499
13.0289	826.5
-47.7365	970.8
50.0013	1166.2
-18.6261	1341.4
0.993973	5395
0.536078	10185

The critical properties from the current standards [4] were used in the nonlinear regression. Since the critical point values were treated as adjustable parameters with this fitting technique, the critical point values calculated using the new formulation changed slightly from those of [4]. The Younglove EOS was published in 1984 [14], before the new ITS-90 temperature scale was adopted. In the ITS-90 scale, the triple point of parahydrogen is a fixed point. The triple point temperatures used in this work are consistent with ITS-90. The critical and triple point values used in the new parahydrogen EOS are shown in Table 6.4.

Table 6.4 Critical and Triple Point Properties used by the New Parahydrogen EOS.

	Temperature (K)	Pressure (MPa)	Density ($mol \cdot L^{-1}$)
Critical Point	32.938	1.2858	15.538
Triple Point	13.8033	0.007041	38.185

The critical density is difficult to reproduce because of the small change in slope of the critical isotherm very near to the critical pressure. To locate the critical density for parahydrogen, the rectilinear diameter method was used. The rectilinear diameter method uses a plot of the average values of the saturated liquid density and saturated vapor density along the liquid-vapor coexistence curve. Plotting these averaged densities versus temperature results in a nearly straight line to aid in finding the value of the critical density used in the

formulation. Figure 6.1 shows the rectilinear diameter plot of a preliminary version of the new parahydrogen EOS with an incorrect critical density.

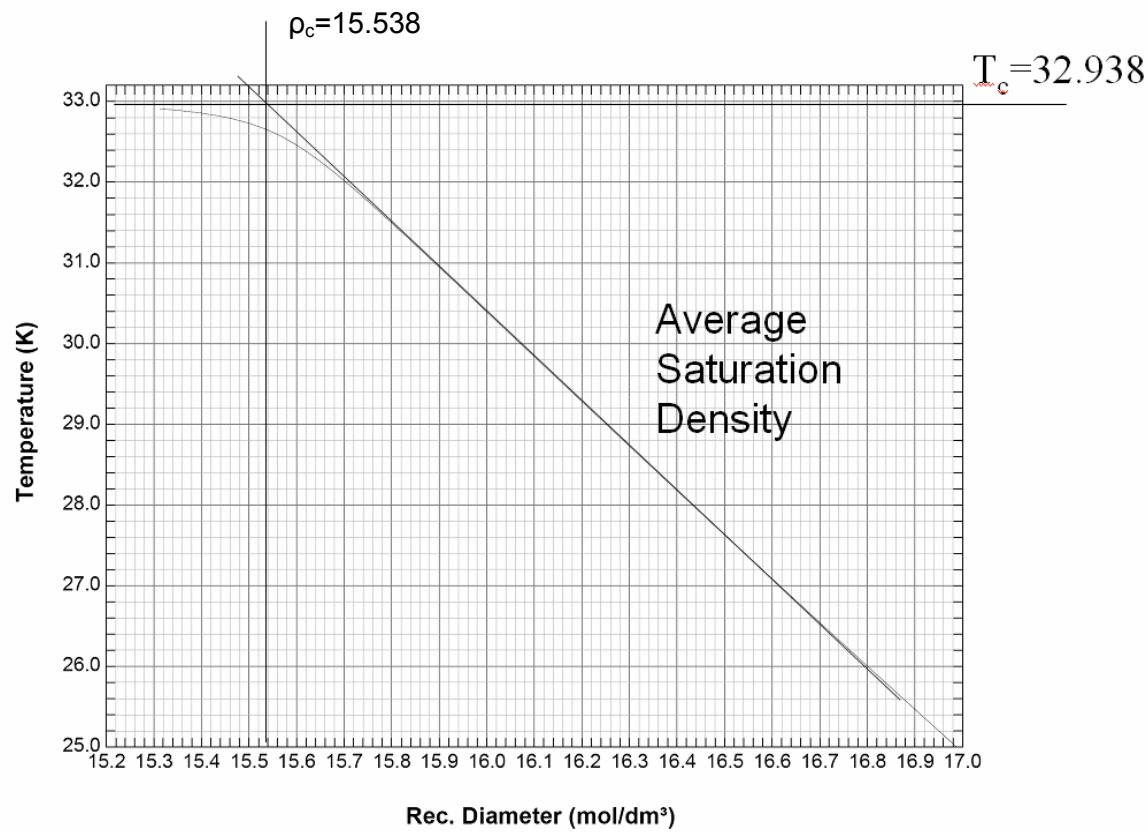

Figure 6.1 Rectilinear Diameter Plot of a Preliminary New Parahydrogen EOS Displaying an Incorrect Critical Density.

The shape of the fluid surface for certain properties gives an indication of how well the functional form of the formulation obeys correct thermodynamic theory. Trends in caloric properties can be an indication of fundamentally correct or incorrect behavior of formulations. For instance, saturation curves are theoretically monotonic. Figure 6.2 shows the isochoric heat capacity plotted versus temperature for the parahydrogen equation of state of Younglove [14]. The large curl in the isochoric heat capacity along the saturated liquid line below 20 kelvin indicates fundamentally incorrect behavior. This behavior was corrected in the formulation presented in this thesis. The isochoric heat capacity plotted versus temperature for the new parahydrogen formulation is shown in Figure 6.3.

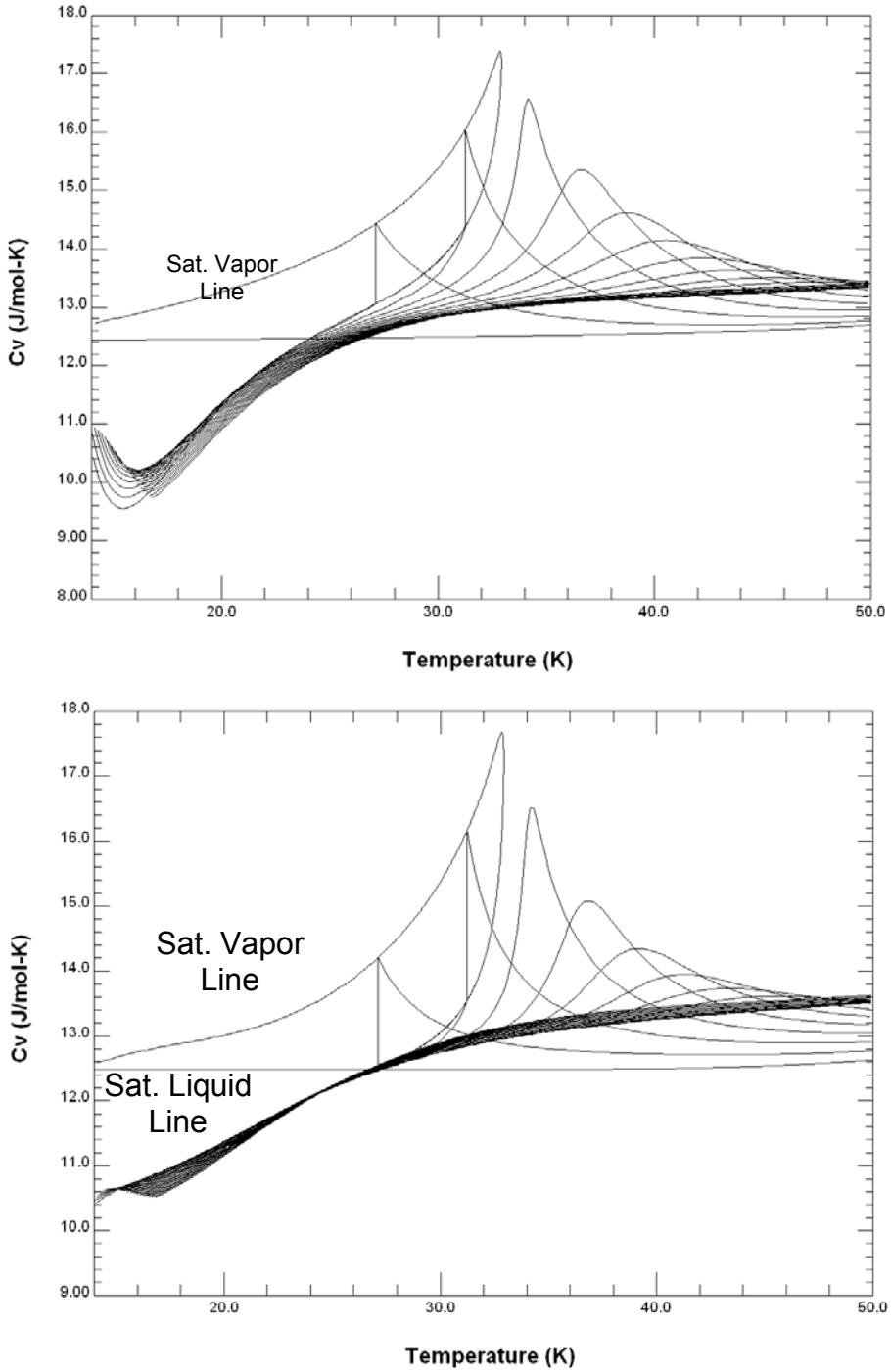

Figure 6.2 Calculated Isochoric Heat Capacity plotted versus Temperature for the Parahydrogen EOS of Younglove [14] (top) and the New Parahydrogen EOS (bottom) (Isobars are shown between 0 and 10 MPa in 0.5 MPa increments).

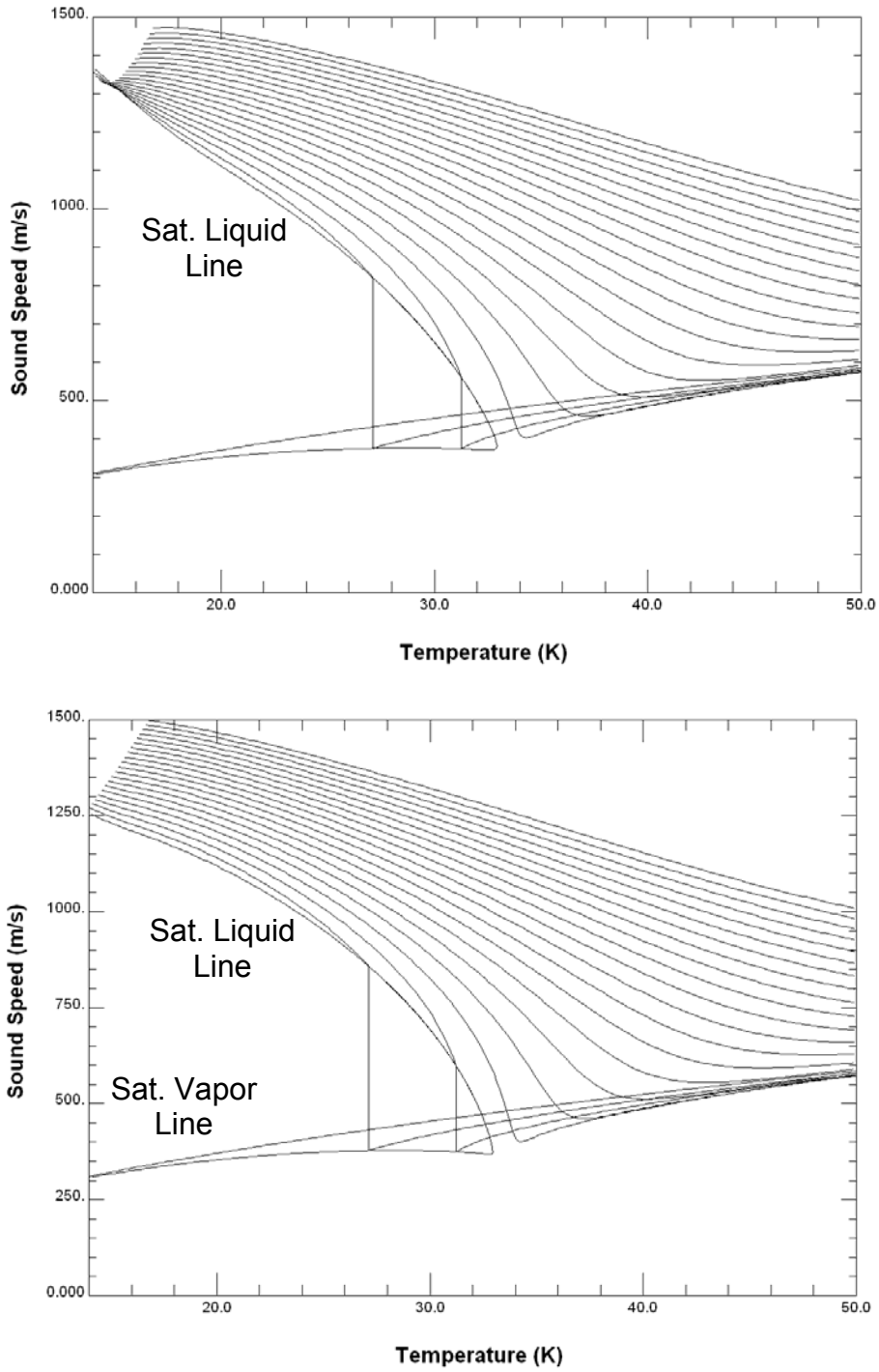

Figure 6.3 Calculated Speed of Sound plotted versus Temperature for the Parahydrogen EOS of Younglove [14] (top) and the new Parahydrogen EOS (bottom) (Isobars are shown between 0 and 10 MPa in 0.5 MPa increments).

In addition to the isochoric heat capacity, the speed of sound should exhibit monotonic behavior of the saturation lines and the single phase liquid region should have symmetric isobars. The calculated speed of sound is plotted versus temperature in Figure 6.3 for the parahydrogen EOS of Younglove [14. The speed of sound along the saturated liquid line deviates from classical monotonic behavior below 20 kelvin and the single phase isobars are not parallel. This behavior was corrected in the new parahydrogen formulation. The calculated speed of sound plotted versus temperature for the new parahydrogen formulation is shown in Figure 6.3.

Another test of equation behavior occurs at extrapolated temperatures, densities, and pressures. The behavior of equations of state at extreme conditions varies, incredibly with many equations having areas of negative pressures, which are not physically meaningful. Some formulations have isotherms that become parallel to one another or cross each other. This behavior is also not appropriate at these conditions. Figure 6.6 shows the extrapolated behavior of the parahydrogen EOS of Younglove [14] indicating that the isotherms cross at extreme densities. This is verified by the inaccurate behavior of the melting line.

To straighten the isotherm behavior at high densities for the new EOS for parahydrogen, the t=1 d=4 combination with a positive coefficient was chosen for the polynomial term with the highest d value. This term is dominant at high densities. The use of the t=1 eliminates the temperature dependence at extreme conditions. If a value less than 1 were to be used, the isotherms would become parallel and a value greater than 1 would cause the isotherms to cross. The analytical details of this approach are given by Lemmon and Jacobsen [119]. Figure 6.4 shows the isothermal behavior of the new parahydrogen EOS at extrapolated pressures and densities.

The comparisons of the formulation to experimental data are given in Section 7.1.

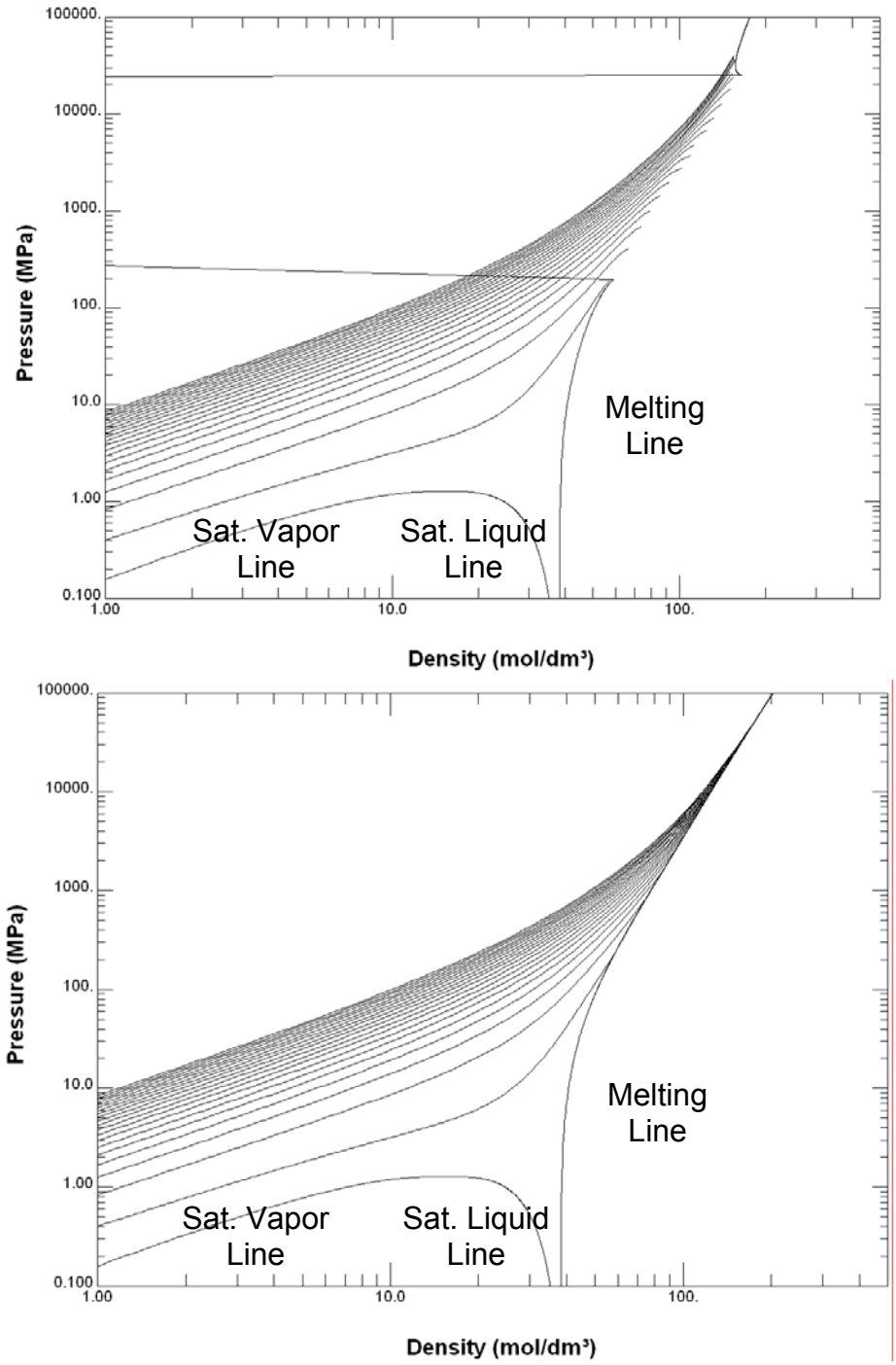

Figure 6.4 Isothermal Behavior of the Parahydrogen EOS of Younglove [14] (top) and the New Parahydrogen EOS (bottom) at Extreme Conditions of Density and Pressure. (Isotherms are spaced in 50 K increments starting with 50 K and ending at 1000 K.)

6.3 New Thermodynamic Property Formulation for Normal Hydrogen

After the parahydrogen EOS was developed, the new normal hydrogen EOS was formulated using the real fluid portion of the parahydrogen EOS. To represent the normal hydrogen surface, the equation was refitted with the normal hydrogen critical property values and a new normal hydrogen ideal gas heat capacity equation. The parahydrogen critical region data points were replaced by normal hydrogen data where available. Where no replacement normal hydrogen data existed, other properties in the region or predicted properties calculated using the Quantum Law of Corresponding States were used.

The parameters and coefficients of the new equation of state for normal hydrogen are shown in Table 6.5, and the parameters of the Gaussian terms are shown in Table 6.6.

Table 6.5 Parameters and Coefficients of the New Normal Hydrogen Equation of State.

i	N_i	t_i	d_i	p_i
1	-6.93643	0.6844	1	0
2	0.01	1	4	0
3	2.1101	0.989	1	0
4	4.52059	0.489	1	0
5	0.732564	0.803	2	0
6	-1.34086	1.1444	2	0
7	0.130985	1.409	3	0
8	-0.777414	1.754	1	1
9	0.351944	1.311	3	1
10	-0.0211716	4.187	2	--
11	0.0226312	5.646	1	--
12	0.032187	0.791	3	--
13	-0.0231752	7.249	1	--
14	0.0557346	2.986	1	--

Table 6.6 Parameters of the Gaussian Terms in the New Normal Hydrogen Equation of State.

i	φ_i	β_i	γ_i	D_i
10	-1.685	-0.171	0.7164	1.506
11	-0.489	-0.2245	1.3444	0.156
12	-0.103	-0.1304	1.4517	1.736
13	-2.506	-0.2785	0.7204	0.67
14	-1.607	-0.3967	1.5445	1.662

The normal hydrogen ideal gas heat capacity equation is of the same form as equation 5.2 but was fitted to match the existing normal hydrogen ideal gas heat capacity data. The parameters and coefficients are shown in Table 6.7.

Table 6.7 Parameters and Coefficients of the Normal Hydrogen Ideal Gas Heat Capacity Equation.

n_i	t_i
2.5	0.0
v_i	u_i
1.616	531
-0.4117	751
-0.792	1989
0.758	2484
1.217	6859

The critical point values used in the REFPROP formulation for normal hydrogen have not been measured experimentally since 1950. The critical temperature was determined based on vapor pressure data and the critical density fitted with the equation of state. In addition, the available normal hydrogen density data near the critical point are not suitable for correlation because the precision is quite low. The data of Goodwin *et al.* [47] and Roder *et al.* [50] were transformed using the Quantum Law of Corresponding States into predicted values for normal hydrogen. These data are described in Section 7.2. Using these data and a direct transformation of the critical point, new values were determined for the critical point of normal hydrogen (Table 6.8).

Table 6.8 Critical and Triple Point Properties used by the New Normal Hydrogen EOS.

	Temperature (K)	Pressure (MPa)	Density ($mol \cdot L^{-1}$)
Critical Point	33.145	1.2964	15.508
Triple Point	13.957	0.00736	38.2

The real fluid portions of the new normal hydrogen and parahydrogen equations of state are very similar. Comparisons of the new normal hydrogen equation of state to the existing standard will be discussed in Section 7.2.

6.4 New Thermodynamic Property Formulation for Orthohydrogen

Section 2 established the difficulties in preparing a pure sample of orthohydrogen. Since no experimental thermodynamic properties of orthohydrogen have ever been measured directly, orthohydrogen data had to be calculated using the Quantum Law of Corresponding States with the new parahydrogen EOS as a reference fluid. Only data at states where there are both normal hydrogen and parahydrogen measurements in the same region were transformed, so the accuracy of the transformation could be estimated. At temperatures above 70 K the differences in measured densities between orthohydrogen and parahydrogen are smaller than the experimental uncertainty so the original normal hydrogen data were used. The predicted data and the property held constant during the transformation are listed in Table 6.9.

The normal parameters and coefficients of the new orthohydrogen equation of state are shown in Table 6.10, and the parameters of the Gaussian terms are shown in Table 6.11.

Table 6.9 Data Sets Selected for Transformation to the Orthohydrogen Surface.

Data Set	Hydrogen Form	Experimental Property held constant During Transformation
Goodwin *et al.* [47]	Parahydrogen	Density
Roder *et al.* [50]	Parahydrogen	Density
van Dael *et al.* [46]	Parahydrogen	Speed of Sound
van Itterbeek *et al.* [54,55]	Parahydrogen	Speed of Sound
New Parahydrogen EOS	Parahydrogen	Vapor Pressure

Table 6.10 Parameters and Coefficients of the Orthohydrogen Equation of State.

i	N_i	t_i	d_i	p_i
1	-6.83148	0.7333	1	0
2	0.01	1	4	0
3	2.11505	1.1372	1	0
4	4.38353	0.5136	1	0
5	0.211292	0.5638	2	0
6	-1.00939	1.6248	2	0
7	0.142086	1.829	3	0
8	-0.87696	2.404	1	1
9	0.804927	2.105	3	1
10	-0.710775	4.1	2	--
11	0.0639688	7.658	1	--
12	0.0710858	1.259	3	--
13	-0.087654	7.589	1	--
14	0.647088	3.946	1	--

Table 6.11 Parameters of the Gaussian Terms in the Orthohydrogen Equation of State.

i	φ_i	β_i	γ_i	D_i
10	-1.169	-0.4555	1.5444	0.6366
11	-0.894	-0.4046	0.6627	0.3876
12	-0.04	-0.0869	0.763	0.9437
13	-2.072	-0.4415	0.6587	0.3976
14	-1.306	-0.5743	1.4327	0.9626

The orthohydrogen ideal gas heat capacity equation is of the same form as Equation 5.2 and that of normal hydrogen and parahydrogen. The normal hydrogen ideal gas heat capacity equation was refitted to match the

orthohydrogen ideal heat capacity data given in Woolley *et al.* [8]. The parameters and coefficients are shown in Table 6.12.

Table 6.12 Parameters and Coefficients of the Orthohydrogen Ideal Gas Heat Capacity Equation.

n_i	t_i
2.5	0.0
v_i	u_i
2.54151	856
-2.3661	1444
1.00365	2194
1.22447	6968

To determine the critical point properties, initial interpolation of the normal hydrogen and parahydrogen critical point values were estimated. The final critical point values were fitted using the transformed critical region data of Goodwin *et al.* [47] and Roder *et al.* [50]. The values for the critical point of orthohydrogen used by the equation of state are shown in Table 6.13.

Table 6.13 Critical and Triple Point Properties used by the Orthohydrogen EOS.

	Temperature (K)	Pressure (MPa)	Density ($mol \cdot L^{-1}$)
Critical Point	33.22	1.31065	15.445
Triple Point	14.008	0.007461	38.2

Since the real fluid portions of the new orthohydrogen, normal hydrogen and parahydrogen equations of state are very similar, comparisons of the fluid surfaces will not be made here. Comparisons of the orthohydrogen EOS to the transformed data will be made in Section 7.3.

7. Comparison of Calculated Thermophysical Properties of Hydrogen to Data

To illustrate the accuracy of an EOS, plots are created to show the deviations of property values calculated using the EOS from the experimental values obtained in the same region. In this section all calculated properties compared with data values are determined using the standard equations of state (This Work) in the top or right of each figure, and the new equation of state in the bottom or left of each figure. These plots show comparisons among data from different sources in the same or adjacent regions of the surface of state. Figures 7.1-7.16 illustrate selected comparisons for thermodynamic properties of parahydrogen, Figures 7.17-7.31 illustrate those for normal hydrogen, and Figures 7.31-7.36 illustrate those for orthohydrogen. Data selected for these comparisons are those which have been cited by others as accurate.

7.1 Comparison of Calculated Parahydrogen Properties to Data

Some normal hydrogen density data were included in the parahydrogen density and pressure deviation plots. This illustrates the difference between the densities of parahydrogen and normal hydrogen.

Figures 7.1 and 7.2 display the calculated differences in the second and third virial coefficient data from Goodwin *et al.* [66] from the predicted values of the equations of state. It has been established that the second virial coefficient becomes negative very rapidly approaching zero deviation [121]. The large deviation at low temperatures observed in Figures 7.1 and 7.2 was not apparent throughout the entire regression and did not appear until the slope of the 14 K isotherm on a $(Z-1)/\rho$ versus ρ plot was forced to be negative at zero density. The reason for this discrepancy is unknown.

Figure 7.3 shows the deviation of saturation heat capacity. Below 17 K the Johnston *et al.* [64] and Younglove and Diller [65] data sets show differing trends.

This region of the surface was fit using speed of sound data and vapor pressure data. The resulting fit of the new parahydrogen equation of state predicts saturation heat capacity values in between those of the two data sets. As the critical temperature is approached the Younglove and Diller [65] data set deviates systematically from the values calculated by the equation of state. This trend in saturation heat capacity data has been observed in other fluids measured by this apparatus [122].

The percent deviation of isochoric heat capacity is shown in Figure 7.4. Below 17 K the trend in the Younglove and Diller [51] data suggests a change in sign of the second derivative of the saturated liquid line on a C_v-T plot similar to the trend displayed in Figure 6.2. In an effort to keep this curve monotonic the data were not included in the fit below 17 K. The other points with large deviations occur near 33 K. The isochoric heat capacity theoretically goes to infinity at the critical point. To accomplish this in a formulation, special critical enhancement terms must be included. These terms were not included in this formulation.

Figure 7.5 displays the isobaric heat capacity deviations of the new and old parahydrogen equations of state. The precision of the Medvedev [52] data is quite low and despite efforts, no discernable trend could be observed in the data.

Speed of sound deviations for the new and old parahydrogen equations of state are shown in Figure 7.6. The Younglove [53] data was chosen as primary along the saturated liquid line and at temperatures higher than the critical temperature. The change in axis scale between the top graph and the bottom graph suggests a significant improvement in the representation of the data with the new parahydrogen equation of state. The critical pressure sees some significant deviations due to the lack of critical enhancement terms that would cause the speed of sound to go to zero at the critical point.

Figure 7.7 shows the deviations of vapor pressure. In the 21-32.8 K range the Weber *et al.* [61] data set was chosen as primary. In the 13.8-21 K range the Kemp and Kemp [59] was chosen as primary. The later data set were used as fixed points in the ITS-90 temperature scale and chosen as the primary point to fit at the normal boiling point. Comparison to the deviations of the old parahydrogen equation of state indicates a significant improvement of the representation with the new equation of state.

Figure 7.8-7.14 display deviations in density. The data are separated into increments of temperature in Figures 7.9-7.14. In most of the plots the new equation of state displays significant improvement over the old parahydrogen equation of state. It can be seen in the 60-70 K plot of Figure 7.9 that the difference between the parahydrogen and normal hydrogen experimental density data becomes undetectable with the apparatus used to make the measurements. In the 90-100 K plot of Figure 7.10 the data of Michels *et al.* [79] was taken as primary at higher temperatures, deviates systematically from the data of Goodwin *et al.* [47] that was considered primary at lower temperatures. The normal hydrogen data of Johnston *et al.* [74] trends with the Goodwin *et al.* [47] data. All three apparatus used were similar in construction so the cause of the deviation is unknown. Figure 7.8 shows that the new parahydrogen equation of state more accurately reproduces the Liebenberg *et al.* [76] high pressure data. The black lines of data displayed on the old equation of state plot indicate errors in the programs interpretation of the data at these high pressures. The cause of these errors is likely due to isotherms crossing each other at these pressures.

Figures 7.15 and 7.16 show deviations in pressure near the critical point and deviation in density plotted versus temperature, respectively. The estimated uncertainties in the equation of state based on the deviations shown in Figures 7.1-7.16 in density are 0.1% at temperatures from the triple point to 250 K and at pressures up to 40 MPa, except in the critical region, where an uncertainty of 0.2% in pressure is generally observed. In the region between 250 and 450 K

and at pressures from 0.1 to 300 MPa, the uncertainty in density is 0.04%. At temperatures between 450 and 1000 K, the uncertainty in density increases to 1%. At pressures between 300 and 2000 MPa, the uncertainty in density is 8%. Speed of sound data are represented within 0.5% below 100 MPa. The estimated uncertainty for heat capacities is 1.0%. The estimated uncertainties of vapor pressures and saturated liquid densities calculated using the Maxwell criterion are 0.1% for each property.

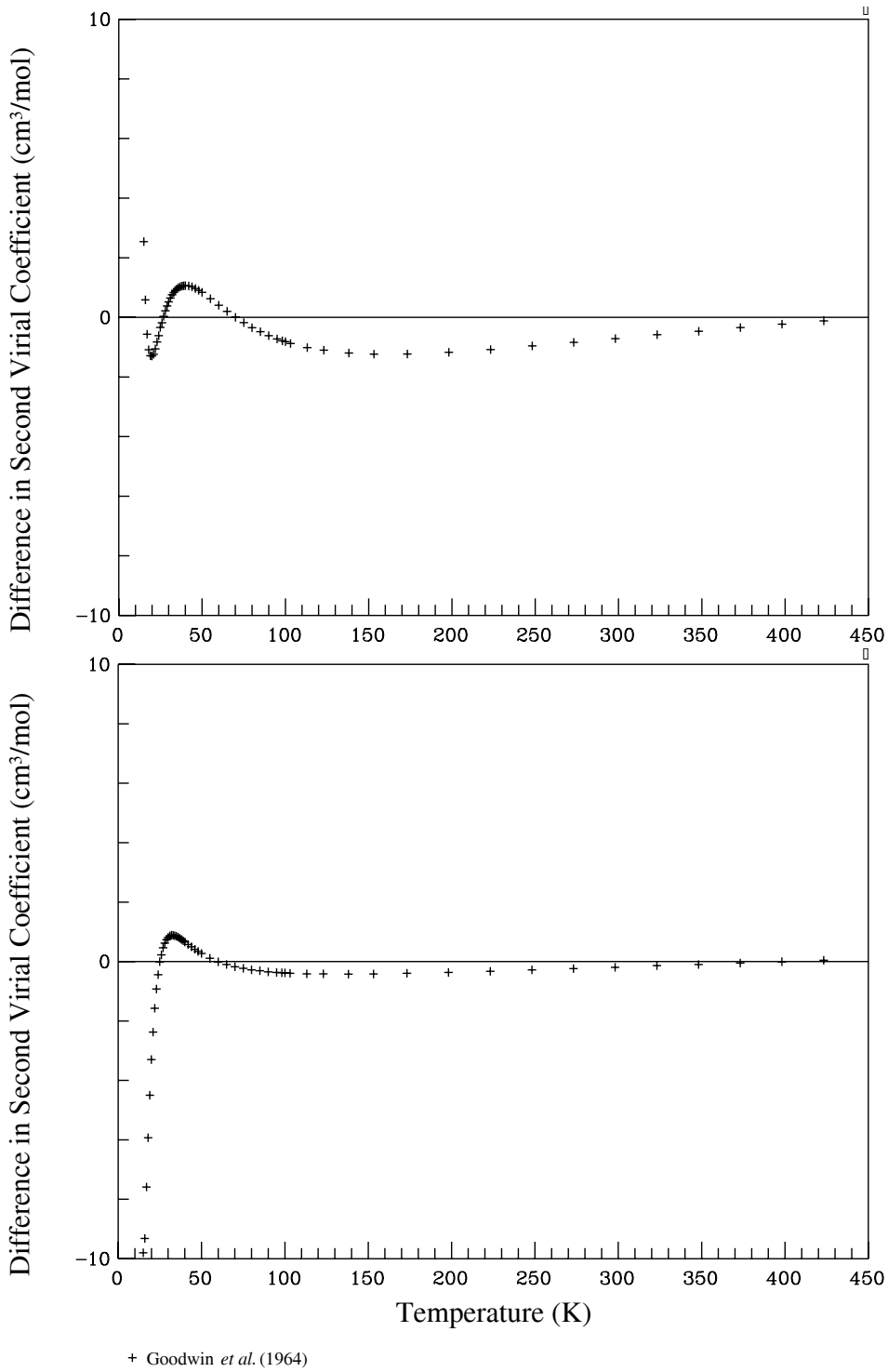

Figure 7.1 Difference in Second Virial Coefficient plotted versus Temperature for the Parahydrogen EOS of Younglove [14] (top) and the New Parahydrogen EOS (bottom) from experimental data.

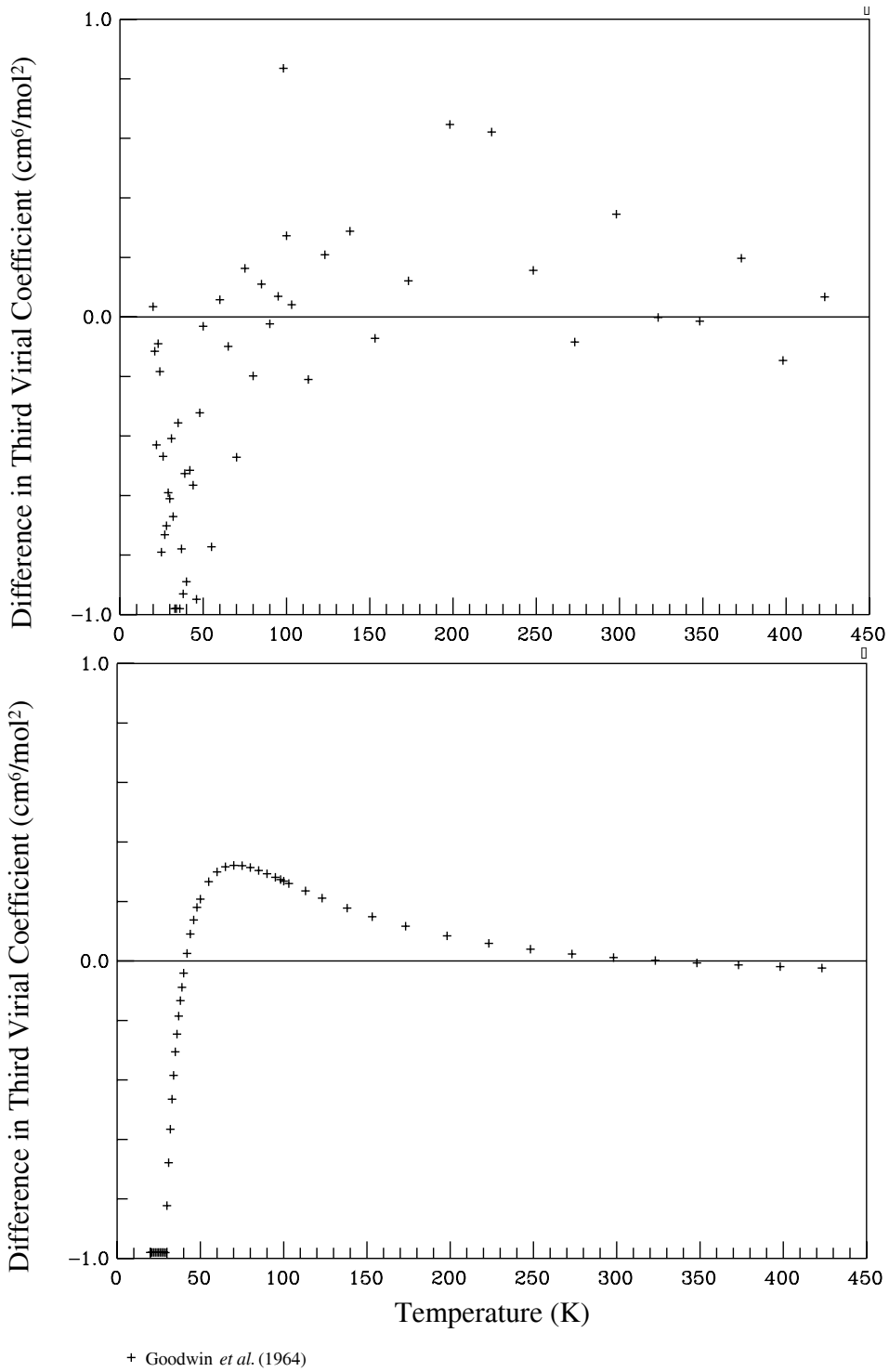

Figure 7.2 Difference in Third Virial Coefficient plotted versus Temperature for the Parahydrogen EOS of Younglove [14] (top) and the New Parahydrogen EOS (bottom) from experimental data.

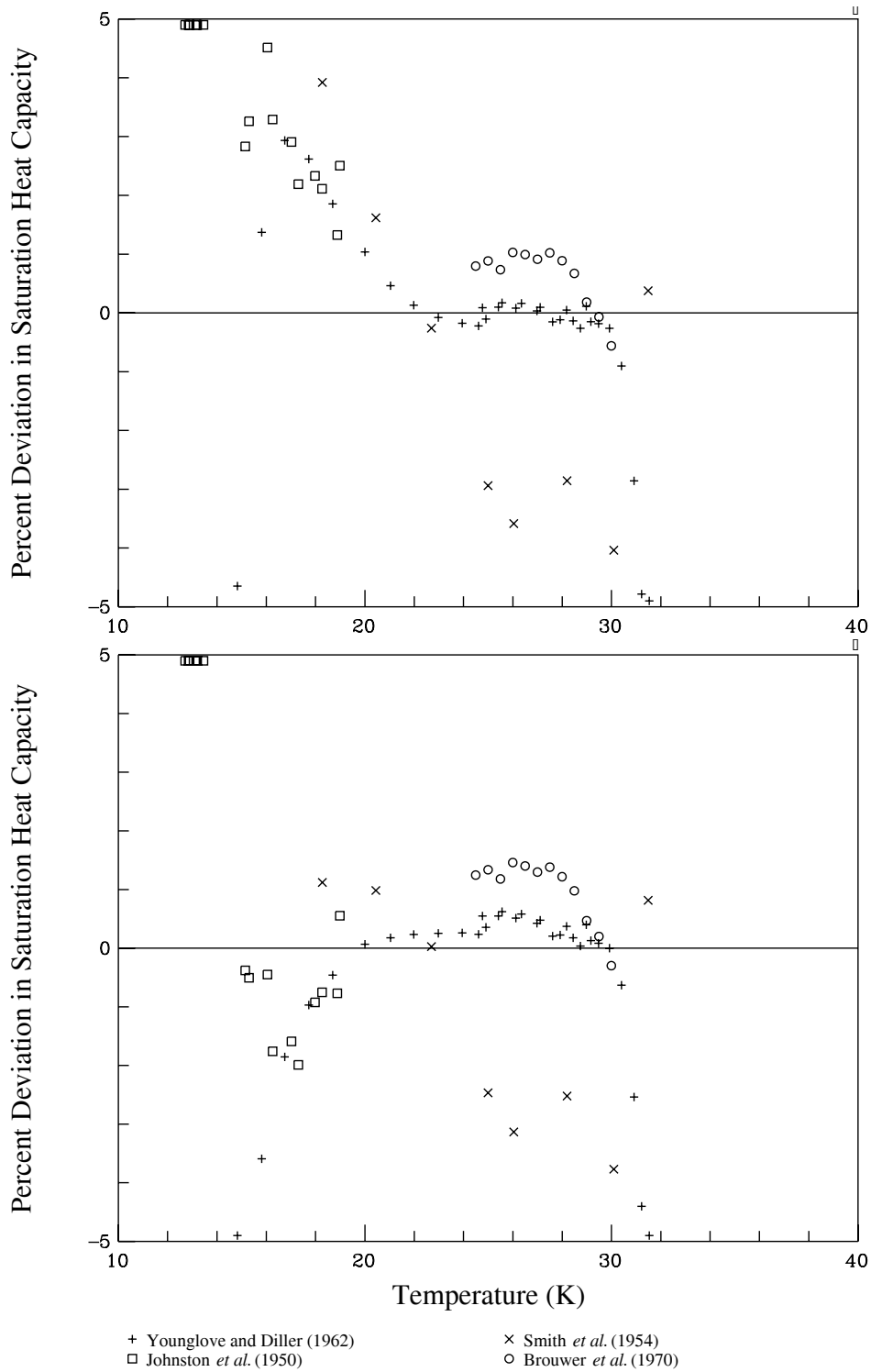

Figure 7.3 Deviation of Saturation Heat Capacity for the Parahydrogen EOS of Younglove [14] (top) and the new Parahydrogen EOS (bottom) from experimental data.

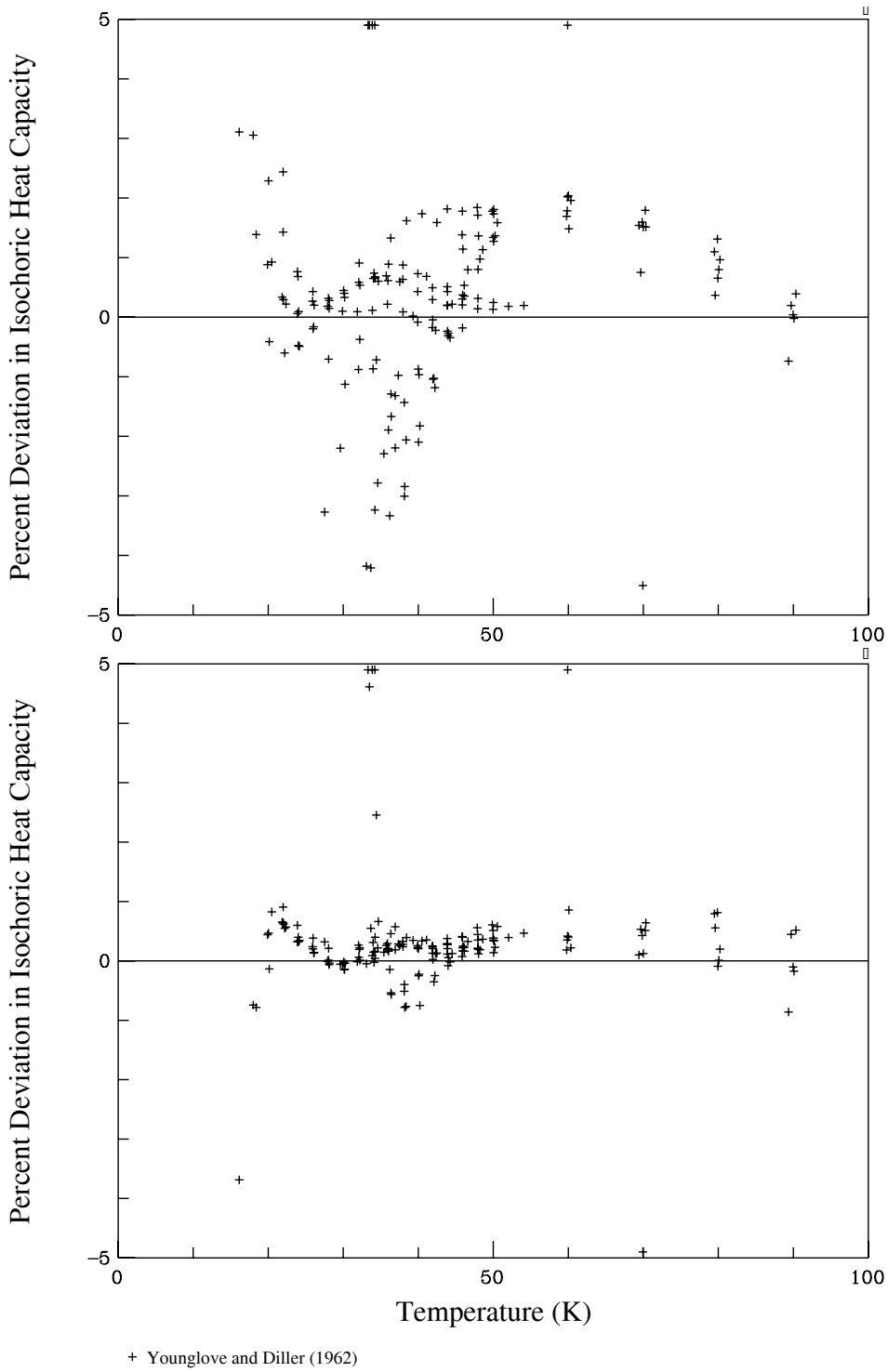

Figure 7.4 Deviation of Isochoric Heat Capacity of the Parahydrogen EOS of Younglove [14] (top) and the new Parahydrogen EOS (bottom) from experimental data.

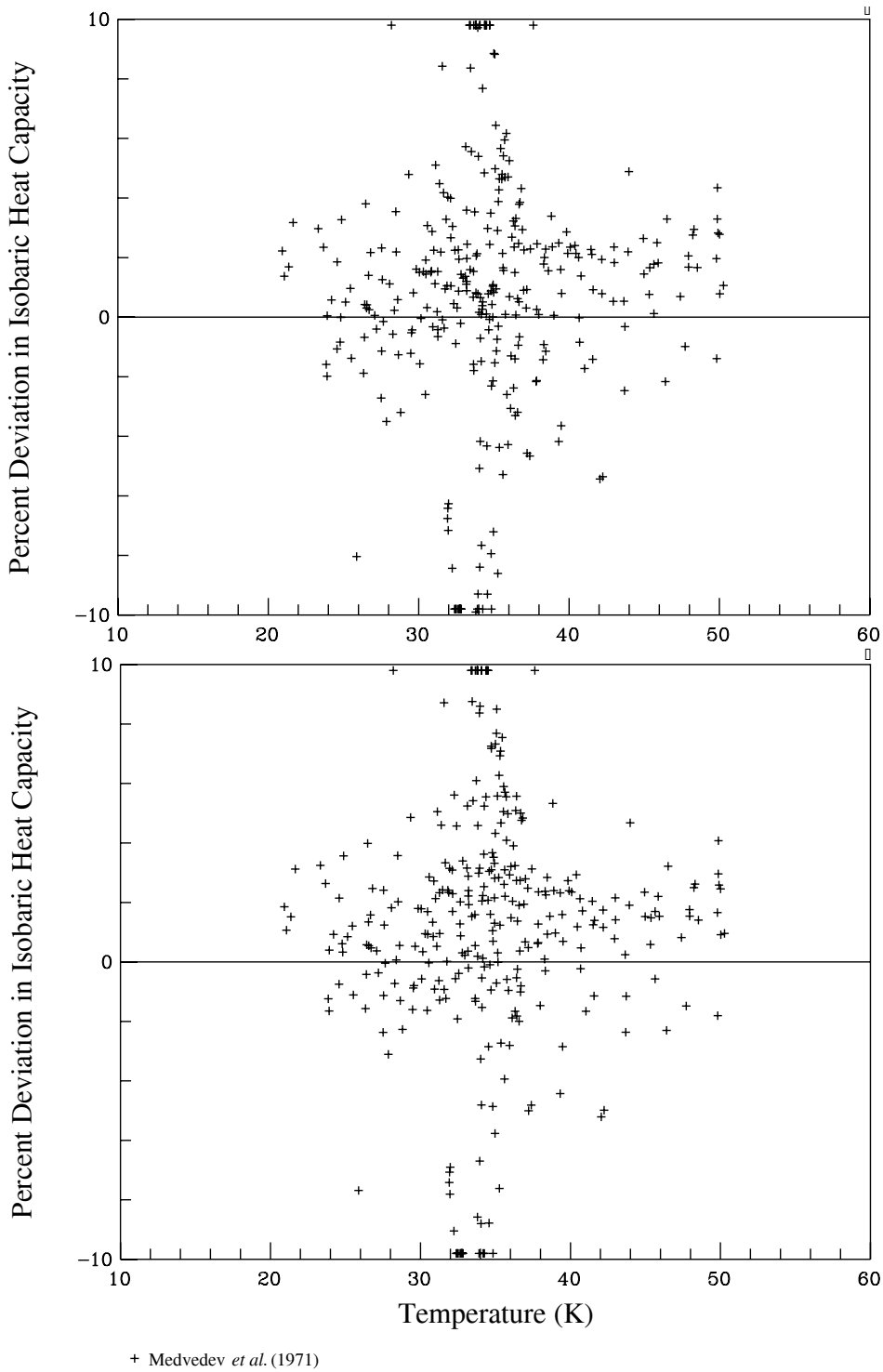

Figure 7.5 Deviation of Isobaric Heat Capacity of the Parahydrogen EOS of Younglove [14] (top) and the new Parahydrogen EOS (bottom) from experimental data.

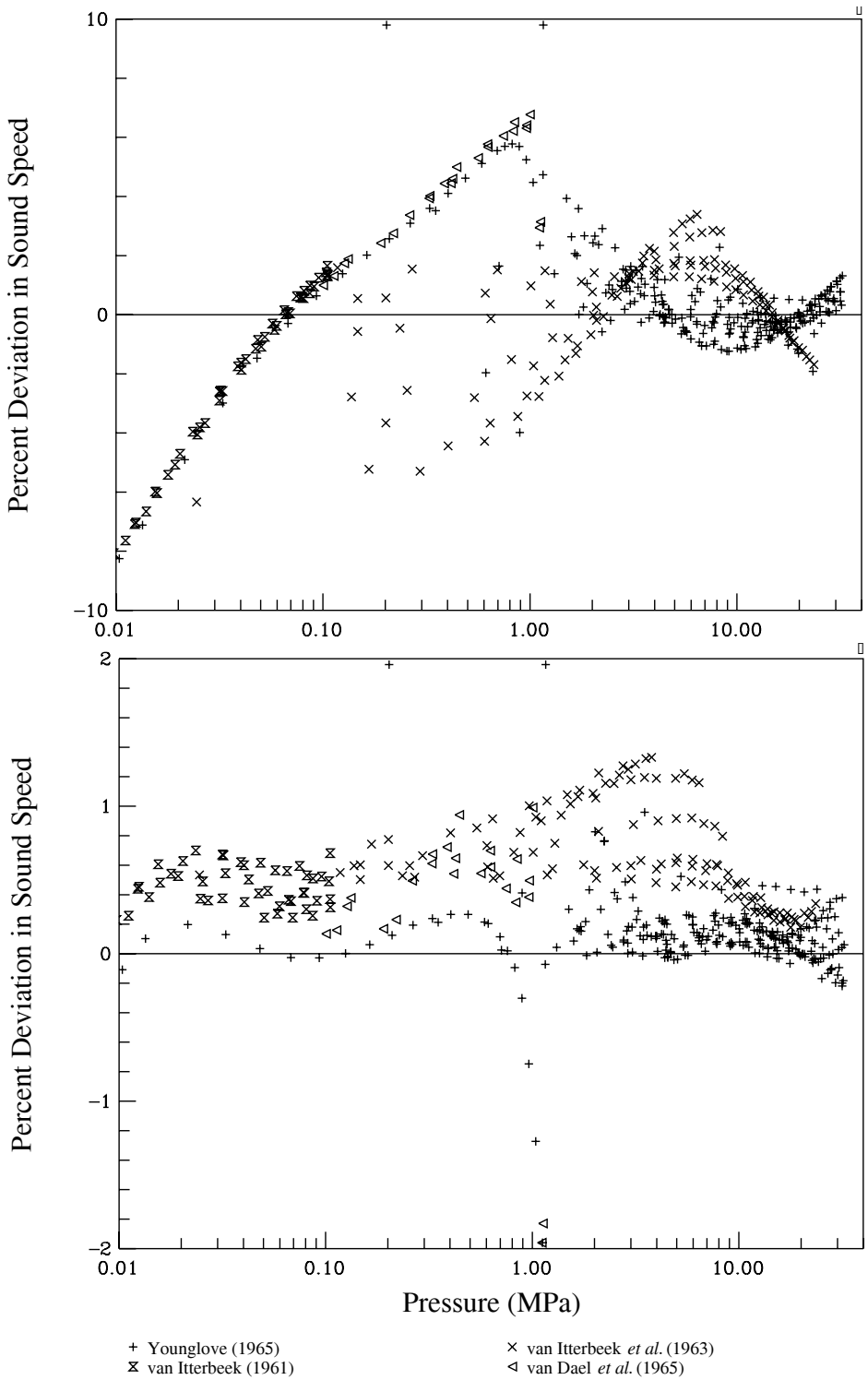

Figure 7.6 Deviation of Sound Speed of the Parahydrogen EOS of Younglove [14] (top) and the new Parahydrogen EOS (bottom) from experimental data.

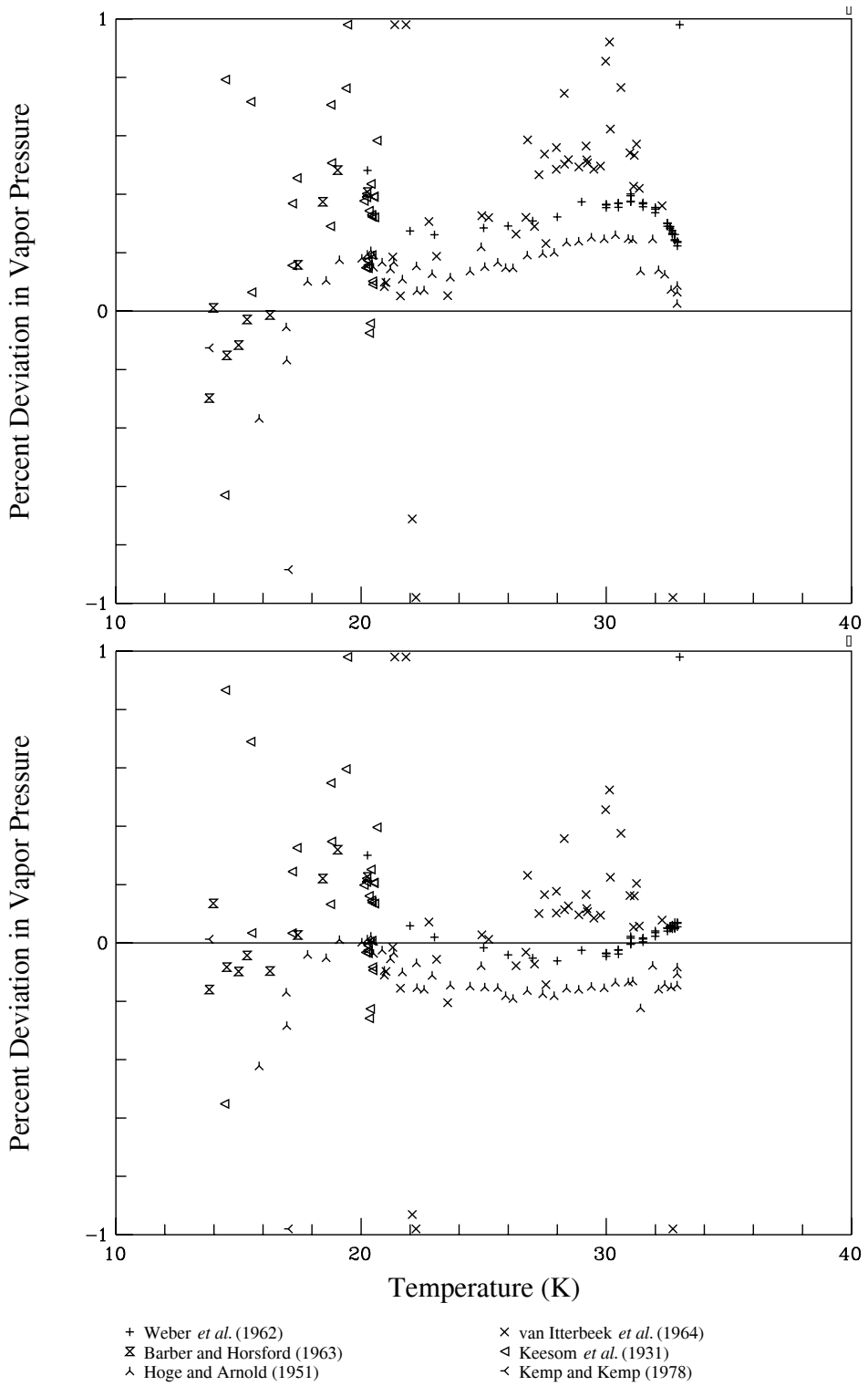

Figure 7.7 Deviation of Vapor Pressure of the Parahydrogen EOS of Younglove [14] (top) and the new Parahydrogen EOS (bottom) from experimental data.

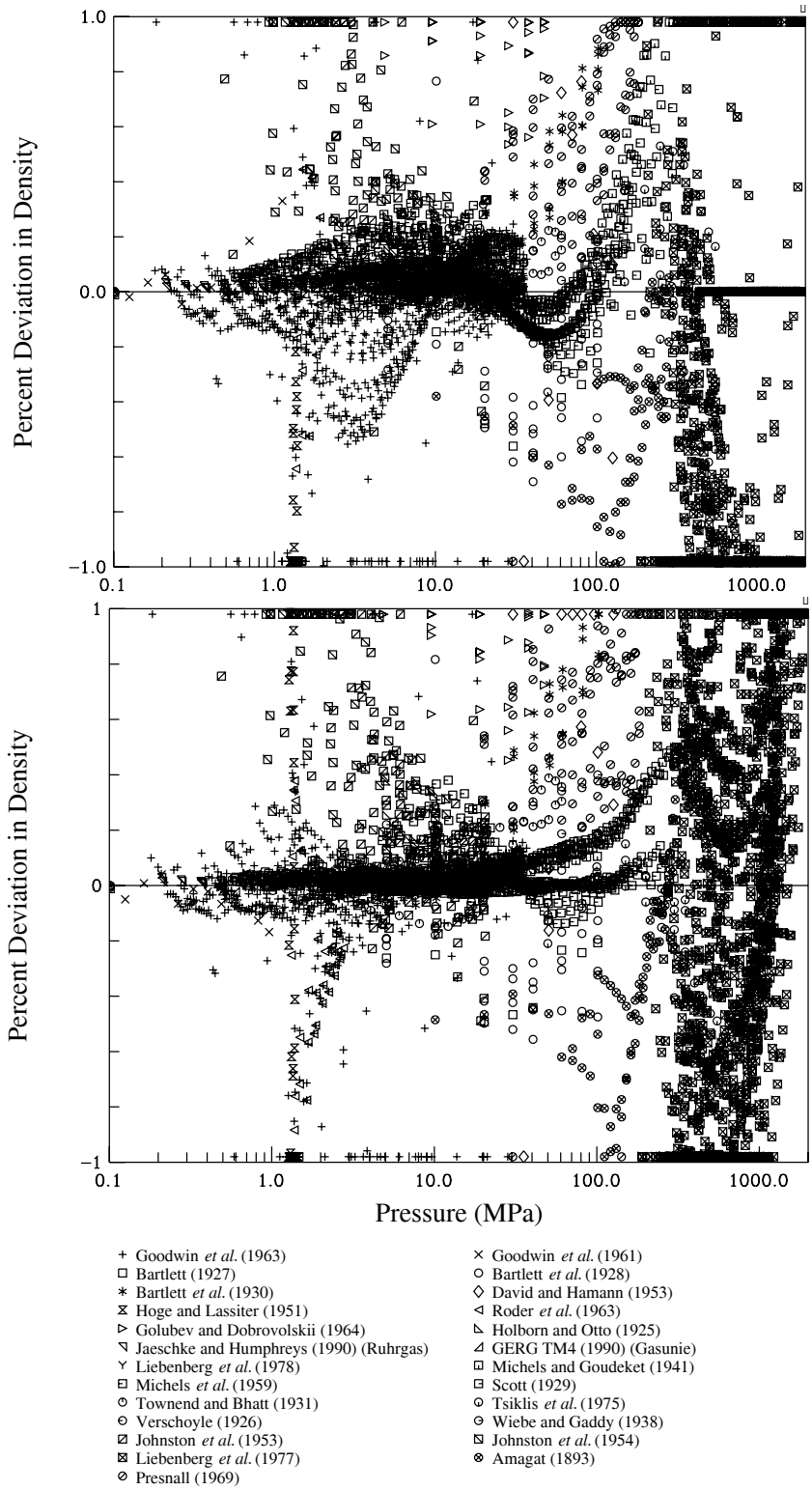

Figure 7.8 Deviation of Density of the Parahydrogen EOS of Younglove [14] (top) and the new Parahydrogen EOS (bottom) from experimental data (Data plotted against Pressure).

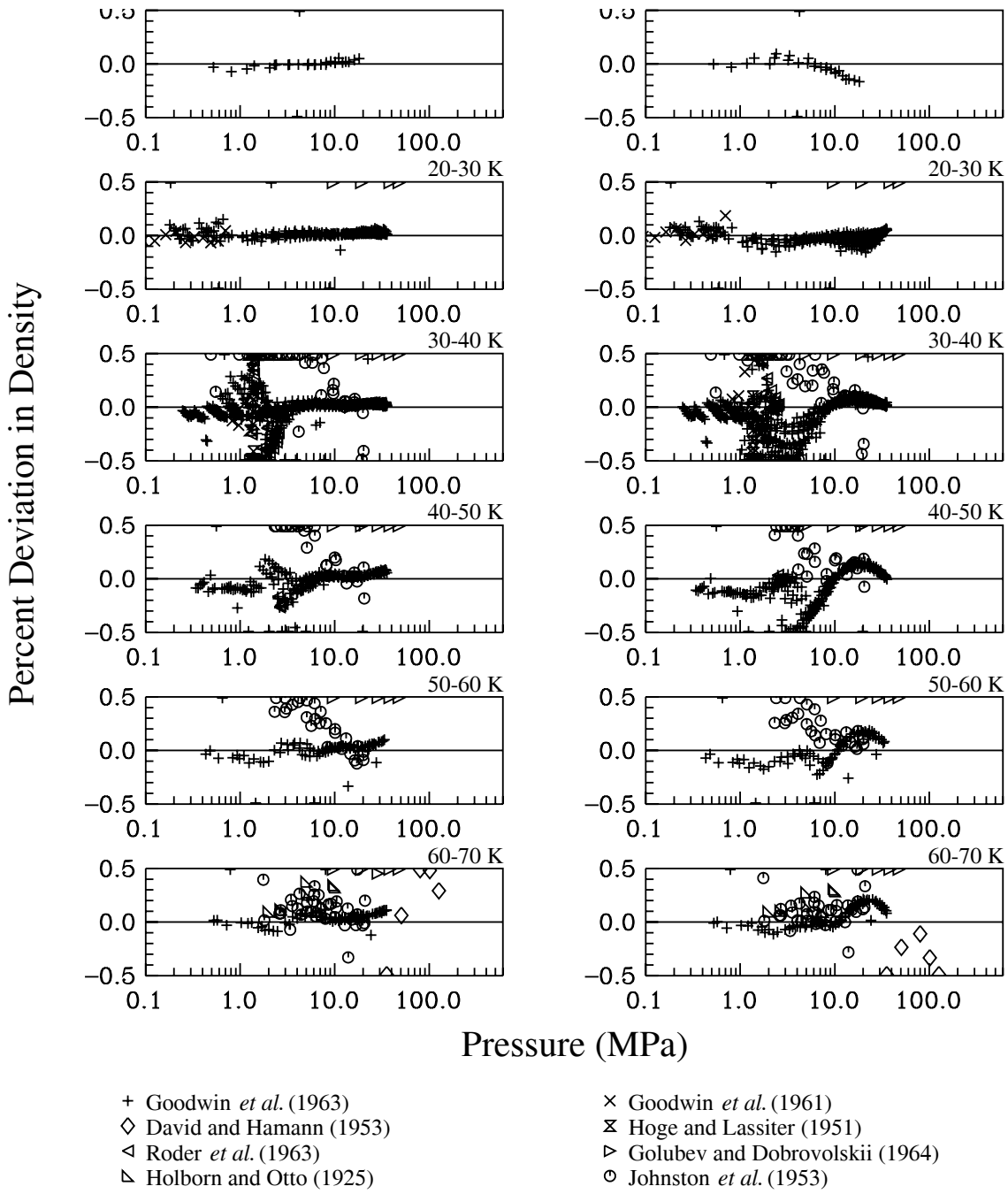

Figure 7.9 Deviation of Density of the Parahydrogen EOS of Younglove [14] (right) and the new Parahydrogen EOS (left) from experimental data. (Data displayed in 10 K increments from 10-70 K)

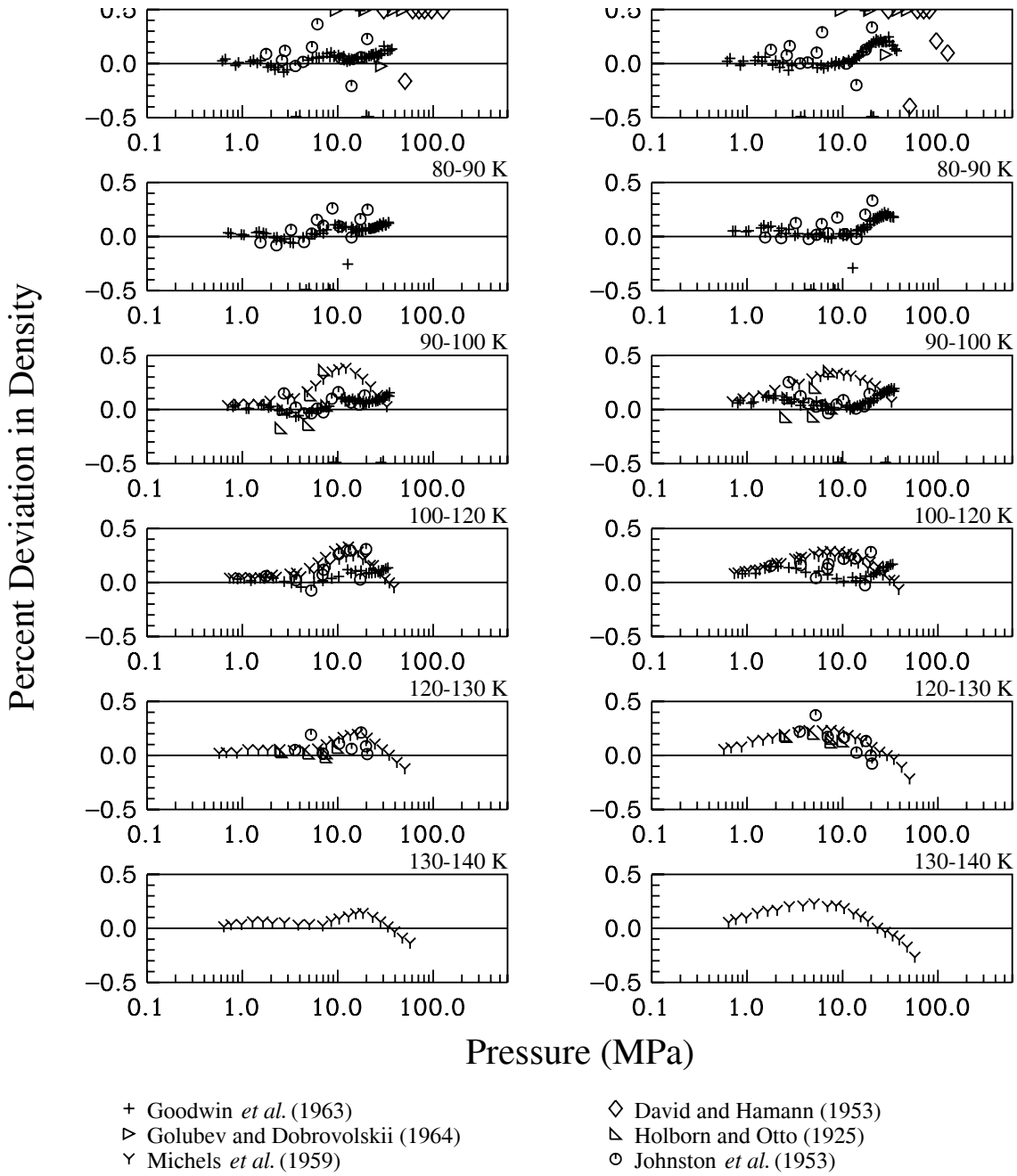

Figure 7.10 Deviation of Density of the Parahydrogen EOS of Younglove [14] (right) and the new Parahydrogen EOS (left) from experimental data. (Data displayed in 10 K increments from 70-140 K)

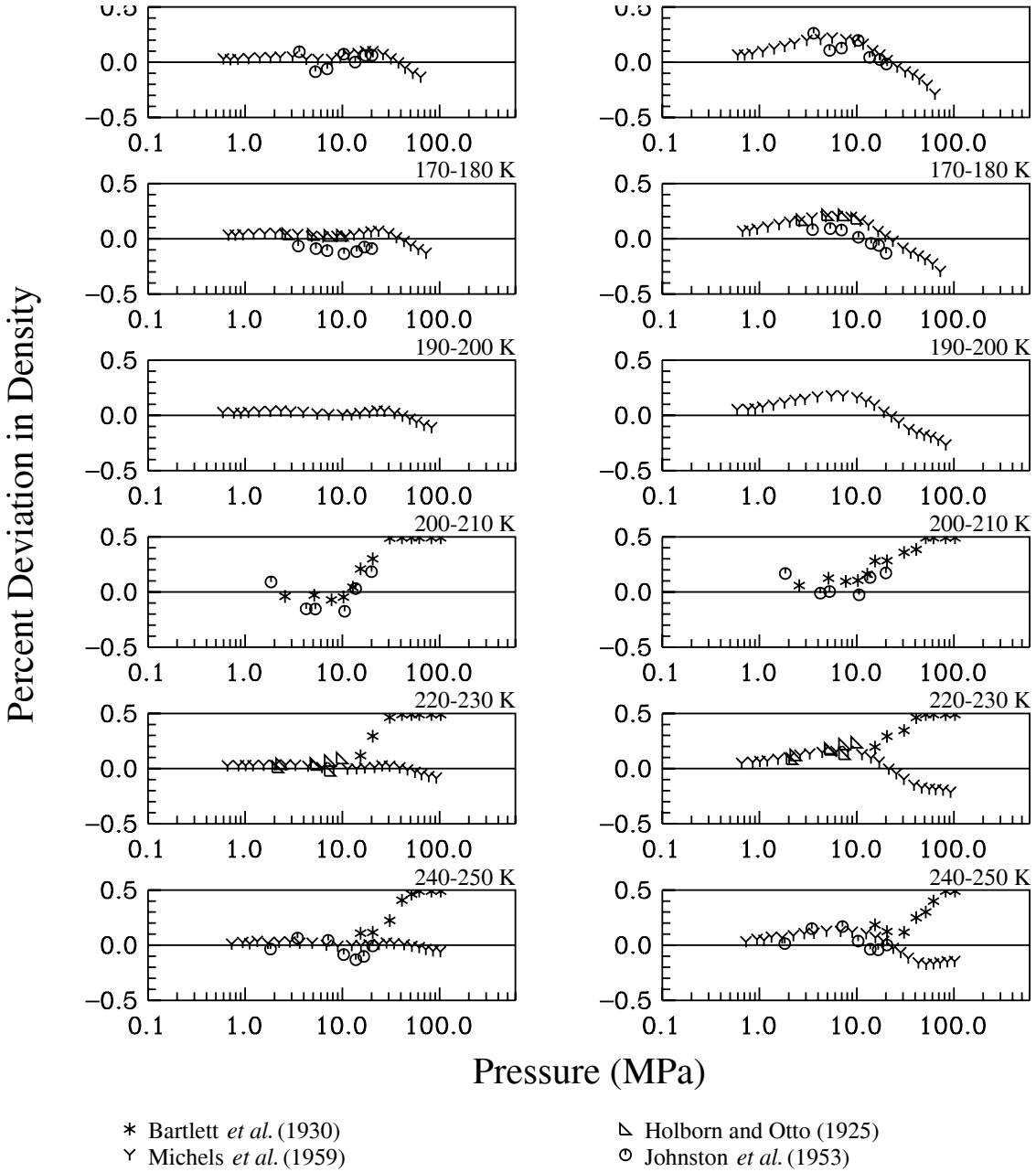

Figure 7.11 Deviation of Density of the Parahydrogen EOS of Younglove [14] (right) and the new Parahydrogen EOS (left) from experimental data. (Data displayed in 10 K increments from 150-250 K)

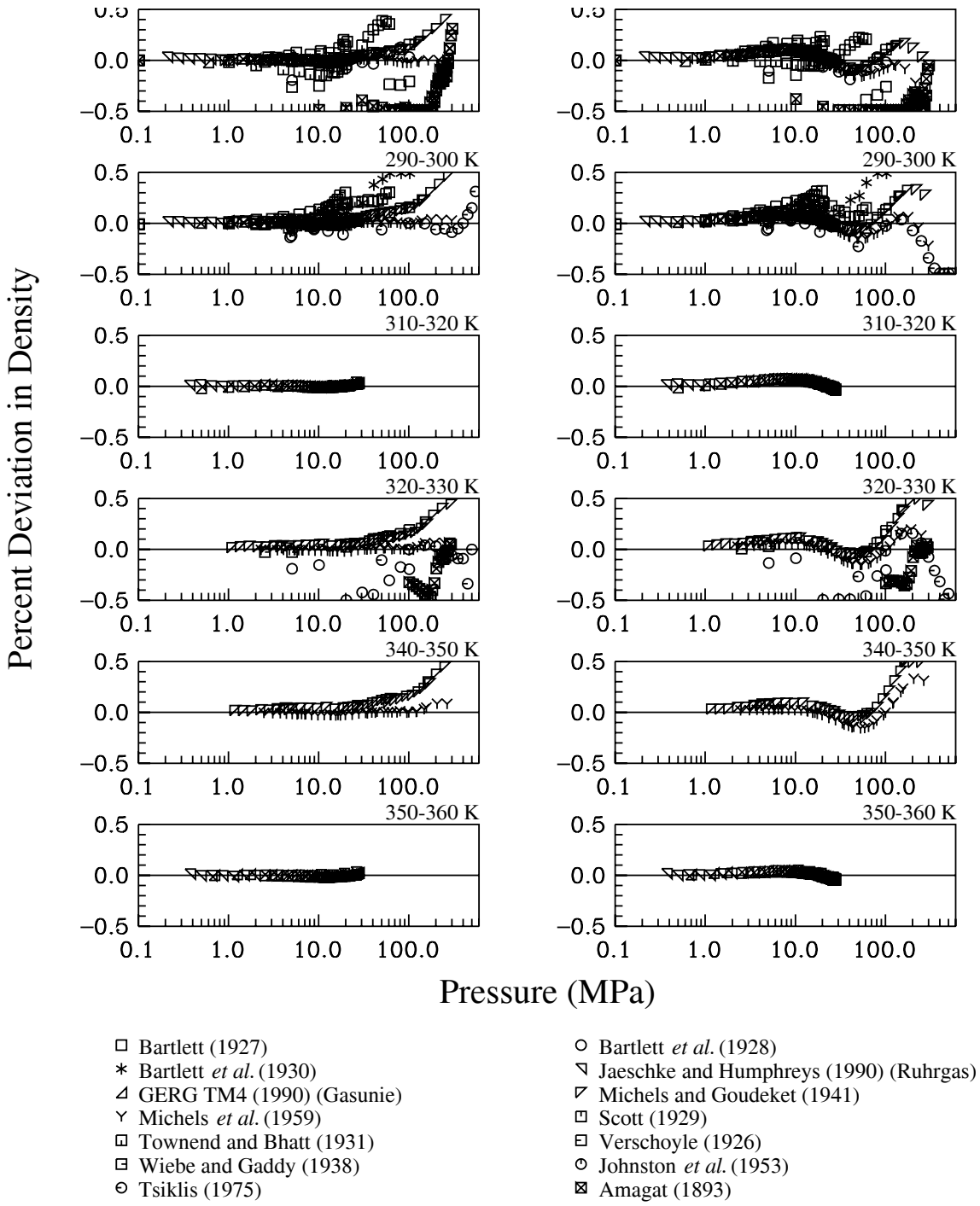

Figure 7.12 Deviation of Density of the Parahydrogen EOS of Younglove [14] (right) and the new Parahydrogen EOS (left) from experimental data. (Data displayed in 10 K increments from 270-360 K)

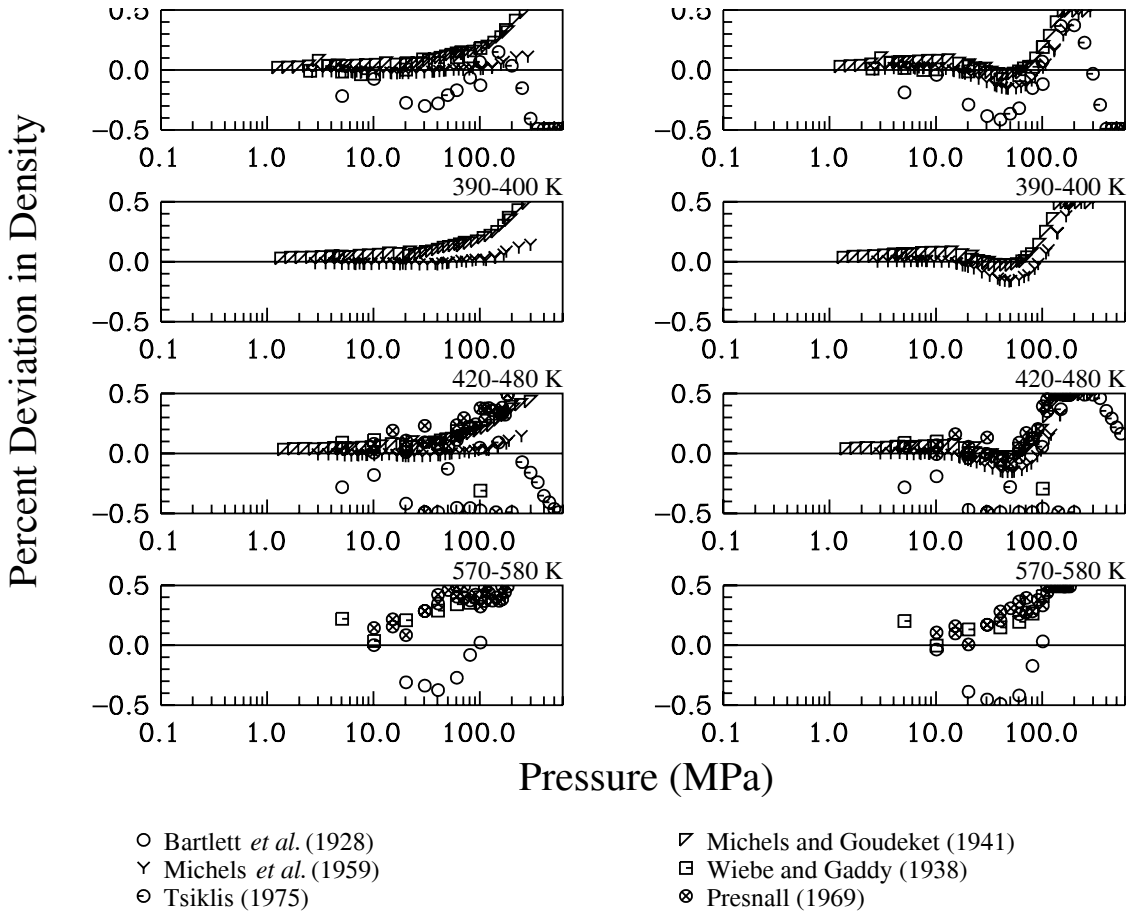

Figure 7.13 Deviation of Density of the Parahydrogen EOS of Younglove [14] (right) and the new Parahydrogen EOS (left) from experimental data. (Data displayed in listed increments from 370-580 K)

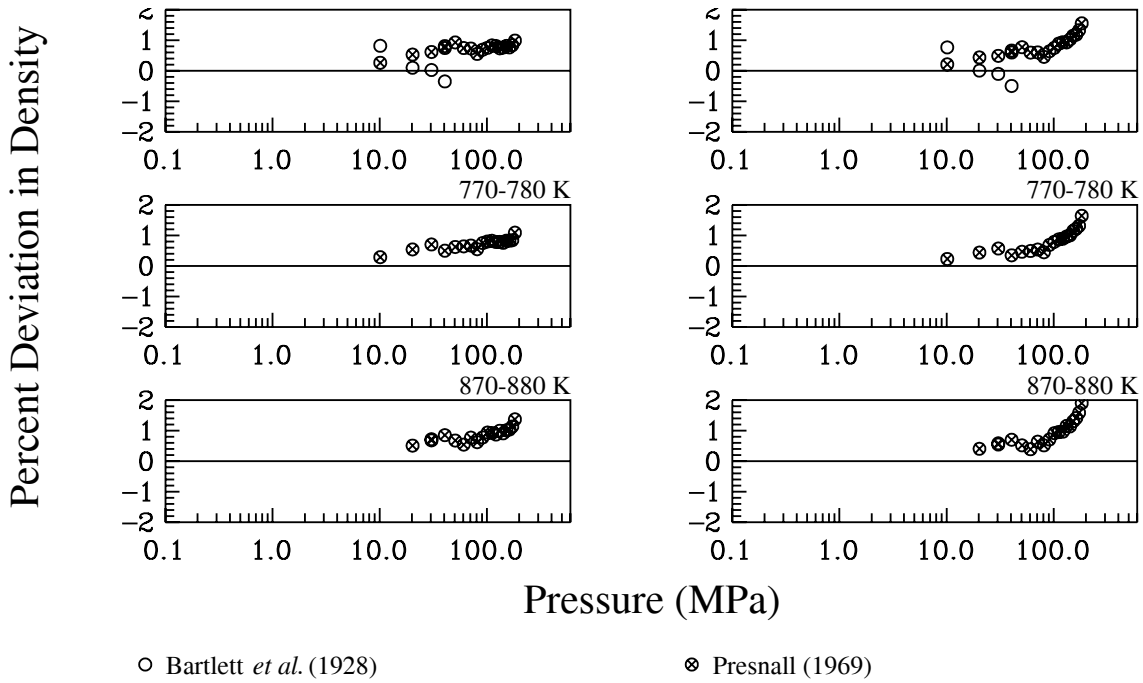

Figure 7.14 Deviation of Density of the Parahydrogen EOS of Younglove [14] (right) and the new Parahydrogen EOS (left) from experimental data. (Data displayed in 10 K increments from 670-880 K)

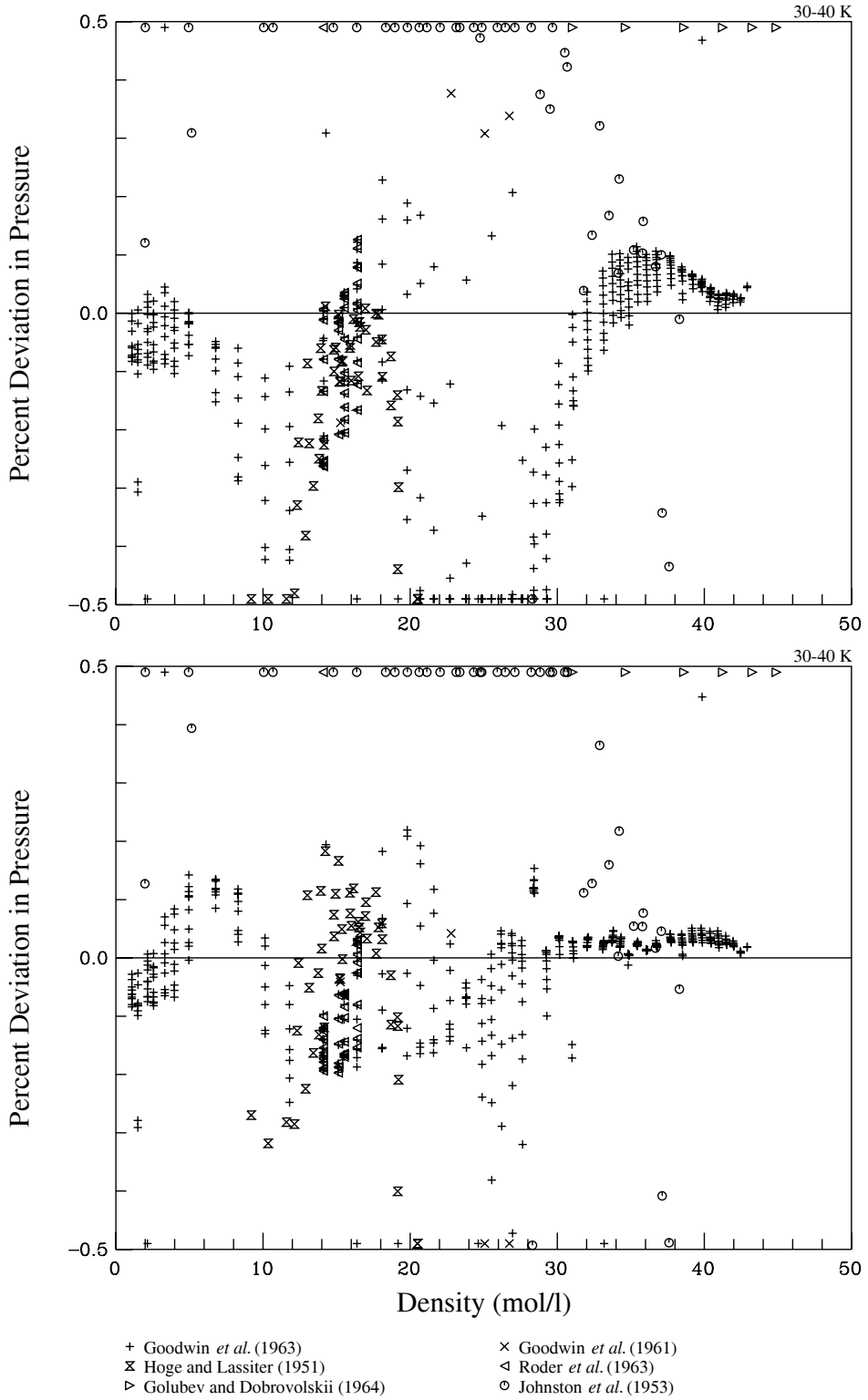

Figure 7.15 Deviation of Pressure of the Parahydrogen EOS of Younglove [14] (top) and the new Parahydrogen EOS (bottom) from experimental data. (Data displayed in 10 K increment from 30-40 K)

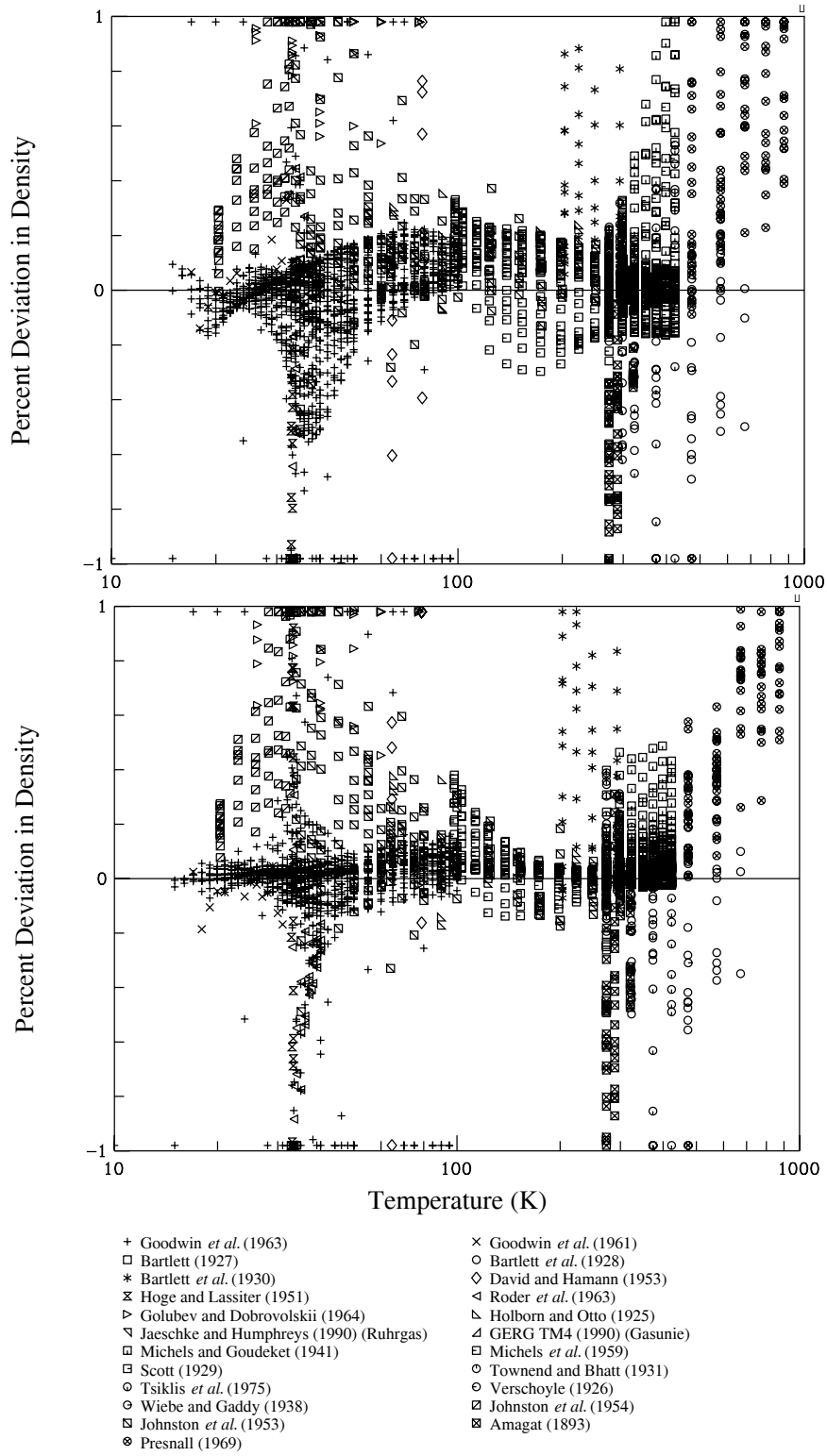

Figure 7.16 Deviation of Density of the Parahydrogen EOS of Younglove [14] (top) and the new Parahydrogen EOS (bottom) from experimental data. (Data plotted against temperature)

7.2 Comparison of Calculated Normal Hydrogen Properties to Data

Figures 7.17-7.31 display comparison plots for the new and old normal hydrogen equations of state. Due to the similar form of the new parahydrogen and new normal hydrogen equations of state, similar trends and uncertainties exist with the formulations. Notable exceptions will be discussed here.

The deviation of Vapor Pressure plotted versus temperature is displayed in Figure 7.21. The change in scale of the y-axis between plots indicates a significant improvement in representation of the new normal hydrogen equation of state. The Hiza [95] data are the most recent available. The Scott [97] data were chosen as primary below the normal boiling point. The significant improvement over the old equation of state is due to the old normal hydrogen equation of state predicting the same vapor pressures as the parahydrogen equation of state. This is due to the real fluid portion of the formulations being identical.

Figure 7.22 is the same as the bottom plot of Figure 7.21 except that Figure 7.22 includes data predicted using the Quantum Law of Corresponding States. Vapor pressure values were calculated using the new parahydrogen equation of state and transformed to the normal hydrogen surface using the procedure discussed in Section 3.3. The deviations indicate the predicted data trend with the Hiza [95] data set and indicate the Scott [97] data are the closest data set to the predicted in the low temperature range. This indicated the accuracy of the Quantum Law of Corresponding States as a tool for prediction of normal hydrogen and orthohydrogen properties near the critical region.

Figures 7.23-7.30 display deviations in density for the new normal hydrogen and old normal hydrogen equations of state. The Quantum Law of Corresponding States was used to transform the single phase data of Goodwin *et al.* [47] and Roder *et al.* [50] to the normal hydrogen surface of state; once transformed the data agreed fairly closely to those of Johnston *et al.* [74]. The deviations of

density from the transformed data are included in Figures 7.23, 7.24, and 7.30. The deviations of pressure from the transformed data are included in Figure 7.31. The original Goodwin *et al.* [47] and Roder *et al.* [50] data are included in the figures to display similarities between the normal hydrogen and parahydrogen surface of state. At pressures over 20 MPa the deviations between original and transformed data become small.

The estimated uncertainties in the normal hydrogen equation of state based on the deviations shown in Figures 7.17-7.31 are similar to the new parahydrogen equation of state. The deviation in density are 0.1% at temperatures from the triple point to 250 K and at pressures up to 40 MPa, except in the critical region, where an uncertainty of 0.2% in pressure is generally observed. In the region between 250 and 450 K and at pressures from 0.1 to 300 MPa, the uncertainty in density is 0.04%. At temperatures between 450 and 1000 K, the uncertainty in density increases to 1%. At pressures between 300 and 2000 MPa, the uncertainty in density is 8%. Speed of sound data are represented within 0.5% below 100 MPa. The estimated uncertainty for heat capacities is 1.0%. The estimated uncertainties of vapor pressures and saturated liquid densities calculated using the Maxwell criterion are 0.2% for each property. The increased uncertainty near the critical region versus the new parahydrogen EOS is evident the large deviations among data sets in that region.

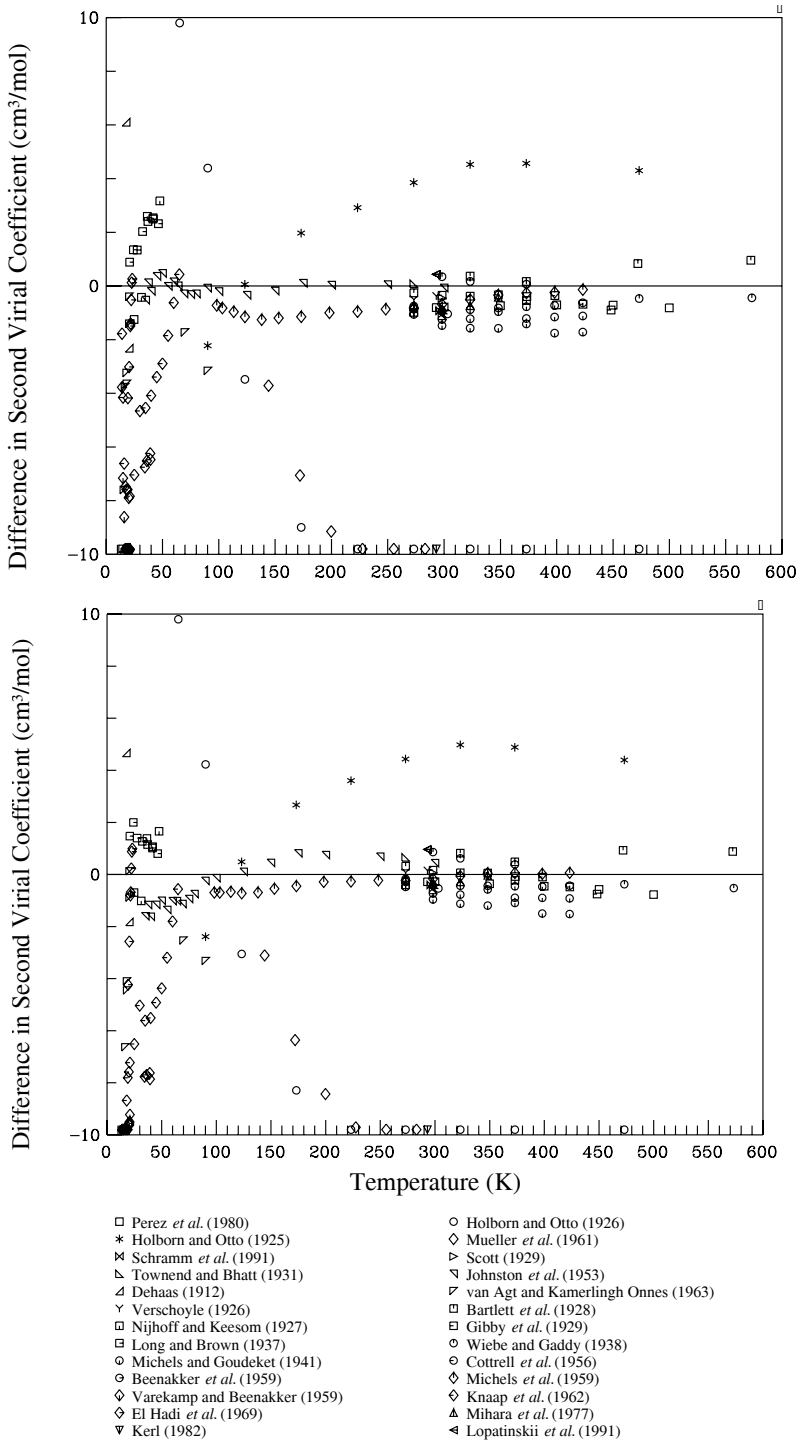

Figure 7.17 Difference in Second Virial Coefficient plotted versus Temperature for the Normal Hydrogen EOS of REFPROP [4] (top) and the New Normal Hydrogen EOS (bottom) from experimental data.

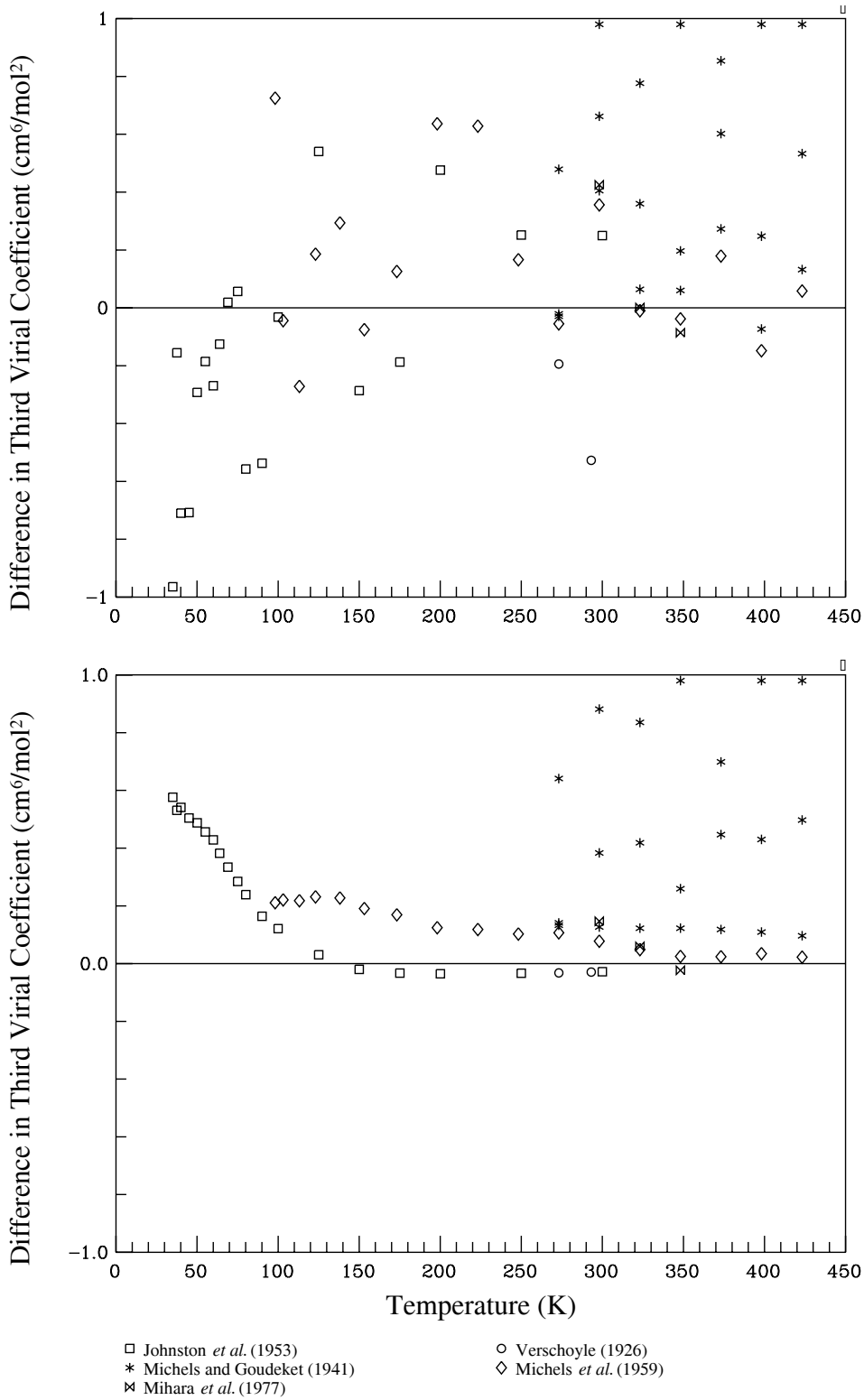

Figure 7.18 Difference in Third Virial Coefficient plotted versus Temperature for the Normal Hydrogen EOS of REFPROP [4] (top) and the New Normal Hydrogen EOS (bottom) from experimental data.

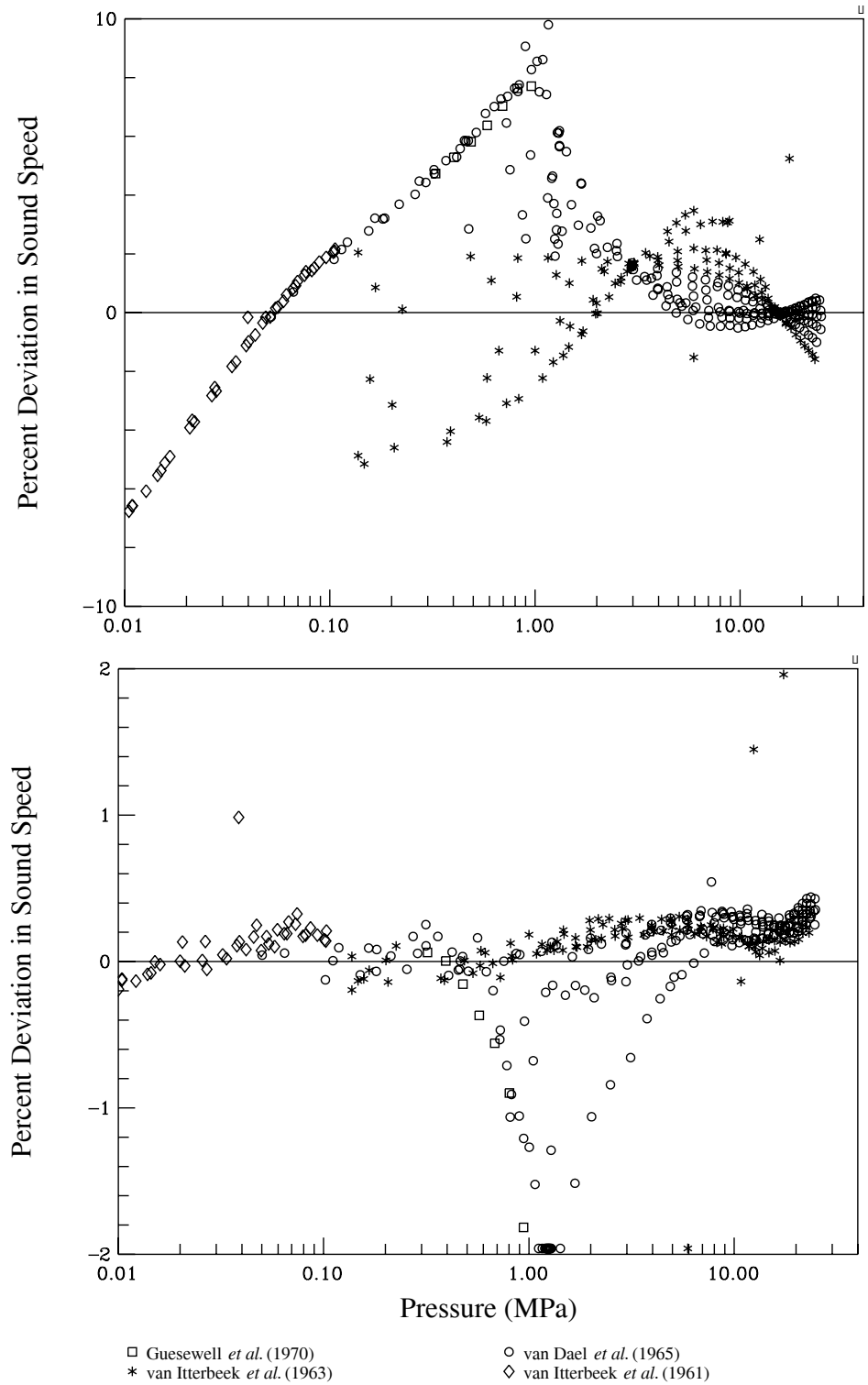

Figure 7.19 Deviation of Sound Speed plotted versus Pressure for the Normal Hydrogen EOS of REFPROP [4] (top) and the New Normal Hydrogen EOS (bottom) from experimental data.

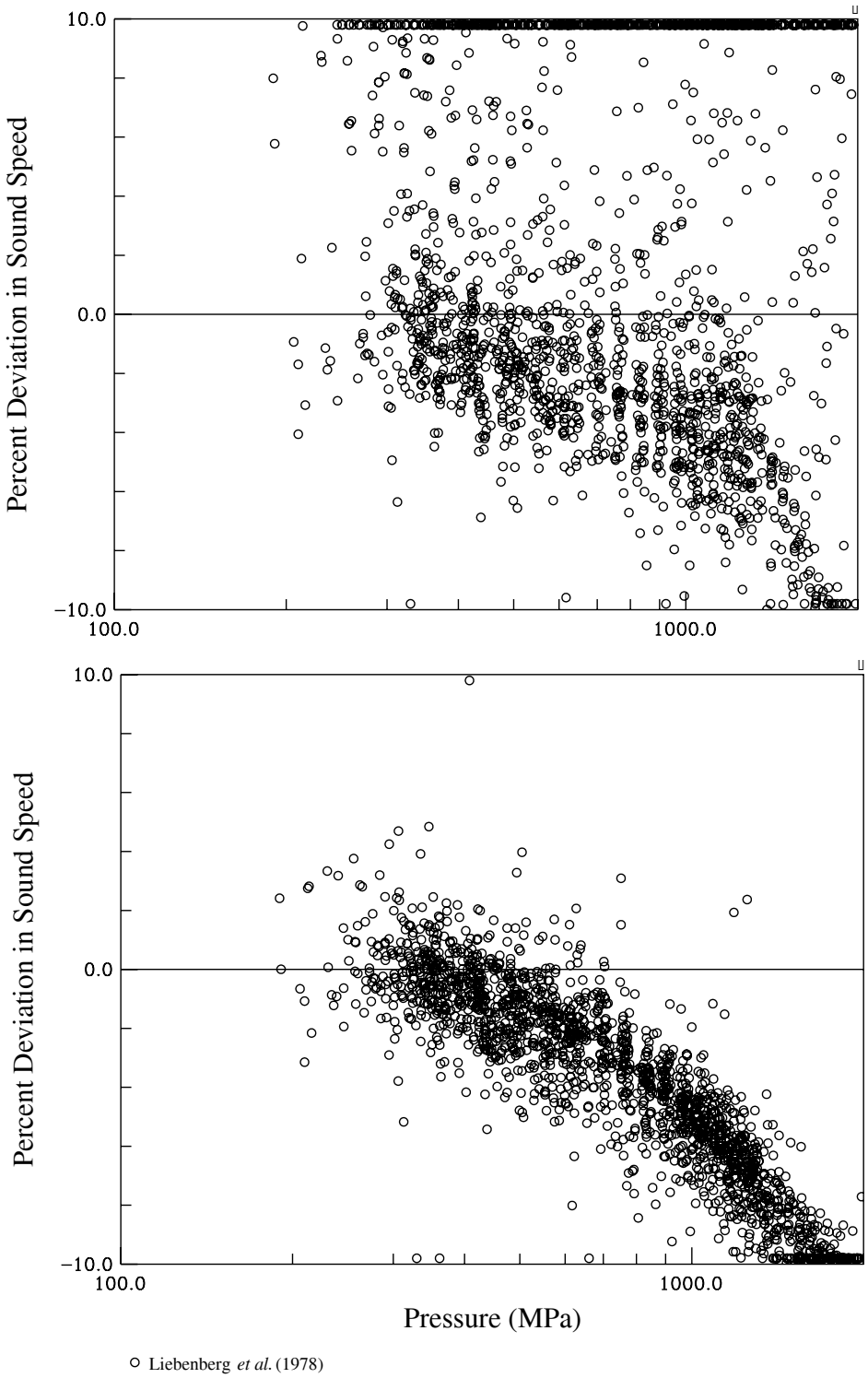

Figure 7.20 Deviation of Sound Speed plotted versus Pressure for the Normal Hydrogen EOS of REFPROP [4] (top) and the New Normal Hydrogen EOS (bottom) from high pressure experimental data.

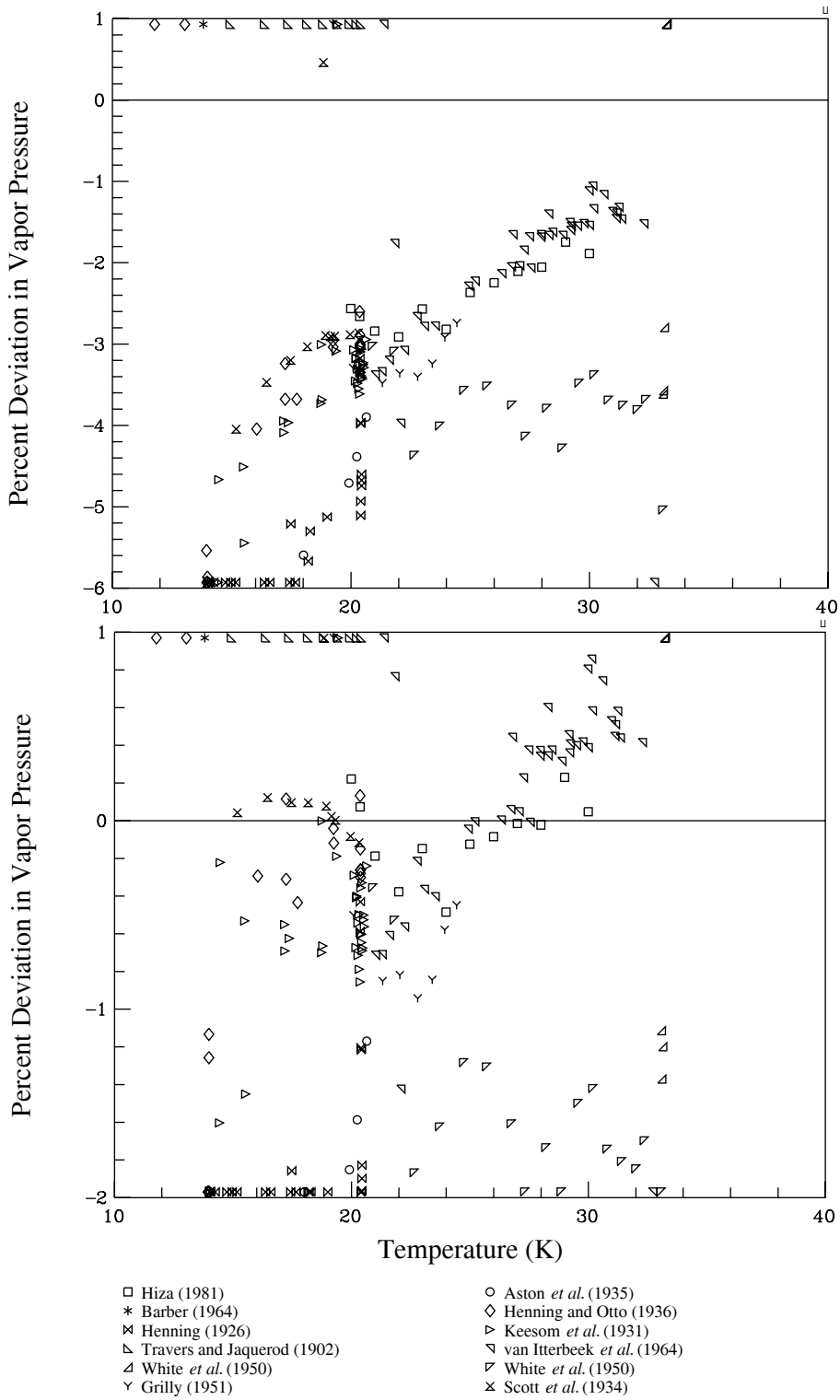

Figure 7.21 Deviation of Vapor Pressure plotted versus Temperature for the Normal Hydrogen EOS of REFPROP [4] (top) and the New Normal Hydrogen EOS (bottom) from experimental data.

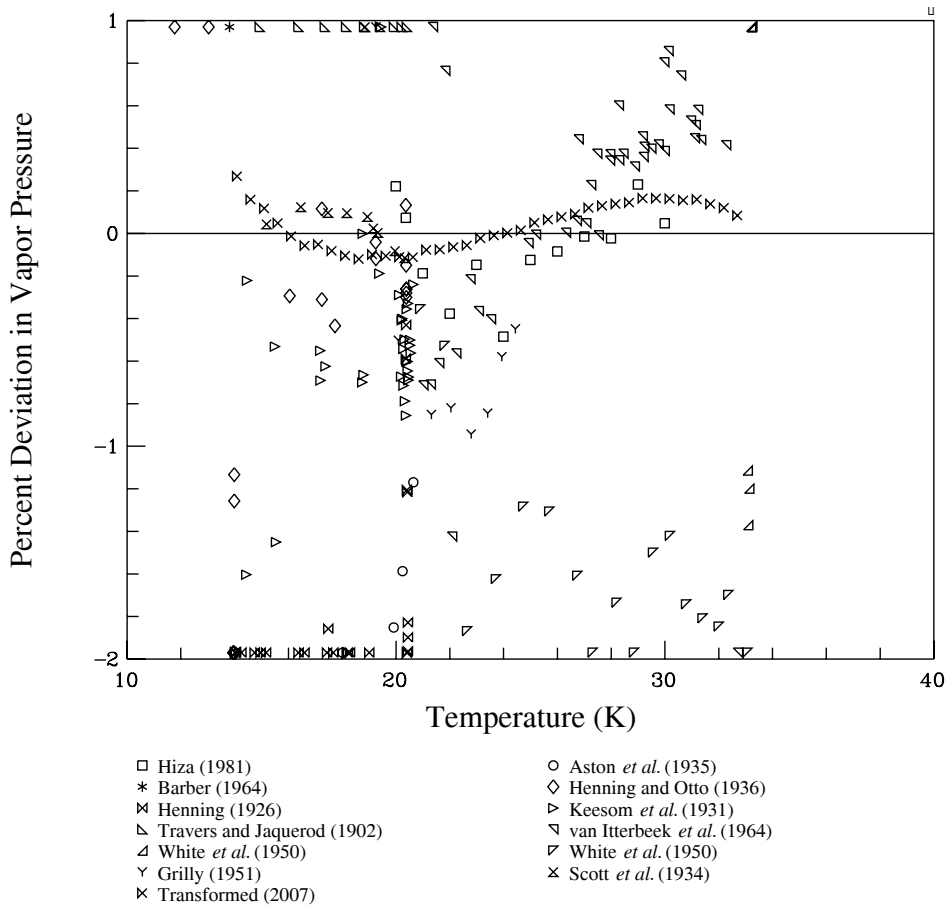

Figure 7.22 Deviation of Vapor Pressure plotted versus Temperature for the New Normal Hydrogen EOS with Transformed Parahydrogen data.

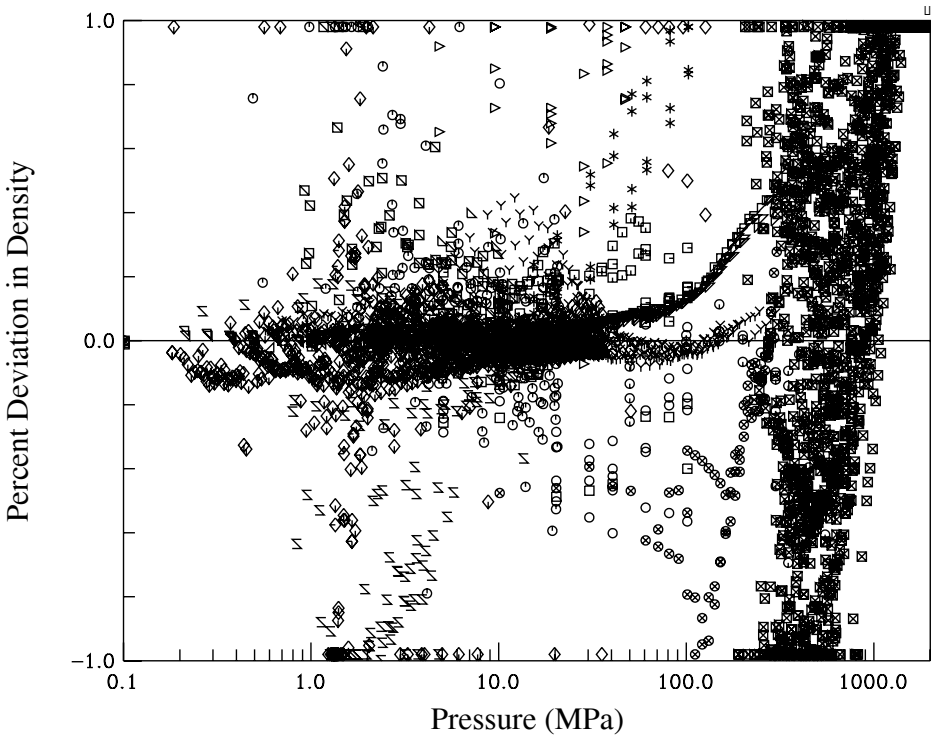

- Bartlett (1927)
- Bartlett *et al.* (1928)
- Bartlett *et al.* (1930)
- David and Hamann (1953)
- Golubev and Dobrovolskii (1964)
- Holborn and Otto (1925)
- Jaeschke and Humphreys (1990) (Ruhrgas)
- GERG TM4 (1990) (Gasunie)
- Michels and Goudeket (1941)
- Michels *et al.* (1959)
- Scott (1929)
- Townend and Bhatt (1931)
- Verschoyle (1926)
- Wiebe and Gaddy (1938)
- Johnston *et al.* (1953)
- Tsiklis *et al.* (1975)
- Transformed Goodwin *et al.* (2007)
- Transformed Roder *et al.* (2007)
- van Itterbeek *et al.* (1966)
- Johnston *et al.* (1954)
- Liebenberg *et al.* (1977)
- Amagat (1893)

Figure 7.23 Deviation of Density plotted versus Pressure for the New Normal Hydrogen EOS.

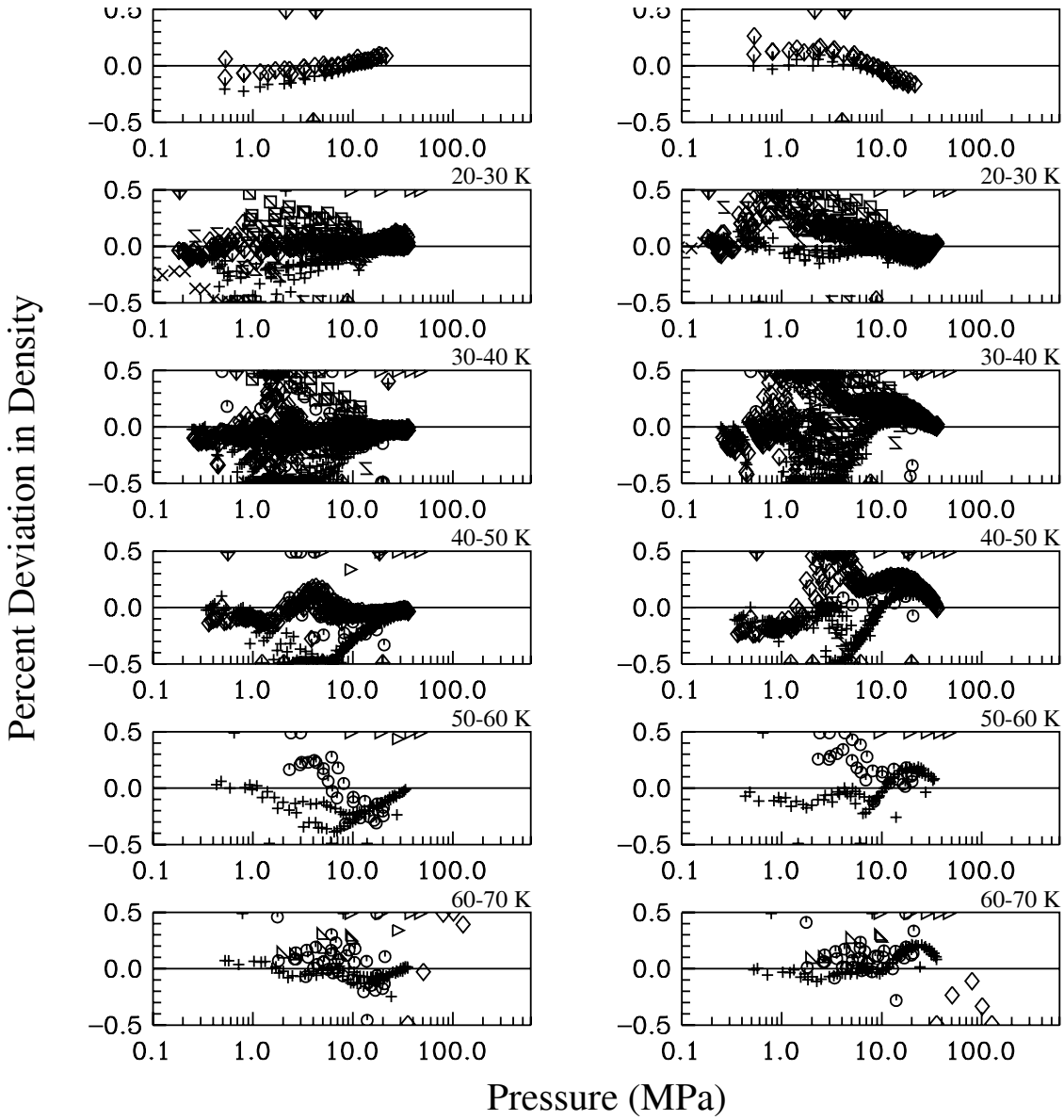

Figure 7.24 Deviation of Density plotted versus Pressure for the Normal Hydrogen EOS of REFPROP [4] (right) and the New Normal Hydrogen EOS (left) from experimental data (Data plotted in 10 K increments from 10-80 K).

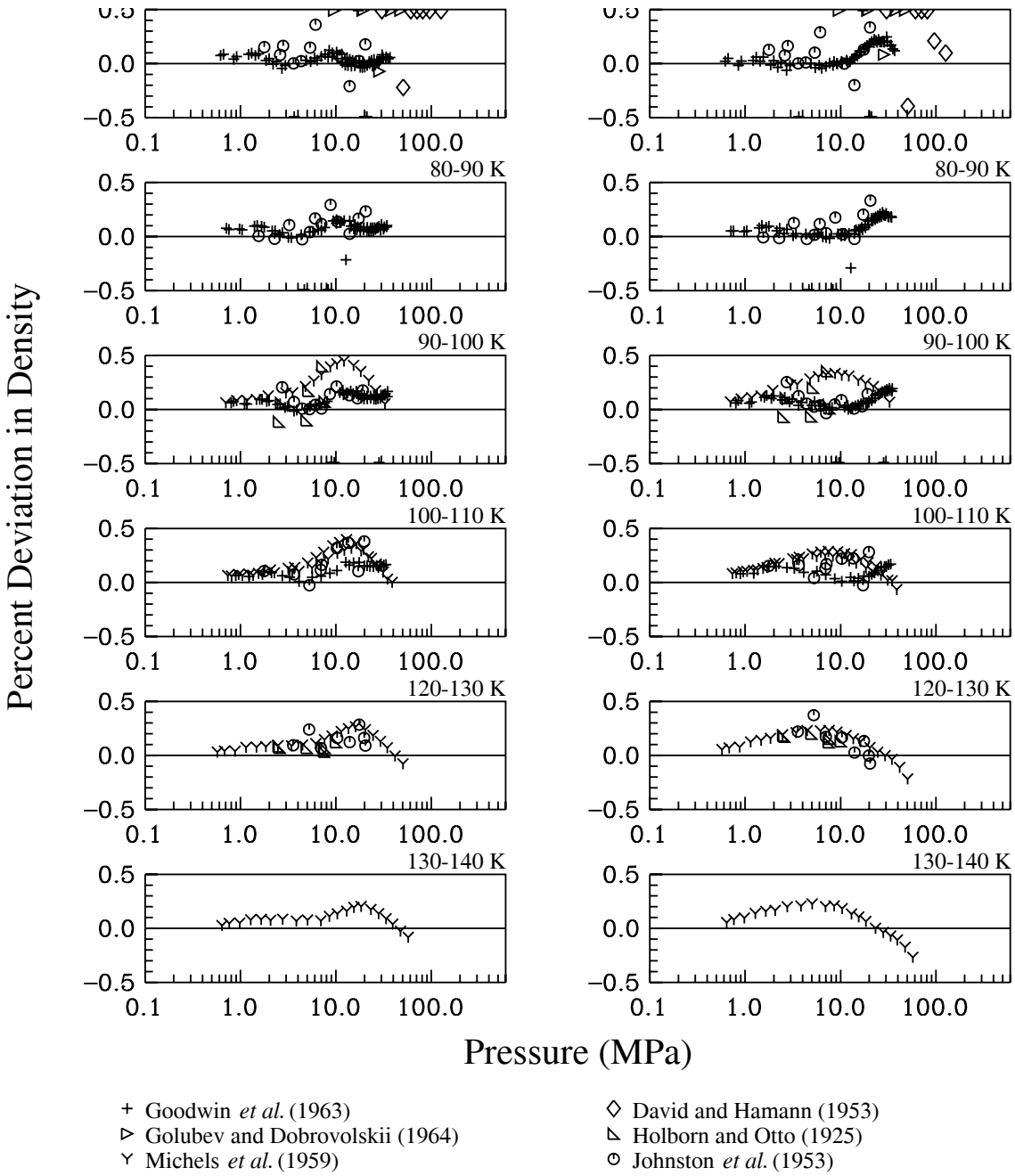

Figure 7.25 Deviation of Density plotted versus Pressure for the Normal Hydrogen EOS of REFPROP [4] (right) and the New Normal Hydrogen EOS (left) from experimental data (Data plotted in 10 K increments from 70-140 K).

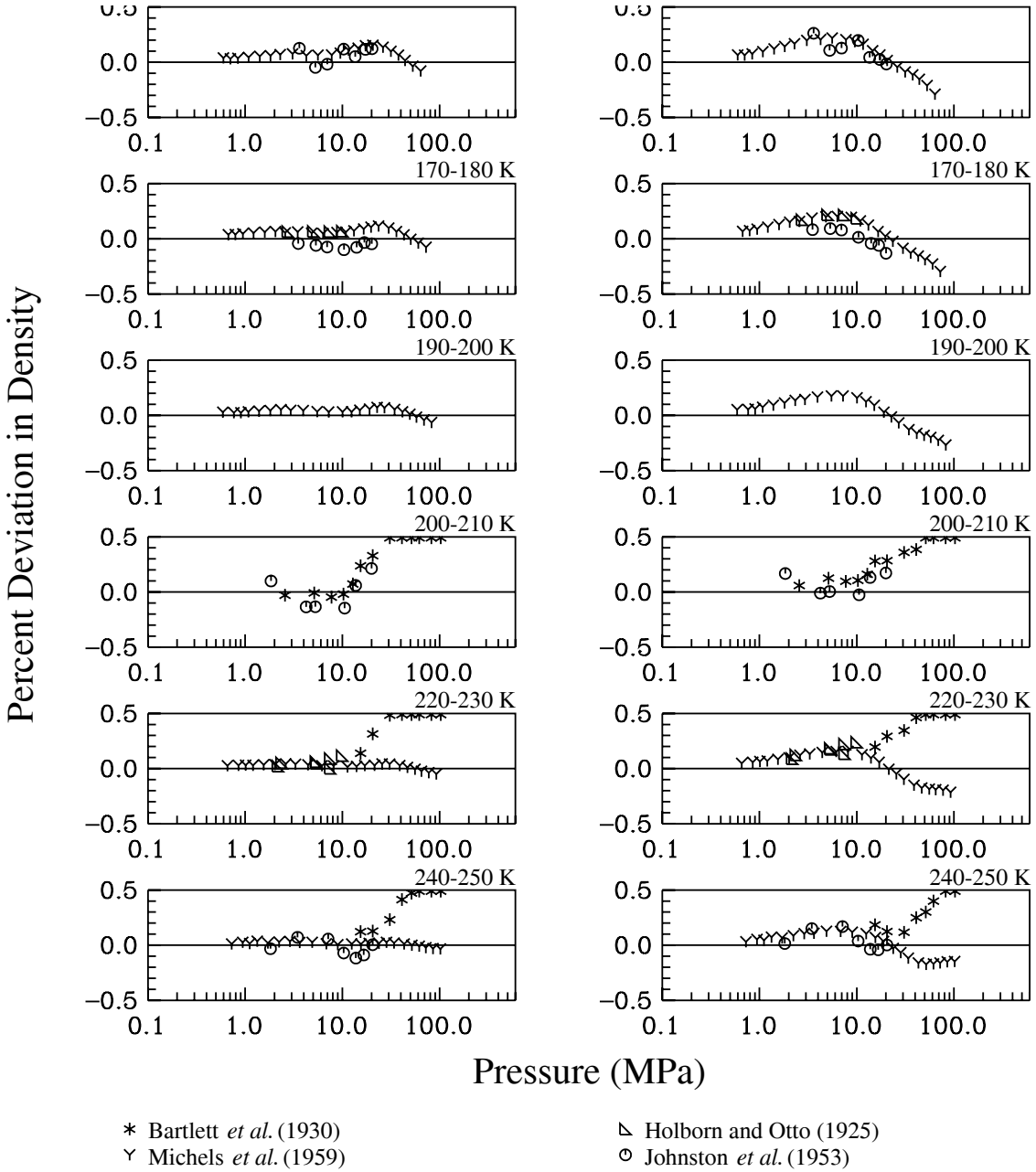

Figure 7.26 Deviation of Density plotted versus Pressure for the Normal Hydrogen EOS of REFPROP [4] (right) and the New Normal Hydrogen EOS (left) from experimental data (Data plotted in 10 K increments from 150-250 K).

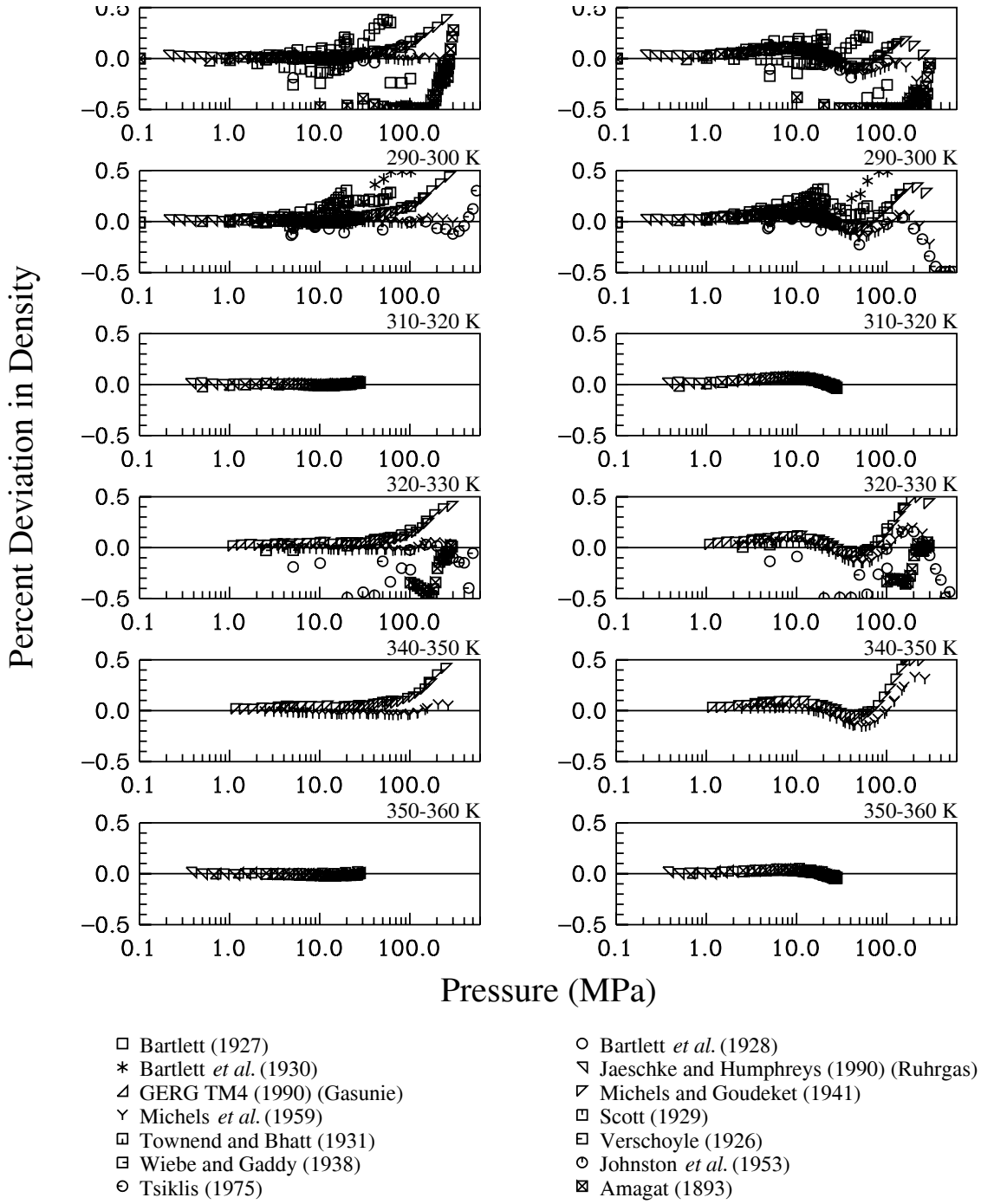

Figure 7.27 Deviation of Density plotted versus Pressure for the Normal Hydrogen EOS of REFPROP [4] (right) and the New Normal Hydrogen EOS (left) from experimental data (Data plotted in 10 K increments from 270-360 K).

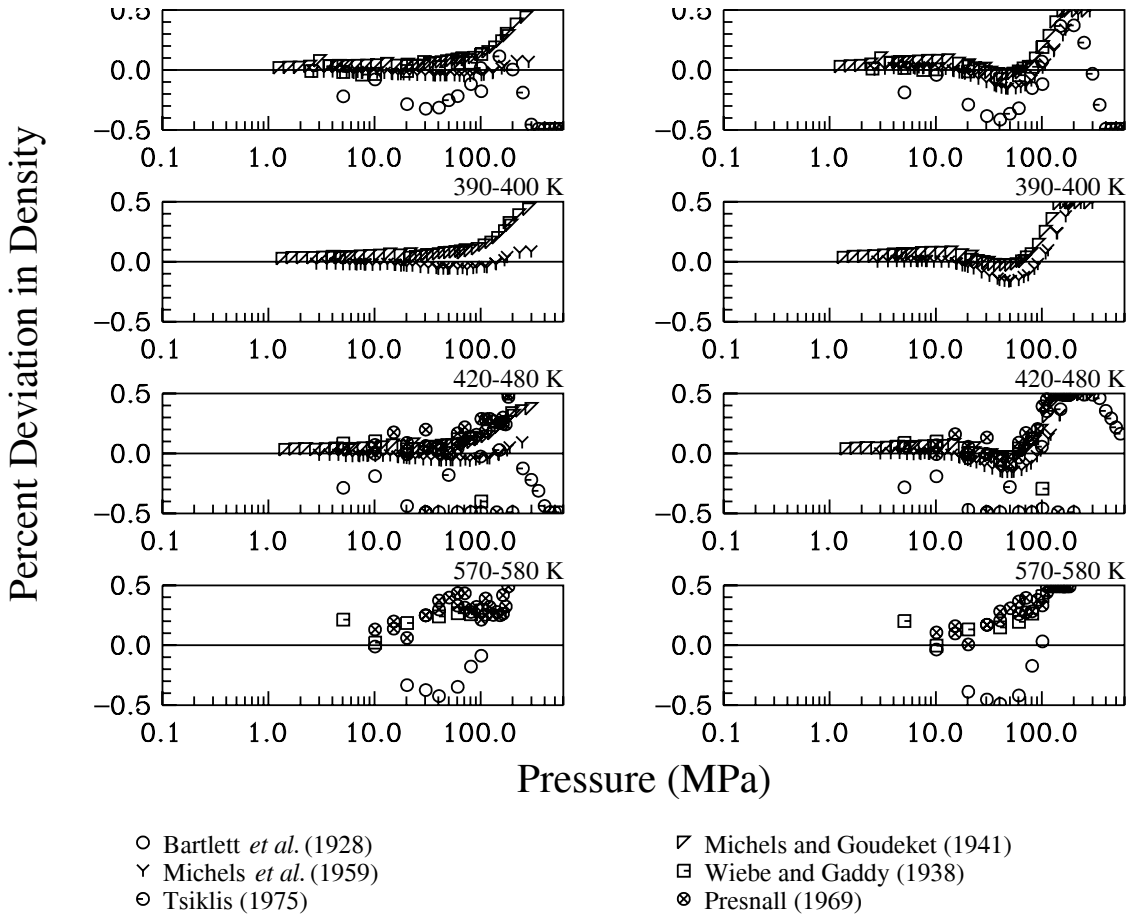

Figure 7.28 Deviation of Density plotted versus Pressure for the Normal Hydrogen EOS of REFPROP [4] (right) and the New Normal Hydrogen EOS (left) from experimental data (Data plotted in listed increments from 370-580 K).

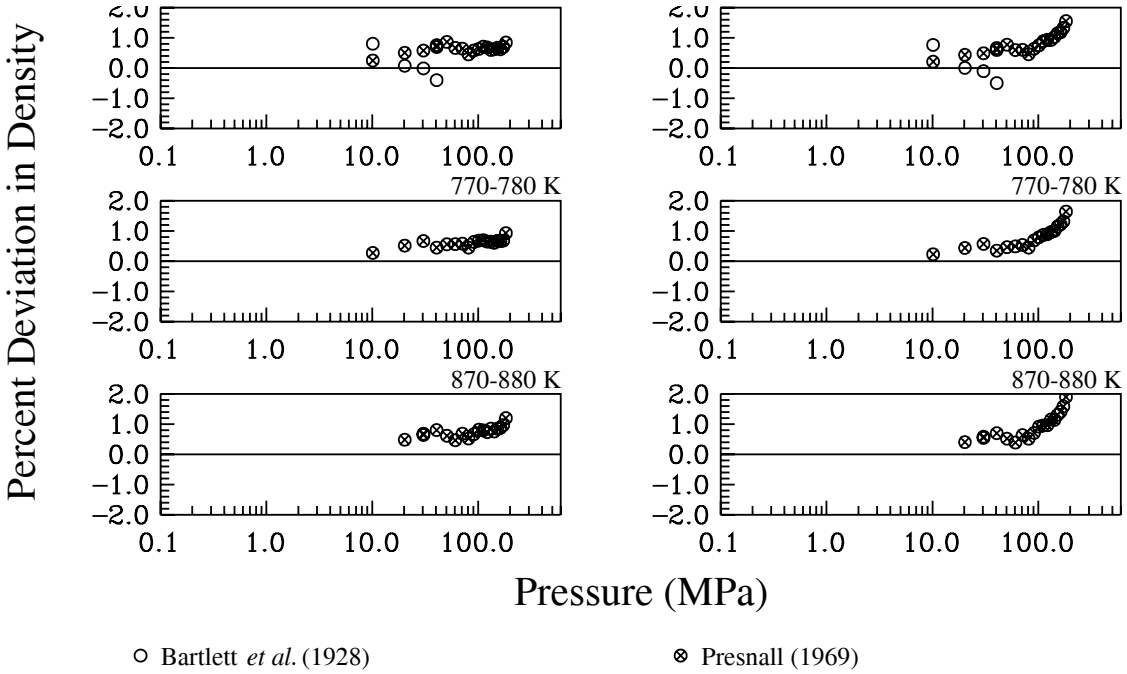

Figure 7.29 Deviation of Density plotted versus Pressure for the Normal Hydrogen EOS of REFPROP [4] (right) and the New Normal Hydrogen EOS (left) from experimental data (Data plotted in listed increments from 670-880 K).

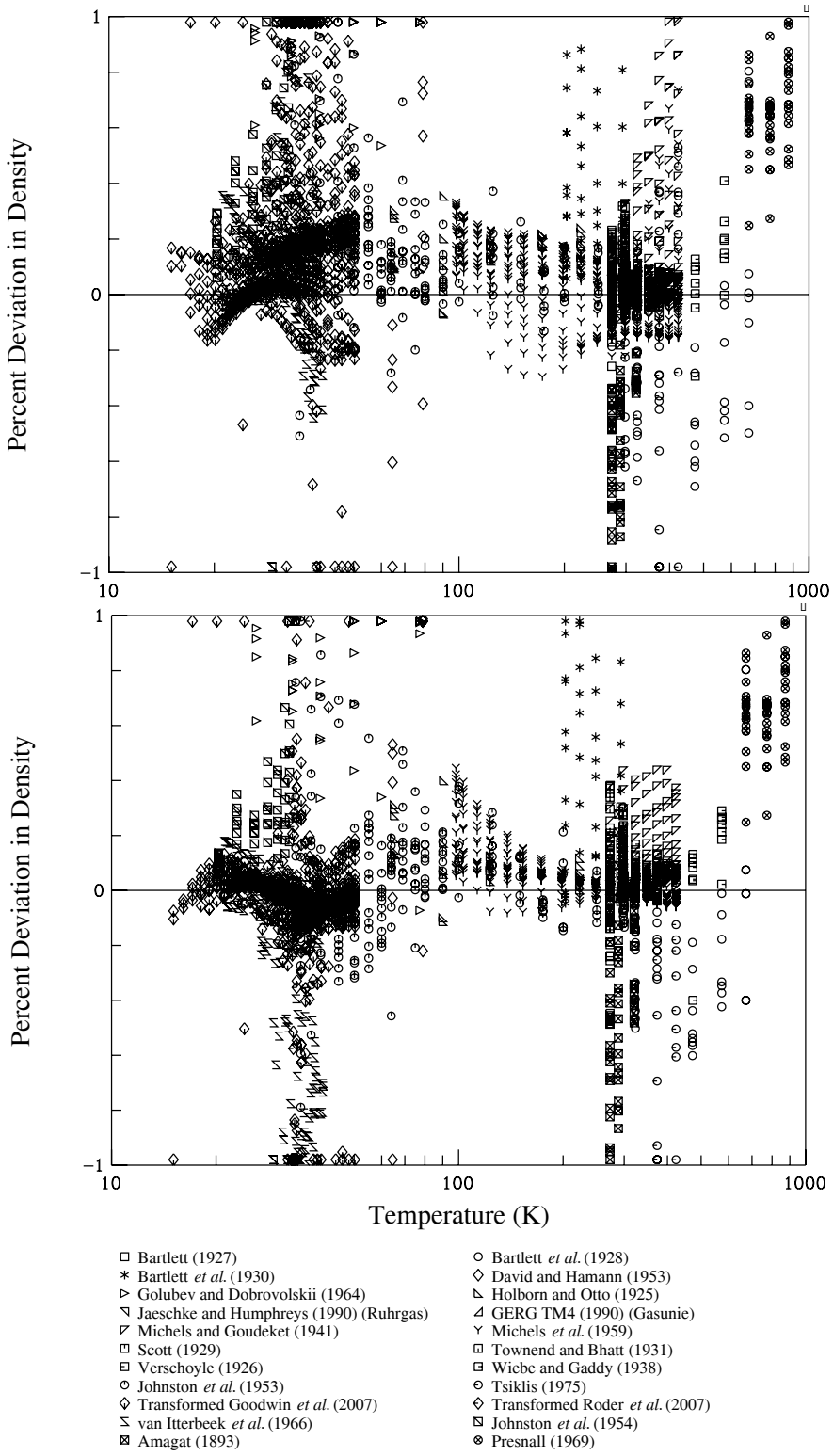

Figure 7.30 Deviation of Density plotted versus Temperature for the Normal Hydrogen EOS of REFPROP [4] (top) and the New Normal Hydrogen EOS (bottom) from experimental data.

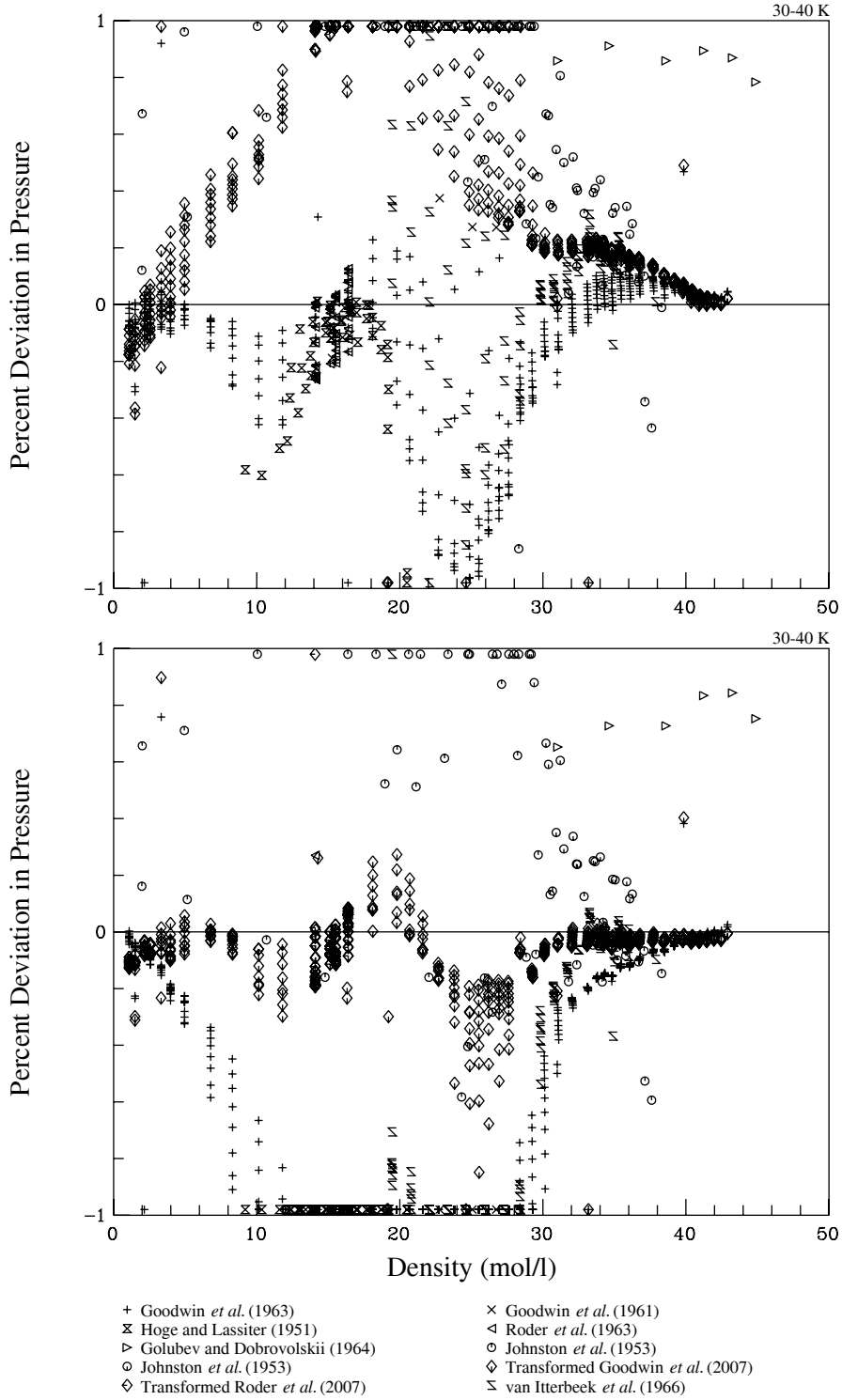

Figure 7.31 Deviation of Pressure plotted versus Density for the Normal Hydrogen EOS of REFPROP [4] (top) and the New Normal Hydrogen EOS (bottom) from experimental data (Data displayed in one 10 K increment from 30-40 K).

7.3 Comparison of Calculated Orthohydrogen Properties to Data

Due to the similarities between the normal hydrogen and orthohydrogen surfaces of state, normal hydrogen data is included in the graphs of this section for comparison. Only data that could be verified by comparison with existing experimental data was selected for transformation to the orthohydrogen surface of state.

Figure 7.33 displays the deviations from predicted speed of sound data for the orthohydrogen equation of state. All of the available measurements near the critical region for the speed of sound of normal hydrogen except those of Gusewell *et al.* [86] were transformed to the orthohydrogen surface. The normal hydrogen data were selected because the differences in parahydrogen sound speed data sets are larger than the predicted difference between the orthohydrogen and parahydrogen surfaces of state. These differences in the experimental data sets may be resolved in future work.

Figures 7.34-7.36 display deviations in density including data transformed to the orthohydrogen surface of state. The deviations are similar to those for the parahydrogen and normal hydrogen formulations. Although no comparisons to actual orthohydrogen experimental data can be made, the uncertainties in the new orthohydrogen formulation are similar to those of the normal hydrogen and parahydrogen formulations due to the similarities of the formulations.

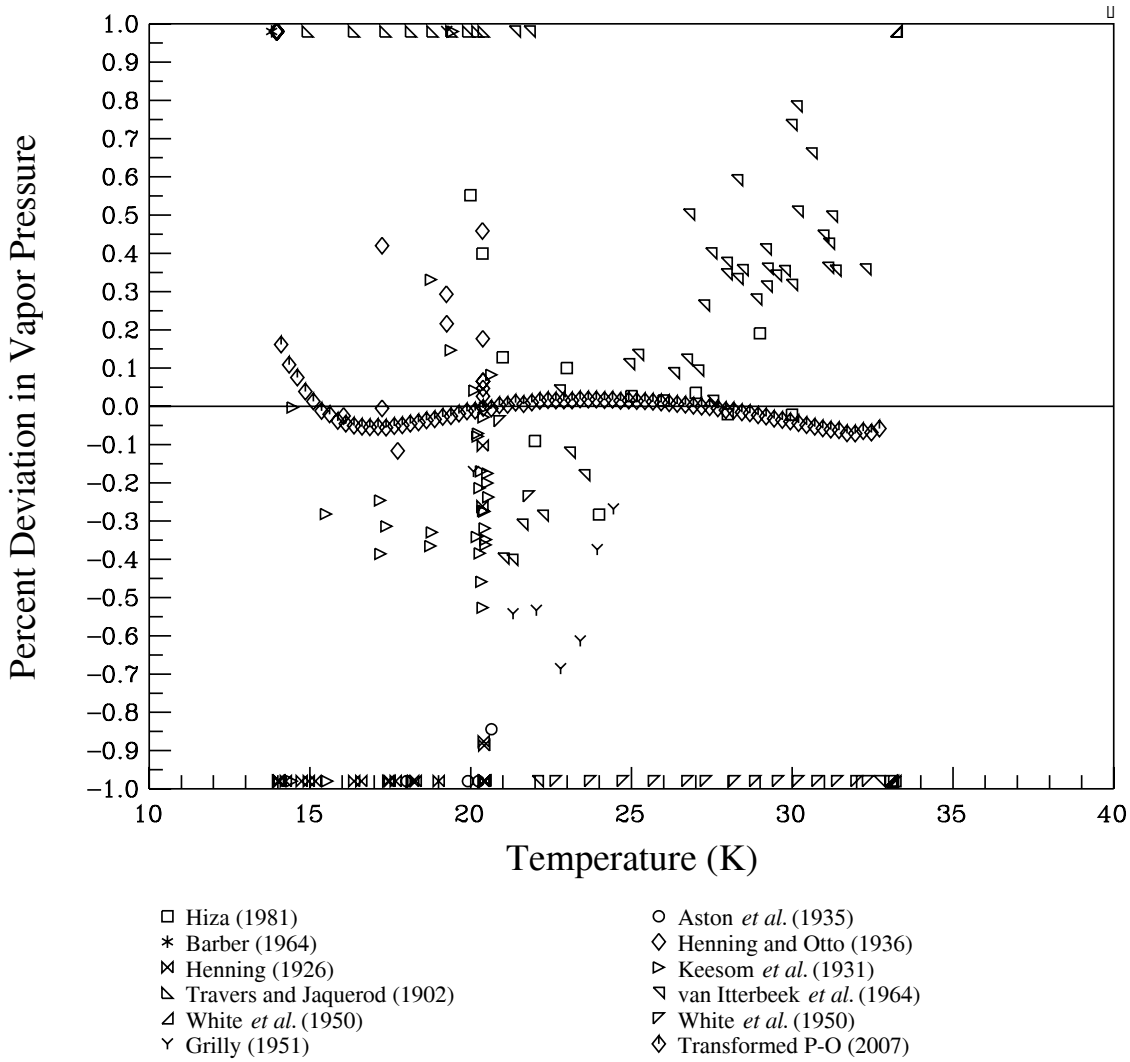

Figure 7.32 Deviation of Vapor Pressure plotted versus Temperature for the New Orthohydrogen EOS from Experimental and Predicted data.

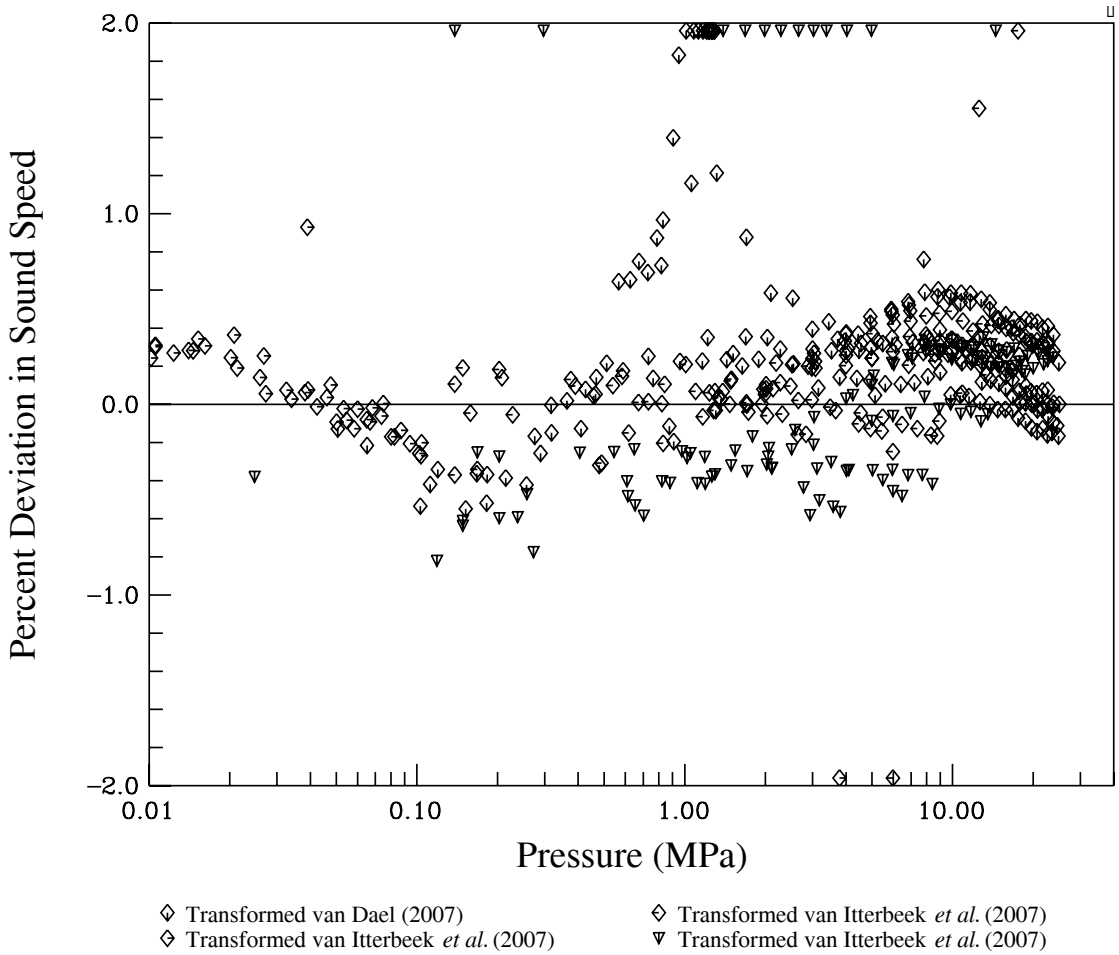

Figure 7.33 Deviation of Sound Speed plotted versus Pressure for the New Orthohydrogen EOS from Predicted data.

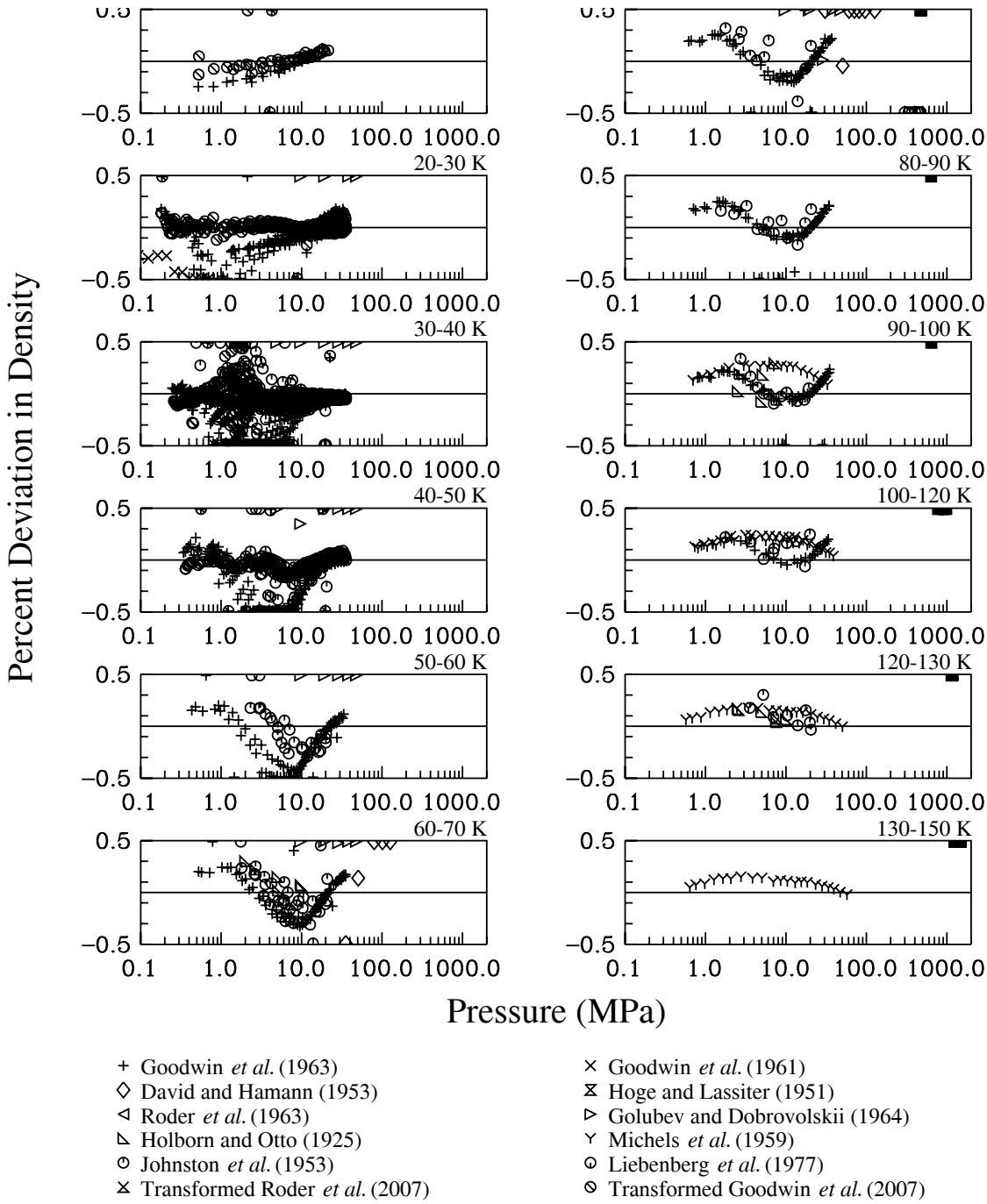

Figure 7.34 Deviation of Density plotted versus Pressure for the New Orthohydrogen EOS from Experimental and Predicted data. (Data shown in increments from 10-150 K)

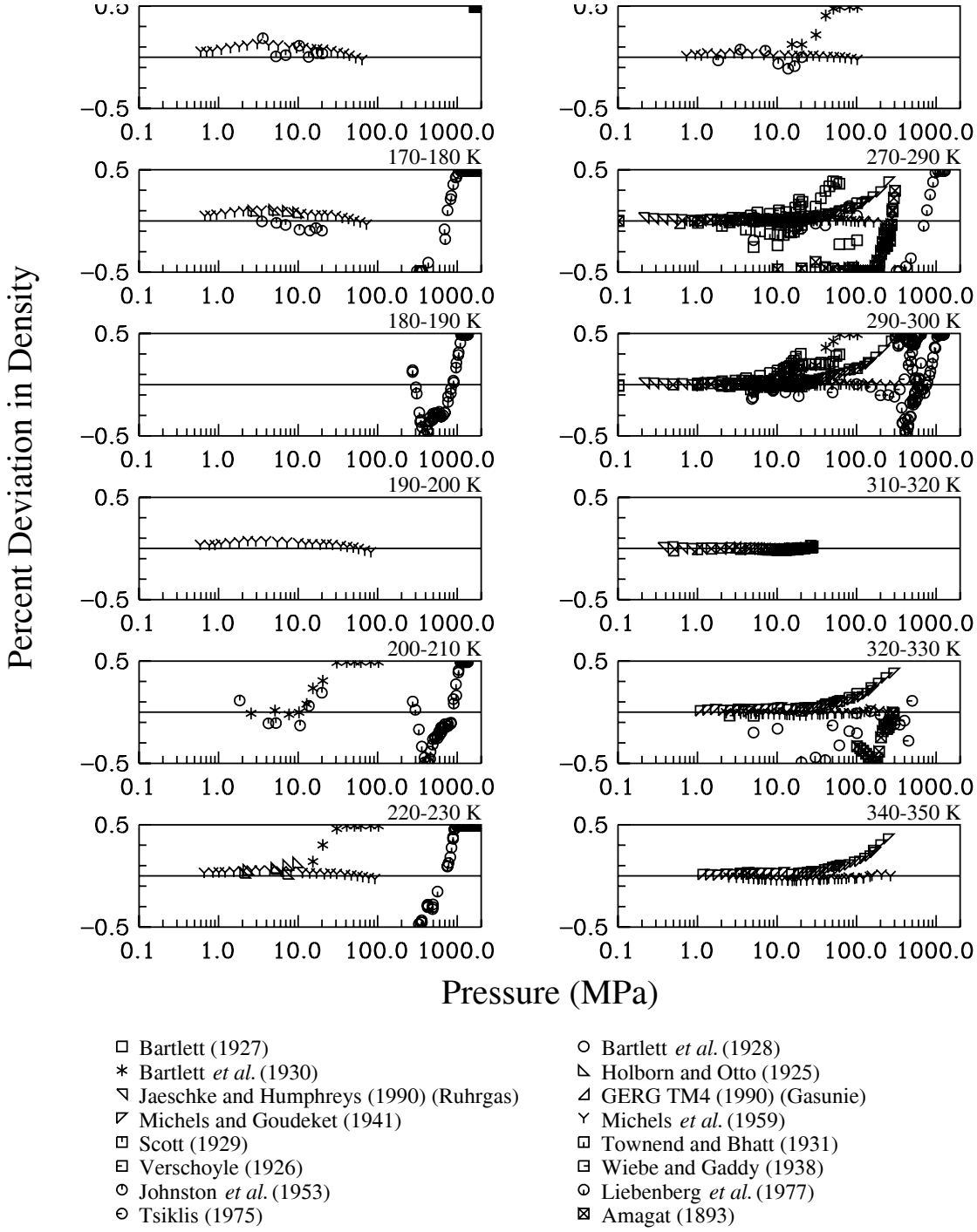

Figure 7.35 Deviation of Density plotted versus Pressure for the New Orthohydrogen EOS from Experimental and Predicted data. (Data shown in increments from 150-350 K)

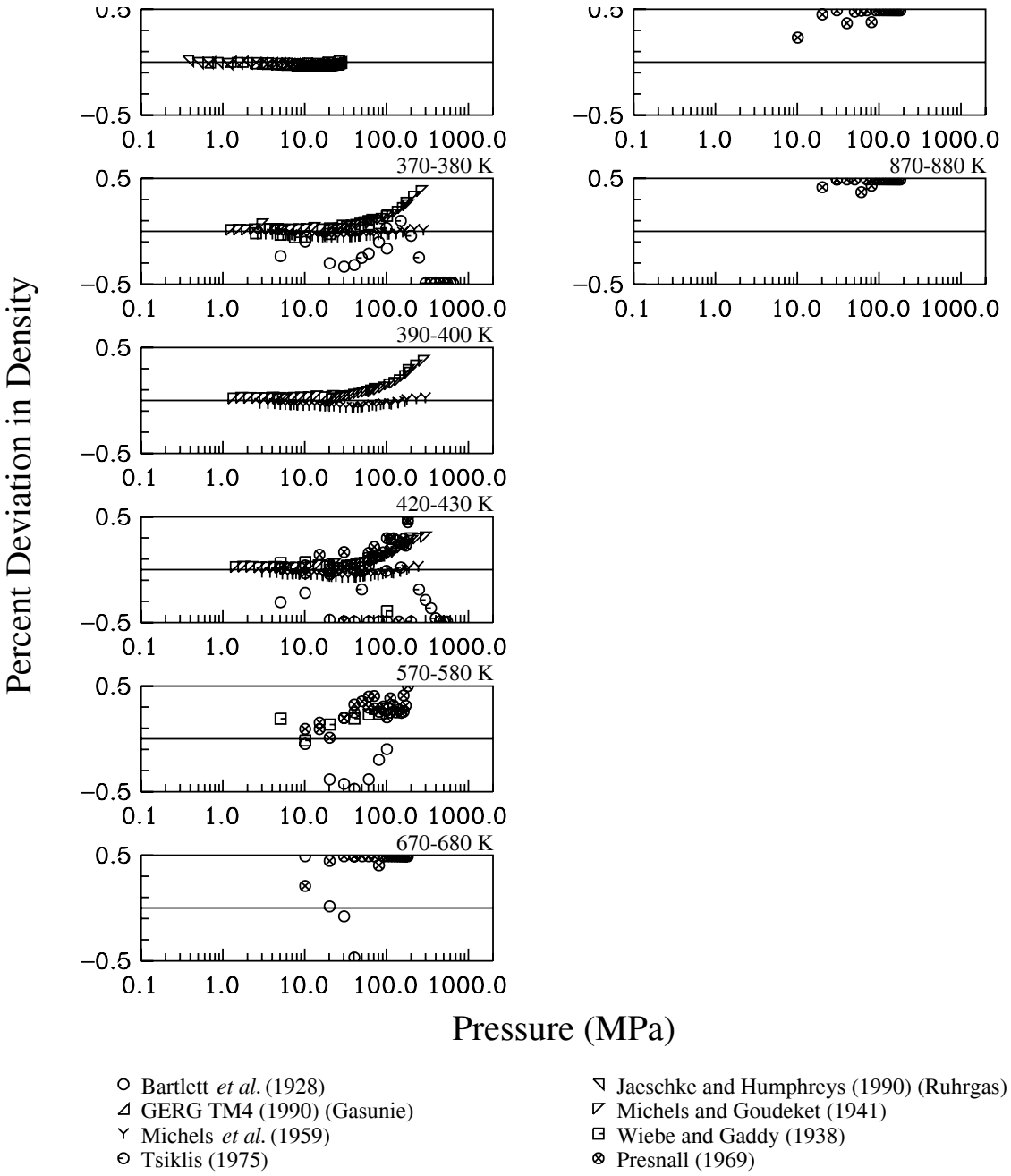

Figure 7.36 Deviation of Density plotted versus Pressure for the New Orthohydrogen EOS from Experimental and Predicted data. (Data shown in increments from 350-880 K)

8. Current Status and Recommendations for Future Research

Three new fundamental equations of state for parahydrogen, normal hydrogen, and orthohydrogen have been developed. The equations represent the available experimental data to within the estimated uncertainty of the data. The formulations extend the existing range of property prediction from an EOS and improve the uncertainty in properties predicted. The formulations predict different caloric and near critical region properties between parahydrogen, orthohydrogen, and their mixture normal hydrogen. The Quantum Law of Corresponding States was used to create data for orthohydrogen and normal hydrogen in regions where little data existed or the trends in existing data were unclear.

Although calculated vapor pressure, experimental density, and experimental sound speed data were transformed to the normal hydrogen and orthohydrogen surface, no attempt was made to transform other experimental data. This is due to no experimental data existing to evaluate the accuracy of the transformation. The calculated heat capacities of the normal hydrogen and orthohydrogen equations, therefore, have never compared to experimental data because none exist for comparison.

There are many applications of hydrogen in mixtures of other fluids including natural gas which may contain greater than 20 percent hydrogen at various equilibrium states. The equations of state created in this work could be used in a mixture model to accurately determine these properties which are not yet available.

9. References

1. Wikipedia contributors, 'Whistler, British Columbia', *Wikipedia, The Free Encyclopedia,* 2006,<http://en.wikipedia.org/w/index.php?title=Whistler%2C_British_Columbia&oldid=55117469> [accessed 5 March 2006].
2. 'Hydrogen Fueling Stations and Vehicle Demonstration Programs', California Fuel Cell Partnership, 2005. <http://www.cafcp.org/fuel-vehl_map.html> [accessed 6 June 2006].
3. Veziroglu, TN; Barbir, F., "Hydrogen: the wonder fuel" International Journal of Hydrogen Energy 17 (1992) 391-404.
4. Lemmon, E.W., McLinden, M.O., Huber, M.L. NIST Standard Reference Database 23: Reference Fluid Thermodynamic and Transport Properties-REFPROP, Beta Version 7.1 National Institute of Standards and Technology, Standard Reference Data Program, Gaithersburg, 2005.
5. Jacobsen, R.T, Leachman, J.W., "A Review of the Status of the Thermophysical Properties of Hydrogen Including Thermodynamic Properties and Transport Properties." Report to National Institute of Standards and Technology on Order NO. RA 1341-05-SE-6352, June 2006.
6. Jacobsen, R.T, Leachman, J.W., Penoncello, S.G., Lemmon, E.W., "Current Status of Thermodynamic Properties of Hydrogen." International Journal of Thermophysics, currently in review, 2006.
7. Leachman, J.W., Jacobsen, R.T, Penoncello, S.G., Huber, M.L., "Current Status of Transport Properties of Hydrogen." International Journal of Thermophysics, currently in review, 2006.
8. Woolley, H.W., Scott, R.B., and Brickwedde, F.G., Compilation of Thermal Properties of Hydrogen in Its Various Isotopic and Ortho-Para Modifications, Natl. Bur. Stand., Res. Paper RP1932, 379-475 pp, 1948.
9. Hust, J.G. and Stewart, R.B., A Compilation of the Property Differences of Ortho and Para Hydrogen or Mixtures of Ortho and Para Hydrogen, Natl. Bur. Stand., Rep. 8812, 38 pp, 1965.
10. McCarty, R.D. and Weber, L.A., Thermophysical Properties of Parahydrogen from the Freezing Liquid Line to 5000 R for Pressures to 10,000 Psia, Natl. Bur. Stand., Tech. Note 617, 1972.
11. McCarty, R.D., Hydrogen Technological Survey - Thermophysical Properties, NASA Spec. Publ. (NASA-SP-3089), 1975.
12. Vargaftik, N.B., Tables on the Thermophysical Properties of Liquids and Gases, Hemisphere Publishing Company, 1975.
13. McCarty, R.D., Hord, J., and Roder, H.M., "Selected Properties of Hydrogen (Engineering Design Data)", Natl. Bur. Stand., Monogr. 168, 1981.

14. Younglove, B.A., " Thermophysical Properties of Fluids. I. Argon, Ethylene, Parahydrogen, Nitrogen, Nitrogen Trifluoride, and Oxygen," J. Phys. Chem. Ref. Data, 14(2):619, 1982.
15. Souers, P.C., "Hydrogen Properties for Fusion Energy" University of California Press, (1986).
16. Verkin, B.I., "Handbook of Properties of Condensed Phases of Hydrogen and Oxygen", Hemisphere Publishing Corporation, 1991.
17. National Institute of Standards and Technology Physical and Chemical Properties Division, "Thermophysical Properties of Hydrogen", <http://www.boulder.nist.gov/div838/Hydrogen/Publications/ Publicationsmain.htm>, [accessed January 4th 2006].
18. Spritzer, Michael H.; "Supercritical Water Partial Oxidation", Hydrogen, Fuel Cells, and Infrastructure Technologies, 2003, <http://www.eere.energy.gov> [accessed 5 March 2006].
19. Wikipedia contributors, 'Syngas', *Wikipedia, The Free Encyclopedia,* 2006, <http://en.wikipedia.org/w/index.php?title=Syngas&oldid=55099460> [accessed 5 March 2006].
20. Wikipedia contributors, 'Fischer-Tropsch process', *Wikipedia, The Free Encyclopedia,* 2006, <http://en.wikipedia.org/w/index.php?title=Fischer-Tropsch_process&oldid=55025810> [accessed 5 March 2006].
21. U.S. Department of Energy Energy Information Agency, "U.S. Daily Average Supply and Disposition of Crude Oil and Petroleum Products, 2004", 2005, <www.eia.doe.gov> [accessed 5 March 2006].
22. Wikipedia contributors, 'Hydrogen economy', *Wikipedia, The Free Encyclopedia,* 2006, <http://en.wikipedia.org/w/index.php?title=Hydrogen_economy&oldid=56948710> [accessed 5 March 2006].
23. U.S. Department of Energy Office of Nuclear Energy, "Advanced Nuclear Research: Nuclear Hydrogen Initiative", 2004, <http://www.ne.doe.gov/hydrogen/hydrogenBG.html> [accessed 5 March 2006].
24. U.S. Department of Energy Office of Science, "Basic Research Needs for the Hydrogen Economy", 2004, pg 32. <http://www.sc.doe.gov/bes/hydrogen.pdf> [accessed 5 March 2006].
25. U.S. Department of Energy Energy Efficiency and Renewable Energy, "Hydrogen Storage" 2006, <http://www.eere.energy.gov/hydrogenandfuelcells/storage/hydrogen_storage.html> [accessed 6 June 2006].
26. The National Hydrogen Association, "Frequently Asked Questions" 2007, <http://www.hydrogenassociation.org/general/faqs.asp> [accessed 2 April 2007].
27. U.S. Department of Energy Energy Information Agency, "Retail Gasoline Historical Prices", 2006 http://www.eia.doe.gov/oil_gas/petroleum/data_publications/wrgp/mogas_history.html> [accessed 6 June 2006].

28. Hydropole-The Swiss Hydrogen Association, "Properties of Hydrogen," <http://www.hydropole.ch/Hydropole/Intro/Hydrogen.htm> [accessed 9 March 2006].
29. Bonhoeffer, K.F. and Harteck, P., "About Para- and Orthohydrogen," (In German) Z. Physic. Chem. 4B (1929) 113.
30. Eucken, A. and Hiller, K., "The proof of a change of the Orthohydrogen in Parahydrogen by measurement of the specific heat," (In German) Z. Physic. Chem., 4B (1929) 142.
31. Heisenberg, V.W., "Mehrkörper probleme und Resonanz in der Quantenmechanik. II.," (In German) Z. Physik, 41 (1927), 239.
32. Farkas, Adalbert, "Orthohydrogen, parahydrogen and heavy hydrogen" Cambridge at the University Press (1935).
33. Ishii, Y., "Theory of non-dissociative ortho-para conversion on magnetic surfaces." Progress in Surface Science, 21(2) (1986), 163-208.
34. Milenko, Yu.Ya, Sibileva, R.M., and Strzhemechny, M.A., "Natural ortho-para Conversion Rate in Liquid and Gaseous Hydrogen," J. Low Temp. Phys. 107 (1997), 77-92.
35. Schmauch, G.E., Singleton, A.H., "Technical aspects of Ortho-Parahydrogen Conversion." Industrial and Engineering Chemistry, 56(5) (1964) 20-31.
36. Wigner, E., Z. Phys. Chem., B23 (1933) 28.
37. Kasai, H., Diño, W.A., and Huhida, R., "Surface Science-based reaction design: increasing the ortho-para hydrogen conversion yield via molecular orientation, a case study". Prog. Surf. Sci. 72 (2003) 53-86.
38. Stewart, A.T., Squires, G.L., "Analysis of ortho- and para-hydrogen mixtures by the thermal conductivity method," J. Sci. Instrum. 32 (1955) 26-29.
39. Bradshaw, T.W., Norris, J.O.W., "Observations on the use of a thermal conductivity cell to measure the para hydrogen concentration in a mixture of para and ortho hydrogen gas." Rev. Sci. Instrum. 58(1) (1987) 83-85.
40. Zhou, D., Ihas, G.G., Sullivan, N.S., "Determination of the ortho-para ratio in gaseous hydrogen mixtures," J. Low Temp. Phys. V. 134(1/2) (2004) 401-406.
41. Leachman, J.W., Jacobsen, R.T, Penoncello, S.G., "Near Critical Region Properties of Parahydrogen, Orthohydrogen, and Normal Hydrogen and the Quantum Law of Corresponding States." To be published, 2007.
42. Hirschfelder, J.O., Curtiss, C.F., Bird, R.B., "Molecular Theory of Gases and Liquids" John Wiley & Sons, Inc. (1954).
43. de Boer, J., "Gquantum Theory of Condensed Permanent Gases I: The Law of Corresponding States." Physica, 14(2-3) (1948) 139-148.
44. Hirschfelder, J.O., Curtiss, C.F., Bird, R.B., "Molecular Theory of Gases and Liquids" John Wiley & Sons, Inc. (1954).

45. Knaap, H.F., Beenakker, J.J., “The Lennard-Jones 6-12 Potential Parameters of H(2) and D(2).” Physica, 27 (1961) 523-530.
46. van Dael, W., van Itterbeek, A., Cops, A., Thoen, J., “Velocity of Sound in Liquid Hydrogen.” Cryogenics, (1965) 207-212.
47. Goodwin, R.D., Diller, D.E., Roder, H.M., and Weber, L.A., “Pressure-Density-Temperature Relations of Fluid Parahydrogen from 15 to 100 K at Pressures to 350 atmospheres,” J. Res. Nat. Bur. Stand. (U.S.) 67A(2): 173-192, 1963.
48. Goodwin, R.D., Diller, D.E., Roder, H.M., and Weber, L.A., "The Densities of Saturated Liquid Hydrogen," Cryogenics, 2(2):81-3, 1961.
49. Hoge, H.J. and Lassiter, J.W., "Critical Temperatures, Pressures, and Volumes of Hydrogen, Deuterium, and Hydrogen Deuteride," J. Res. Natl. Bur. Stand., 47(2):75-9, 1951.
50. Roder, H.M., Diller, D.E., Weber, L.A., and Goodwin, R.D., "The Orthobaric Densities of Parahydrogen, Derived Heats of Vaporization, and Critical Constants," Cryogenics, 3(1):16-22, 1963.
51. Younglove, B.A. and Diller, D.E., "The Specific Heat at Constant Volume of Para-Hydrogen at Temperatures from 15 to 90 Degrees K and Pressures to 340 Atm," Cryogenics, 2(6):348-52, 1962.
52. Mevedev, V.A., Dedikov, Yu. A., Orlova, M.P., “Isobaric Heat Capacity of Para-Hydrogen at 20 to 31 kgf cm(-2) and 20-50 degrees K.” Russ. J. Phys. Chem. (Engl. Transl.), 45(3)297-9, 1971.
53. Younglove, B.A., "Speed of Sound in Fluid Parahydrogen," J. Acoust. Soc. Am., 38(3):433-8, 1965.
54. van Itterbeek, A., van Dael, W., and Cops, A., "Velocity of Ultrasonic Waves in Liquid Normal and Para Hydrogen," Physica (Amsterdam), 27:111-6, 1961.
55. van Itterbeek, A., van Dael, W., and Cops, A., "The Velocity of Sound in Liquid Normal and Para Hydrogen as a Function of Pressure," Physica (Amsterdam), 29:965-73, 1963.
56. Barber, C.R., Horsford, A., "The determination of the boiling and triple points of equilibrium hydrogen and its vapour pressure-temperature relation." Br. J. Appl. Phys., 14:920-3, 1963.
57. Hoge, H.J. and Arnold, R.D., "Vapor Pressures of Hydrogen, Deuterium, and Hydrogen Deuteride and Dew-Point Pressures of their Mixtures," J. Res. Natl. Bur. Stand., 47(2):63-74, 1951.
58. Keesom, W.H., Bijl, A., and van der Horst, H., "Determination of the Boiling Points and the Vapour-Pressure Curves of Normal Hydrogen and of Para-Hydrogen. The Normal Boiling Point of Normal Hydrogen as a Basic Point in Thermometry," Commun. Kamerlingh Onnes Lab. Univ. Leiden (217A):1-9, 1931.
59. Kemp, R.C., Kemp, W.R., “The Triple Point, Boiling Point and 17 K Point of Equilibrium Hydrogen.” Metrologia, 15 (1979) 155-159.

60. van Itterbeek, A., Verbeke, O., Theewes, F., Staes, K., and de Boelpaep, J., "The Difference in Vapour Pressure between Normal and Equilibrium Hydrogen. Vapour Pressure of Normal Hydrogen between 20 Degrees K and 32 Degrees K," Physica (Amsterdam), 30:1238-44, 1964.
61. Weber, L.A., Diller, D.E., Roder, H.M., and Goodwin, R.D., "The Vapour Pressure of 20 Degrees K Equilibrium Hydrogen," Cryogenics, 2(4):236-8, 1962.
62. Brouwer, J.P., van den Meijdenberg, C.J.N., Beenakker, J.J.M., “Specific Heat of the Liquid Mixtures of Neon and Hydrogen isotopes in the Phase-Separation Region. I. The system Ne-H(2).” Commun. Kamerlingh Onnes Lab. Univ. Leiden, (380a):1-31, 1970.
63. Smith, A.L., Hallett, N.C., and Johnston, H.L., "Condensed Gas Calorimetry. VI. The Heat Capacity of Liquid Parahydrogen from the Boiling Point to the Critical Point," J. Am. Chem. Soc., 76:1486-8, 1954.
64. Johnston, H.L., Clarke, J.T., Rifkin, E.B., and Kerr, E.C., "Condensed Gas Calorimetry. I. Heat Capacities, Latent Heats and Entropies of Pure Para-Hydrogen from 12.7 to 20.3 Degrees K. Description of the Condensed Gas Calorimeter in Use in the Cryogenic Laboratory of the Ohio State University," J. Am. Chem. Soc., 72:3933-8, 1950.
65. Younglove, B.A. and Diller, D.E., "The Specific Heat of Saturated Liquid Para-Hydrogen from 15 to 32 Degrees K," Cryogenics, 2(5):283-7, 1962.
66. Goodwin, R.D., Diller, D.E., Roder, H.M., and Weber, L.A., "Second and Third Virial Coefficients for Hydrogen," J. Res. Natl. Bur. Stand., Sect. A, 68(1):121-6, 1964.
67. Amagat, E.A., “Reports of the Elasticity and Expansivity of Fluids at Very High Pressures.” Ann. Chem. Phys., 29 (1893) 68-136.
68. Bartlett, E.P., "The Compressibility Isotherms of Hydrogen, Nitrogen and Mixtures of These Gases at 0 Degrees and Pressures to 1000 Atmospheres," J. Am. Chem. Soc., 49:687-701, 1927.
69. Bartlett, E.P., Cupples, H.L., and Tremearne, T.H., "The Compressibility Isotherms of Hydrogen, Nitrogen and a 3:1 Mixture of These Gases at Temperatures between 0 and 400 Degrees and at Pressures to 1000 Atmospheres," J. Am. Chem. Soc., 50:1275-88, 1928.
70. Bartlett, E.P., Hetherington, H.C., Kvalnes, H.M., and Tremearne, T.H., "The Compressibility Isotherms of Hydrogen, Nitrogen and a 3:1 Mixture of These Gases at Temperatures of -70, -50, -25 and 20(and at Pressures to 1000 Atmospheres," J. Am. Chem. Soc., 52:1363-73, 1930.
71. David, H.G. and Hamann, S.D., "The Quantum Behaviour of Compressed Gases," Trans. Faraday Soc., 49: 711-716, 1953.
72. Holborn, L. and Otto, J., "On the Isotherms of Some Gases between +400 and -183 Degrees (in German)," Z. Phys., 33:1-11, 1925.

73. Jaeschke, M. and Humphreys, A.E., The GERG Databank of High Accuracy Compressibility Factor Measurements, GERG Technical Monograph 4, Verlag des Vereins Deutscher Ingenieure: Dusseldorf, Germany, 1990.
74. Johnston, H.L., White, D., Wirth, H., Swanson, C., Jensen, L.H., and Friedman, A.S., "Gaseous Data of State II - The Pressure-Volume-Temperature Relationships of Gaseous Normal Hydrogen From the Critical Temperature to Room Temperature and Up to 200 Atmospheres Pressure," Cryogenic Laboratory -Ohio State University, Columbus, Ohio. Technical Report 264-25 , November 25, 1953.
75. Liebenberg, D.H., Mills, R.L., and Bronson, J.C., "Measurement of P, V, T, and Sound Velocity Across the Melting Curve of n-H(2) and n-D(2) to 19 Kbar," Phys. Rev. B, 18(8):4526-32, 1978.
76. Liebenberg, D.H., Mills, R.L., Bronson, J.C., "P-V-T and Sound Velocity data for fluid n-H2 in the range 75-307 K and 2-20 kbar." Los Alamos Inf. Rep. LA-6641-MS, 1977.
77. Machado, J.R.S., Streett, W.B., and Deiters, U., "PVT Measurements of Hydrogen/Methane Mixtures at High Pressures," J. Chem. Eng. Data, 33(2): 148-152, 1988.
78. Michels, A. and Goudeket, M., "Compressibilities of Deuterium between 0 Degrees C and 150 Degrees C, up to 3000 Atmospheres," Physica (Amsterdam), 8(3):353-60, 1941.
79. Michels, A., De Graaff, W., Wassenaar, T., Levelt, J.M.H., and Louwerse, P., "Compressibility Isotherms of Hydrogen and Deuterium at Temperatures between -175 Degrees C and +150 Degrees C (at Densities up to 960 Amagat)," Physica (Amsterdam), 25:25-42, 1959.
80. Presnall, D.C., “Pressure-volume-temperature measurements on hydrogen from 200 degrees to 600 degrees C and up to 1800 atmospheres.” J. Geophys. Res., 74(25) (1969) 6026-6033.
81. Scott, G.A., "The Isotherms of Hydrogen, Carbon Monoxide and their Mixtures," Proc. R. Soc. London, A125: 330-334, 1929.
82. Townend, D.T.A. and Bhatt, L.A., "Isotherms of Hydrogen, Carbon Monoxide and their Mixtures," Proc. R. Soc. London, A134: 502-512, 1931.
83. van Itterbeek, A., Verbeke, O., Theeuwes, F., Jansonne, V., “The molar volume of liquid normal hydrogen in the temperature range between 21 degrees K and 40 degrees K at pressures up to 150 atm.” Physica, 32(9) (1966) 1591-1600.
84. Verschoyle, T.T.H., "Isotherms of Hydrogen, of Nitrogen, and of Hydrogen-Nitrogen Mixtures, at 0 Degrees and 20 Degrees C., up to a Pressure of 200 Atmospheres," Proc. R. Soc. London, Ser. A, 111:552-76, 1926.
85. Wiebe, R. and Gaddy, V.L., "The Compressibilities of Hydrogen and of Four Mixtures of Hydrogen and Nitrogen at 0, 25, 50, 100, 200 and 300 Degrees and to 1000 Atmospheres," J. Am. Chem. Soc., 60:2300-3, 1938.

86. Gusewell, D., Schmeissner, F., Schmid, J., "Density and Sound Velocity of Saturated Liquid Neon-Hydrogen and Neon-Deuterium Mixtures between 25 and 31 K." Cryogenics, 10, 1970.
87. Matsuishi, K., Gregoryanz, E., Mao, H., Hemley, R., "Equation of state and intermolecular interactions in fluid hydrogen from Brillouin scattering at high pressures and temperatures." J. Chem. Phys. 118, 2003.
88. van Itterbeek, A., van Dael, W., and Cops, A., "Velocity of Ultrasonic Waves in Liquid Normal and Para Hydrogen," Physica (Amsterdam), 27:111-6, 1961.
89. van Itterbeek, A., van Dael, W., and Cops, A., "The Velocity of Sound in Liquid Normal and Para Hydrogen as a Function of Pressure," Physica (Amsterdam), 29:965-73, 1963.
90. Aston, J.G., Willihnganz, E., and Messerly, G.H., "Heat Capacities and Entropies of Organic Compounds. I. A Thermodynamic Temperature Scale in Terms of the Copper-Constantan Thermocouple from 12 to 273 K," J. Am. Chem. Soc., 57:1642-1646, 1935.
91. Barber, C.R., "New Determinations of the Vapor Pressure and of the Triple and Boiling Points of Equilibrium Hydrogen," Com. Int. Poids Mes., Com. Consult. Thermom. [Trav.] (6):94-96, 1964.
92. Grilly, E.R., "The Vapor Pressures of Hydrogen, Deuterium and Tritium up to Three Atmospheres," J. Am. Chem. Soc., 73:843-6, 1951.
93. Henning, F., "Vapor Pressure and Resistance Thermometer in the Temperature Range of Liquid Nitrogen and Hydrogen," Z. Phys., 40:775-785, 1926.
94. Henning, F. and Otto, J., "Vapour Pressure Curves and Triple Points in the Temperature Range from 14° to 90° Absolute," Phys. Z., 37:633-636, 1936.
95. Hiza, M.J., "Liquid-Vapor Equilibria in Binary Systems Containing (4)He or (3)He with nH(2) or nD(2)," Fluid Phase Equilib., 6(3):203-207, 1981.
96. Keesom, W.H., Bijl, A., and van der Horst, H., "Determination of the Boiling Points and the Vapour-Pressure Curves of Normal Hydrogen and of Para-Hydrogen. The Normal Boiling Point of Normal Hydrogen as a Basic Point in Thermometry," Commun. Kamerlingh Onnes Lab. Univ. Leiden (217A):1-9, 1931.
97. Scott, R.B., Brickwedde, F.G., Urey, H.C., Wahl, M.H., J. Chem. Phys., 2 (1934) 454.
98. Traver, M.W., Jaquerod, A., and Senter, G., "Part I. Pressure Coefficients of Hydrogen and Helium; Part II. Vapour Pressures of Liquid Oxygen; Part III. Vapour Pressures of Liquid Hydrogen," Proc. R. Soc. London, 484-491, 1902.
99. van Itterbeek, A., Verbeke, O., Theewes, F., Staes, K., and de Boelpaep, J., "The Difference in Vapour Pressure between Normal and Equilibrium Hydrogen. Vapour Pressure of Normal Hydrogen between 20 Degrees K and 32 Degrees K," Physica (Amsterdam), 30:1238-44, 1964.
100. White, D., Friedman, A.S., and Johnston, H.L., "The Vapor Pressure of Normal Hydrogen from the Boiling Point to the Critical Point," J. Am. Chem. Soc., 72:3927-30, 1950.

101. White, D., Friedman, A.S., and Johnston, H.L., "The Direct Determination of the Critical Temperature and Critical Pressure of Normal Hydrogen," J. Am. Chem. Soc., 72:3565-3568, 1950.
102. Beenakker, J.J.M., Varekamp, F.H., and Van Itterbeek, A., "The Isotherms of the Hydrogen Isotopes and their Mixtures with Helium at the Boiling Point of Hydrogen," Commun. Kamerlingh Onnes Lab. Univ. Leiden (313A):1-16, 1959.
103. Cottrell, T.L., Hamilton, R.A., and Taubinger, R.P., "The Second Virial Coefficients of Gases and Mixtures. Part 2. - Mixtures of Carbon Dioxide with Nitrogen, Oxygen, Carbon Monoxide, Argon and Hydrogen," Trans. Faraday Soc., 52:1310-2, 1956.
104. Dehaas, W.J., "Isotherms of diatomic gases and of their binary mixtures. X. Control measurements with the volumenometer of compressibility of hydrogen at 20 C." Proc. K. Ned. Akad. Wet. 15:295-299, 1912.
105. El Hadi, Z.E.H.A., Dorrepaal, J.A., Durieux, M., "Pressure-volume isotherms of hydrogen gas between 19 and 23 degrees K." Physica (Amsterdam), 41:320-31, 1969.
106. Gibby, C.W., Tanner, C.C., and Masson, I., "The Pressures of Gaseous Mixtures. II - Helium and Hydrogen, and their Intermolecular Forces," Proc. R. Soc. London, Ser. A, 122:283-304, 1929.
107. Holborn, L. and Otto, J., "On the Isotherms of Helium, Hydrogen and Neon below -200 Degrees (in German)," Z. Phys., 38:359-67, 1926.
108. Kerl, K., "Determination of mean molecular polarizabilities and second virial coefficients of gases by scanning-wavelength interferometry." Z. Phys. Chem. (Munich) 129:129-48, 1982.
109. Knaap, H.F.P., Knoester, M., Knobler, C.M., and Beenakker, J.J.M., "The Second Virial Coefficients of the Hydrogen Isotopes between 20 and 70 Degrees K," Commun. Kamerlingh Onnes Lab. Univ. Leiden (330C):1-12, 1962.
110. Long, E.A. and Brown, O.L.I., "A Comparison of the Data of State of Normal and Para Hydrogen from the Boiling Point to 55 Degrees K," J. Am. Chem. Soc., 59:1922-4, 1937.
111. Lopatinskii, E.S., Rozhnov, M.S., Zhdanov, V.I., Pernovskii, S.L., Kudrya, Y.N., "Second virial coefficients of gas mixtures of hydrocarbons, carbon dioxide, and hydrogen with nitrogen and argon." Zh. Fiz. Khim. 65, 2060-5, 1991.
112. Mihara, S., Sagara, H., Arai, Y., and Saito, S., "The Compressibility Factors of Hydrogen-Methane, Hydrogen-Ethane and Hydrogen-Propane Gaseous Mixtures," J. Chem. Eng. Jpn., 10(5):395-9, 1977.
113. Mueller, W.H., Leland, T.W., and Kobayashi, R., "Volumetric Properties of Gas Mixtures at Low Temperatures and High Pressures by the Burnett Method: the Hydrogen-Methane System," AIChE J., 7(2):267-272, 1961.

114. Nijhoff, G.P. and Keesom, W.H., "Isotherms of Di-Atomic Substances and their Binary Mixtures. XXXIV. Isotherms of Hydrogen at Temperatures of 0 Degrees and +100 Degrees C," Commun. Phys. Lab. Univ. Leiden (188D):31-4, 1927.
115. Perez, S., Schmiedel, H., and Schramm, B., "Second Interaction Virial Coefficients of the Nobel Gas-Hydrogen Mixtures Ar-H(2), Kr-H(2), and Xe-H(2)," Z. Physik. Chem., 123:35-38, 1980.
116. Schramm, B., Elias, E., Kern, L., Natour, Gh., Schmitt, A., and Weber, Ch., "Precise Measurements of Second Virial Coefficients of Simple Gases and Gas Mixtures in the Temperature Range below 300 K," Ber. Bunsenges. Phys. Chem., 95(5):615-621, 1991.
117. van Agt, F.P.G.A.J. and Kamerlingh Onnes, H., Isotherms of Monatomic Substances and their Binary Mixtures XXV. Idem of Diatomic Substances XXXI. The Compressibility of Hydrogen and Helium Gas between 90 Degrees and 14 Degrees K, Redstone Sci. Inform. Center, Transl. RSIC-30, 16pp, 1963.
118. Varekamp, F.H. and Beenakker, J.J.M., "The Equation of State of the Hydrogen Isotopes and their Mixtures with Helium below the Boiling Point of Hydrogen," Commun. Kamerlingh Onnes Lab. Univ. Leiden (316C):1-16, 1959.
119. Lemmon, E.W., Jacobsen, R.T, “A new Functional Form and new Fitting Techniques for Equations of State with Application to Pentafluoroethane (HFC-125)” J. Phys. Chem. Ref. Data 34(1):69-108, 2005.
120. Setzmann, U., Wagner, W., J. Phys. Chem. Ref. Data, 25(6) (1966) 1061.
121. Trusler, J.P.M., “The Virial Equation of State” Equations of State for Fluids and Fluid Mixtures: Part I, IUPAC Elsevier, 2000.
122. Lemmon, E.C., Private Communications, 2006.

Appendix 1. Tables of Hydrogen Thermodynamic Data

Table A.1 Calculated Saturation Properties of the New Parahydrogen EOS.

Temperature (K)	Pressure (MPa)	Liquid Density (mol/dm³)	Vapor Density (mol/dm³)	Liquid Cv (J/mol-K)	Vapor Cv (J/mol-K)	Liquid Sound Speed (m/s)	Vapor Sound Speed (m/s)
14	0.007884	38.107	0.068845	10.397	12.571	1256.9	307.55
15	0.013434	37.699	0.11032	10.607	12.663	1231.3	316.83
16	0.021548	37.27	0.1675	10.753	12.745	1210.4	325.43
17	0.032886	36.817	0.24341	10.886	12.815	1190.1	333.38
18	0.048148	36.337	0.34129	11.031	12.875	1168.5	340.72
19	0.068071	35.828	0.46459	11.191	12.935	1144.7	347.42
20	0.093414	35.287	0.61709	11.364	13.002	1118.6	353.5
21	0.12496	34.713	0.80302	11.54	13.083	1090.1	358.93
22	0.1635	34.101	1.0272	11.715	13.185	1059.2	363.71
23	0.20983	33.447	1.2954	11.883	13.312	1025.8	367.82
24	0.26478	32.745	1.6145	12.043	13.469	989.93	371.26
25	0.32917	31.988	1.9931	12.193	13.659	951.22	374.02
26	0.40384	31.166	2.4424	12.337	13.888	909.3	376.1
27	0.48965	30.263	2.9778	12.48	14.162	863.62	377.48
28	0.5875	29.257	3.6211	12.632	14.49	813.32	378.15
29	0.69833	28.115	4.4065	12.809	14.885	757.13	378.08
30	0.82319	26.776	5.3927	13.046	15.37	693.03	377.2
31	0.96329	25.113	6.7006	13.414	15.984	617.44	375.34
32	1.1203	22.77	8.6773	14.131	16.805	522.58	372.03

Table A.2 Calculated Saturation Properties of the New Normal Hydrogen EOS.

Temperature (K)	Pressure (MPa)	Liquid Density (mol/dm³)	Vapor Density (mol/dm³)	Liquid Cv (J/mol-K)	Vapor Cv (J/mol-K)	Liquid Sound Speed (m/s)	Vapor Sound Speed (m/s)
14	0.007541	38.181	0.065838	10.407	12.589	1268.3	307.56
15	0.012898	37.768	0.10589	10.546	12.663	1247.1	316.97
16	0.020755	37.335	0.16125	10.742	12.728	1225.5	325.71
17	0.031759	36.88	0.23491	10.925	12.786	1203.3	333.81
18	0.046602	36.398	0.33001	11.085	12.841	1180.2	341.28
19	0.066006	35.89	0.44989	11.228	12.901	1155.5	348.11
20	0.090717	35.352	0.59818	11.363	12.971	1129.1	354.3
21	0.1215	34.781	0.77889	11.494	13.057	1100.7	359.83
22	0.15913	34.175	0.99661	11.621	13.162	1070.2	364.69
23	0.20438	33.53	1.2567	11.748	13.29	1037.5	368.87
24	0.25807	32.839	1.5657	11.873	13.443	1002.2	372.37
25	0.321	32.096	1.9316	11.999	13.623	964.2	375.19
26	0.39399	31.291	2.3649	12.127	13.833	923.09	377.32
27	0.47789	30.411	2.8799	12.261	14.077	878.37	378.77
28	0.57359	29.436	3.4967	12.408	14.363	829.28	379.54
29	0.68205	28.335	4.2464	12.582	14.7	774.75	379.64
30	0.80432	27.054	5.1811	12.808	15.108	713.05	379.06
31	0.94165	25.488	6.4039	13.14	15.618	641.2	377.79
32	1.0957	23.357	8.1828	13.73	16.294	552.87	375.77

Table A.3 Calculated Saturation Properties of the New Orthohydrogen EOS.

Temperature (K)	Pressure (MPa)	Liquid Density (mol/dm³)	Vapor Density (mol/dm³)	Liquid Cv (J/mol-K)	Vapor Cv (J/mol-K)	Liquid Sound Speed (m/s)	Vapor Sound Speed (m/s)
15	0.012868	37.78	0.10539	10.616	12.644	1244.4	316.98
16	0.0207	37.343	0.16036	10.796	12.687	1224.9	325.79
17	0.031665	36.886	0.23346	10.945	12.749	1205.4	333.84
18	0.046452	36.406	0.32781	11.072	12.813	1184.6	341.26
19	0.065786	35.9	0.4468	11.187	12.874	1162	348.11
20	0.090417	35.364	0.59412	11.299	12.937	1137.1	354.41
21	0.12112	34.795	0.77391	11.412	13.011	1109.8	360.15
22	0.15867	34.191	0.9909	11.526	13.108	1080	365.29
23	0.20388	33.546	1.2506	11.642	13.235	1047.5	369.78
24	0.25755	32.855	1.5598	11.76	13.401	1012.3	373.56
25	0.32051	32.112	1.9266	11.879	13.61	973.92	376.59
26	0.39359	31.306	2.362	12.001	13.869	932.22	378.82
27	0.47765	30.425	2.8802	12.13	14.18	886.71	380.21
28	0.57358	29.448	3.5018	12.272	14.549	836.74	380.72
29	0.68232	28.345	4.2576	12.438	14.983	781.37	380.33
30	0.80489	27.061	5.199	12.65	15.492	719.08	378.99
31	0.94245	25.492	6.4254	12.955	16.092	647.29	376.59
32	1.0964	23.366	8.1867	13.49	16.794	560.44	373.03

Table A.4 Vapor Pressure Data Predicted Using the Quantum Law of Corresponding States.

Parahydrogen (orig.)		Normal Hydrogen		Orthohydrogen	
Temperature (K)	Pressure (MPa)	Temperature (K)	Pressure (MPa)	Temperature (K)	Pressure (MPa)
15	0.013452	15.09888	0.013582	15.10768	0.013601
15.5	0.017154	15.60163	0.017311	15.61057	0.017334
16	0.021578	16.10438	0.021768	16.11347	0.021794
16.5	0.026809	16.60713	0.027039	16.61636	0.027069
17	0.032932	17.10989	0.033207	17.11925	0.033242
17.5	0.040038	17.61264	0.040366	17.62215	0.040407
18	0.048216	18.11539	0.048606	18.12504	0.048653
18.5	0.057559	18.61814	0.058019	18.62793	0.058073
19	0.068162	19.1209	0.068701	19.13083	0.068764
19.5	0.080119	19.62365	0.080747	19.63372	0.080819
20	0.093526	20.1264	0.094255	20.13661	0.094337
20.5	0.10848	20.62915	0.10932	20.63951	0.109415
21	0.12508	21.13191	0.126045	21.1424	0.126152
21.5	0.14343	21.63466	0.144532	21.64529	0.144654
22	0.16361	22.13741	0.164863	22.14819	0.165001
22.5	0.18575	22.64016	0.187168	22.65108	0.187324
23	0.20992	23.14292	0.211519	23.15397	0.211694
23.5	0.23625	23.64567	0.238046	23.65687	0.238242
24	0.26482	24.14842	0.26683	24.15976	0.267048
24.5	0.29575	24.65117	0.297991	24.66265	0.298234
25	0.32913	25.15393	0.331621	25.16555	0.33189
25.5	0.36508	25.65668	0.36784	25.66844	0.368137
26	0.40371	26.15943	0.406759	26.17133	0.407087
26.5	0.44511	26.66218	0.448468	26.67423	0.448829
27	0.48941	27.16494	0.4931	27.17712	0.493495
27.5	0.53672	27.66769	0.540764	27.68001	0.541197
28	0.58716	28.17044	0.591581	28.18291	0.592054
28.5	0.64085	28.67319	0.645673	28.6858	0.646188
29	0.69793	29.17595	0.70318	29.18869	0.70374
29.5	0.75854	29.6787	0.764243	29.69159	0.764851
30	0.82283	30.18145	0.829014	30.19448	0.829673
30.5	0.89097	30.6842	0.897663	30.69737	0.898376
31	0.96316	31.18696	0.970393	31.20027	0.971163
31.5	1.0396	31.68971	1.047405	31.70316	1.048236
32	1.1206	32.19246	1.129011	32.20605	1.129905
32.5	1.2066	32.69521	1.215654	32.70895	1.216617